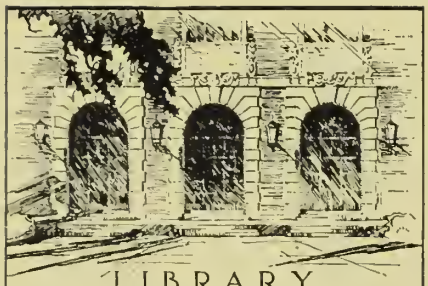

ANTENNA LABORATORY

Technical Report No. 40

A STUDY OF THE COMA-CORRECTED ZONED MIRROR BY DIFFRACTION THEORY

by

Samarendramohon Dasgupta

and

Y. T. Lo

17 July 1959

Contract AF33(616)-6079

Project No. 9-(13-6278) Task 40572

Sponsored by:

WRIGHT AIR DEVELOPMENT CENTER

Electrical Engineering Research Laboratory
Engineering Experiment Station
University of Illinois
Urbana, Illinois

ABSTRACT

A coma-corrected zoned mirror has previously been shown by para-geometrical optics to posess no spherical aberration and no third order coma. However, geometrically defined aberrations provide no information about the diffraction pattern structure which may be of importance in microwave applications. In this investigation a study using a more rigorous boundary value approach has been made of a zoned mirror with emphasis on its effectiveness in coma correction. Because a cylindrical mirror has no astigmatism and other higher types of aberration (according to Nijboer's classification) and because the mathematical analysis is simpler, a two dimensional zoned mirror was chosen for analysis.

The image patterns (the field intensity distributions on the focal plane for various incident angles as commonly used in optics) as well as the main features of the radiation pattern (minor lobe level, gain and beam width for various scan angles as commonly used in antenna engineering) are obtained. These features are compared with those of a smooth parabolic cylinder with same focal length and aperture. It is found that for a system with small F number and nearly uniform illumination, the zoned mirror is much superior to the smooth parabola in coma correction. The gain, minor lobe level and beam width of the radiation pattern for a zoned mirror are relatively constant for a scan angle up to 25^{o}, while those for the corresponding smooth parabola change considerably. The ratio of the two secondary maxima of the intensity distribution in the

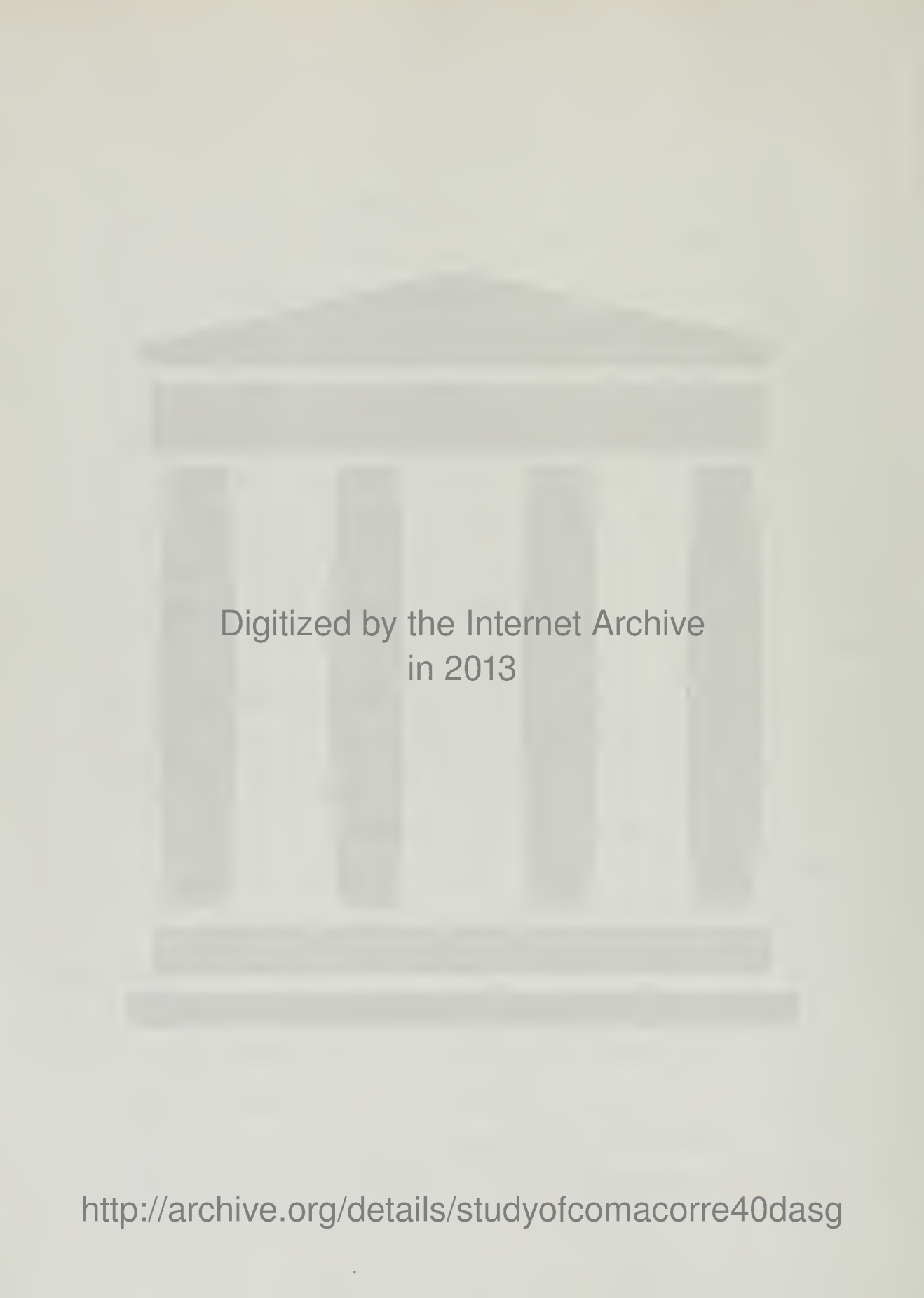

focal plane (a function of the coma aberration only) is substantially equal to unity in the case of a zoned mirror whereas it changes drastically for a smooth parabola.

Calculations of the diffracted fields are based upon three different orders of approximation for the induced current on the mirror, namely, (i) Geometrical optics current distribution (ii) a distribution taking into account the effect of the edges (iii) a distribution taking into account both the edge effect and the first order coupling between zones.

It is found that the field intensity on the focal plane (and by reciprocity, the far field) obtained by using (ii) and (iii) are not significantly different. Results obtained by using approximation (i) follow those obtained by (ii) and (iii) quite closely. Thus the simple and straight-forward physical and optics solution seems to offer a result of good accuracy even with a large number of discontinuities in the diffracting surface as in the present case. However for higher accuracy the edge effect should be considered.

ACKNOWLEDGEMENT

These authors wish to thank Professor V. H. Rumsey for first drawing their attention to this mirror system, and Professors E. C. Jordan, G. A. Deschamps and P. E. Mayes for helpful discussions and for reading the manuscript. They are particularly indebted to Mr. N. E. Wiseman for his assistance in programming the numerical calculation and to the Computer Laboratory of the University of Illinois for providing facilities in computation. It is also a pleasure to acknowledge the sponsorship of the Wright Air Development Center, Wright-Patterson Air Force Base, Ohio, for its investigation.

Lastly, these authors also wish to acknowledge a valuable communication from Dr. Gertrude Blanch of Wright Air Development Center about the convergence and asymptotic solution of Mathieu functions.

CONTENTS

CONTENTS (Continued)

1. INTRODUCTION

For wide angle scanning, the aperture of a microwave reflector is always limited due to the progressive deterioration of the image as the aperture of the system is increased. Although the gain and directivity increase, the scanning performance deteriorates because of spherical aberration, coma, astigmatism etc. which are inherent with wide aperture systems.

The correction of optical errors for wide aperture systems is generally performed by an assembly of lenses which provides the designer, for each element, with two radii of curvature and the index of refraction as the three available parameters for correction of optical errors. In the case of a reflector, however, only the radius of curvature is available as a parameter for correction of optical errors. The correction of aberrations by placing the surfaces of one curvature on the surface of another, such as a zoned mirror, has been suggested by various workers. This method is of practical interest and importance due to its simpler construction and lower cost as compared with a lens system particularly in VHF and UHF ranges.

Ramsay and Jackson[28] have made an experimental investigation of a zoned mirror particularly in comparison with a spherical mirror in scanning performance. Lately Toraldo di Francia[27] and his coworkers have shown by his generalized geometrical optics approach that coma aberration is greatly reduced in a zoned mirror. The purpose of this investigation is to analyze the performance of the zoned mirror as a wide angle scanning antenna by employing a more rigorous boundary value problem approach.

2. COMA-CORRECTED ZONED MIRROR

2.1 Description of the Zoned Mirror

Let us consider a set of confocal paraboloids of focal lengths differing by $\lambda/2$ having the common focus at c and axis VC, (Figure 1). Then the family of the paraboloids will be defined by

$$r = \frac{2(f - n\frac{\lambda}{2})}{1 + \cos\psi}, \qquad n = 0, 1, 2, \ldots \tag{1.1}$$

Where f is the focal length of the paraboloid with largest focal length.

This family of paraboloids will be equiphase in so far as all rays parallel to the axis VC, after reflection from all the parabolic surfaces, will meet at the focus c in phase.

These confocal paraboloids will intersect the spherical surface Σ, having c as the center and f as the radius, as circles represented by P_1, P_2 etc. If a set of planes perpendicular to the axis VC is drawn through the points N_1, N_2 .... representing the intersection of the paraboloids with the axis VC, they will cut the spherical surface Σ in circles represented by Q_1, Q_2 .... etc. A family of coaxial cylinders with VC as the axis and cross sections given by the circles Q_1, Q_2 etc. are drawn. Then the paraboloidal surfaces cut out by these circles form a zoned mirror.

Thus A_1B_1, A_2B_2 etc. are the reflecting zones made of perfect conductor while B_1A_2, B_2A_3 etc. are the sections of coaxial cylinders marking the boundaries of A_1B_1, A_2B_2 etc. which are assumed to play no role in image formation.

It can be proved that all the tangents to these zones at P_1, P_2 etc.

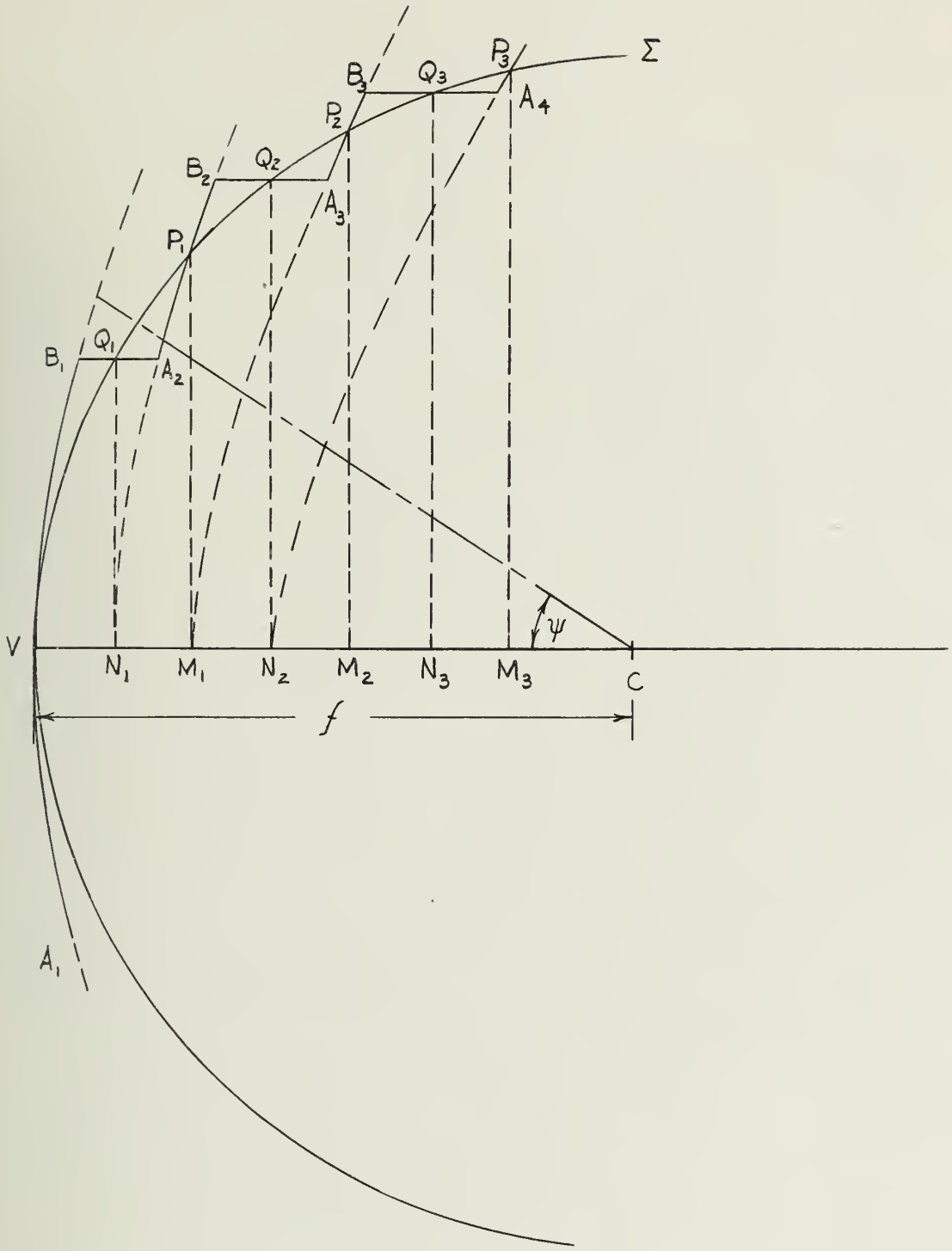

FIGURE 1

pass through V. Thus the parabolic zoned surfaces can be approximated by portions of a set of cones having the same vertex V.

2.2 Some Earlier Works on a Zoned Mirror

Ramsay and Jackson[28] investigated experimentally the performance of a coma corrected zoned mirror similar to the one described above with the modification that the tips and not the centers of the zones were on the spherical surface (coma sphere). This was done presumably for the purpose of simplifying the construction and it was assumed by the authors that this difference did not change the performance to a great extent. Ramsay and Jackson compared the measured gains, side lobe levels and beam widths of the radiation pattern of a zoned mirror with those of a spherical mirror with a feed offset of 15^{o}. They found that the zoned mirror is slightly better than the spherical mirror but this advantage is doubtful when the difficulty of construction is taken into consideration. However, it is felt that they worked with a case where the advantages of a zoned mirror are greatly suppressed due to the following:

(1) The F number, namely f/D ratio used by them is unity, where f is the focal length and D is the diameter of the aperture of the assembly. Thus the dishes used for comparison by them are rather shallow.

(2) A 15 db tapered illumination is used by them. This, in effect, weights heavily a small central portion of the dish which is essentially the same for both the zoned mirror and the spherical mirror.

(3) The zones are not arranged to make their mean surface coincide with the so called "coma circle." In fact except for the first zone, none of the zones has any point lying on the coma circle.

(4) A three dimensional zoned mirror as used by these authors, if coma corrected, will have astigmatism as the main aberration. In their experiment, they seem to have made no effort in differentiating these aberrations.

Ronchi and Toraldo di Francia[27] by employing the theory of "Parageometrical Optics," * have obtained expressions of the fifth order coma and astigmatism for this type of mirror. (The third order coma is absent as a result of the satisfaction of the sine condition.) Toraldo di Francia, very recently reported that their experimental results are in good agreement with the theoretical prediction of the best focal surface for scanning purpose.

* Briefly speaking the parageometrical optics is essentially the theory of geometrical optics generalized for the grating systems which ascertains the relation of the diffracted ray vector in terms of the incident ray vector and the grating system geometry.

3. OUTLINE OF THE PRESENT INVESTIGATION

3.1 Limitations of the Aberration Study by Optical Methods

Aberrations of any system are generally studied by either (1) geometrical optics, namely the ray tracing technique or (2) obtaining the diffraction pattern at the image space with an assumed aberration function at the aperture.[25] The drawback of (2) is obvious in that the over-all performance of a given system is still unknown. About (1), it is well known that geometrical optics loses its effectiveness at microwave frequencies since there exists no definite boundary between the shadow and the illuminated regions, i.e. the image is no longer a well defined geometric one. Thus, aberration defined in terms of geometrical optics loses its clearness of description at lower frequencies. This is particularly true for the region near nulls and minor lobes where even the physical optics method begins to show errors.

It is difficult to translate the geometrical optics evaluation of aberration into a diffraction pattern. However, since the structure of minor lobes and coma effect are closely related (the ratio of the two minor lobe levels on either side of the major lobe is a function of the conventionally defined coma aberration), an investigation of the minor lobes seems to be in order.

For a system like the zoned mirror, having a large number of edges and discontinuities in structure, the physical optics method seems to need further justification. It is reasonable to assume that the diffraction due to the edges and coupling between zones could be important particularly in the regions of nulls and minor lobes upon which the coma aberration

has a dominant effect.

3.2 Plan of the Proposed Investigation

In recent years due to the rapid growth of microwave technology, great interest has been developed in the generalized diffraction theory and many workers, e.g. Fock[6], Braunbeck[3], Keller[15] etc. have propounded various theories for approximate solutions of general diffraction problems. It, therefore, seems that a complete system of relatively simple structure can be analyzed with reasonable accuracy by the "boundary value problem" approach.

The surface of revolution described in 2.1 presents severe mathematical difficulties, however. Therefore a two dimensional version of the zoned mirror with each zone approximated by a strip* is chosen for this investigation. In fact this system is of more interest since, being free from astigmatism, it enables us to evaluate its ability in coma correction exclusively.

It is therefore proposed to

(1) Analyse the cylindrical system using the "Boundary value problem" approach so that more detailed information regarding the performance of the system can be obtained than is possible by other qualitative methods mentioned before.

(2) Provide a comparative study of possible alternative approximations in the analysis.

(3) Provide information on antenna performance, such as gain, side lobe level, beam width, for various scan angles.

---

* The approximation of each zone by a strip is valid for all zones except the central one, for which a correction has been used in later sections.

3.3 Formulation of the Problem

The problem can be stated as follows: Given (a) a two dimensional zoned mirror consisting of a number of perfectly conducting plane strips (1, 2, ... n), infinitely long in z-direction arranged as described before (Figure 2) and (b) a plane electromagnetic field $E_{z_{inc}}$ with the electric field polarized parallel to the edges of the strips, i.e. having only the z component, incident on the zoned mirror; it is required to find the intensity distribution of the electric field on the image plane.

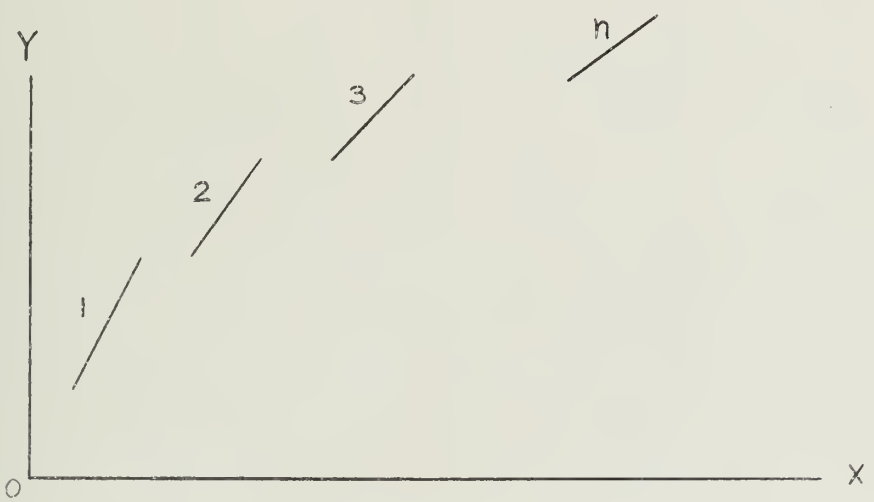

FIGURE 2

When a plane wave is incident on the zoned mirror each element of the zoned mirror will have a current induced on the surface, the distribution of which will depend on the angle of incidence and the width of the strips. It will also depend on the current distribution on the surface of other strips because of the coupling between the strip under consideration and other strips. Once the current distribution on each strip is determined the electric field at any point in space can be evaluated.

This problem can not be solved by the well known method of solution

of the wave equation by separation of variables since the assembly can not be defined by a complete coordinate surface.

However, it is possible to have an integral equation formulation of the problem. Boundary value problems of a conducting or dielectric body in a given electromagnetic field may be formulated by expressing the scattered field in terms of an integral of induced sources over the surface or throughout the volume of the scatterer. The boundary conditions at every point on the scatterer then lead to an integral equation in terms of the induced source function. The integral equation formulation, unlike that of differential equations, contains the boundary condition specified in the formulation, but generally is not traceable. It does not require the system to be separable and often leads to an approximate solution more directly.

Let the currents induced on the surface of the zones 1, 2, 3 ... n etc., be denoted by I_1, I_2 ... I_n etc., respectively.

Then the vector potential has only z component. A_z at any point P due to these currents I_1, I_2, ... I_n etc. is given by

$$A_z = \int_{\text{strip 1}} I_1(s)g(s,s')ds + \int_{\text{strip 2}} I_2(s)g(s,s')ds + \ldots + \int_{\text{strip n}} I_n(s)g(s,s')ds \tag{3.1}$$

where $s(x,y)$ is a point on the strip under consideration, $s'(x',y')$ is the point of observation, and g, the free space Green's function is defined by

$$g = \frac{1}{4i} H_o^{(2)} \left\{ k \sqrt{(x-x')^2 + (y-y')^2} \right\}, \text{ with } k = \frac{2\pi}{\lambda}. \tag{3.2}$$

From Maxwell's equation we have,

$$\bar{H} = \nabla \times \bar{A} \tag{3.3}$$

and

$$\bar{E} = \frac{1}{i\omega\epsilon} \nabla \times \bar{H} \tag{3.4}$$

Hence

$$\bar{E} = \frac{1}{i\omega\epsilon} \nabla \times \nabla \times \bar{A} \tag{3.5}$$

which in our case gives

$$E_z \hat{z} = \frac{1}{i\omega\epsilon} \nabla \times \nabla \times A_z \hat{z} \tag{3.6}$$

or

$$E_z \hat{z} = \frac{1}{y} (\nabla \nabla \cdot A_z \hat{z} - \hat{z} \nabla^2 A_z) = \frac{k^2}{i\omega\epsilon} A_z \hat{z} \tag{3.7}$$

Since

$$\nabla^2 A_z + k^2 A_z = 0$$

and

$$\frac{\partial}{\partial z} A_z = 0$$

At the surface of any strip, the total tangential electric field must be zero. Hence the diffracted tangential field at the surface must be given by

$$E_{Diff} = E_{z_{inc}} \tag{3.8}$$

Therefore

$$\frac{k^2}{i\omega\epsilon} \cdot A_z = - E_{z_{inc}} \tag{3.9}$$

at the surface of any strip. Thus

$$\frac{k^2}{i\omega\epsilon} \left[\int_{\text{strip 1}} I_1(s) g(s,s') ds + \int_{\text{strip 2}} I_2(s) g(s,s') ds + \ldots + \int I_n(s) g(s,s') ds \right]$$

$$= - E_{z_{inc}} \tag{3.10}$$

The above represents n equations for s' lying on any of the n strips.

Representing the operator

$$\frac{k^2}{i\omega\epsilon} \int_q g(s,p)ds$$

by G_{qp} we can express Equation (3.10) symbolically as

$$GI = - E_z \tag{3.11}$$

where

$$G = \begin{bmatrix} G_{11} & G_{21} & \cdots & G_{n1} \\ G_{12} & G_{22} & \cdots & G_{n2} \\ - & - & - & - \\ G_{1n} & G_{2n} & \cdots & G_{nn} \end{bmatrix}$$

$$I = \begin{bmatrix} I_1 \\ I_2 \\ I_n \end{bmatrix}$$

Equation (3.11) represents a set of n simultaneous integral equations which when solved gives the values of the current distributions I_1, I_2, ... I_n on all the n strips.

Let I_i i.e., current on any strip i be represented as

$$I_i = I_{ii} + \sum_{\substack{j=1 \\ j\neq i}}^{n} I_{ij} \tag{3.12}$$

where I_{ii} is the current induced on the surface of the strip i due to an incident plane wave in the absence of other strips, and I_{ij} is the current induced on the surface of the strip i due to the field of I_j of the strip j.

The solution of Equation (3.11) is very difficult to obtain, but a method of successive approximation can be used to obtain the solution to any desired accuracy, at least in principle.

Choosing the i^{th} equation from the set denoted by the Equation (3.11) we have for s' on i

$$\frac{k^2}{i\omega\epsilon}\left[\int_{\text{strip i}} I_i(s)\ (s,s')ds + \sum_{\substack{j=1\\ j\neq i}}^{n} \int_{\text{strip j}} I_j(s)\ g(s,s')ds\right] = -E_{z_{inc}} \tag{3.13}$$

substituting Equation (3.12) in Equation (3.13) we get

$$\sum_{\substack{j=1\\ j\neq i}}^{n}\left[\int_{\text{strip i}} I_{ij}(s)\ g(s,s')ds + \int_{\text{strip j}} I_j(s)\ g(s,s')ds\right] = 0 \tag{3.14}$$

for s' on i

since

$$\frac{k^2}{i\omega\epsilon}\int_{\text{strip i}} I_{ii}(s)\ g(s,s')ds = -E \tag{3.15}$$

which defines the integral equation for the isolated strip i. Using Equation (3.12) again in Equation (3.14) we obtain

$$\sum_{\substack{j=1\\ j\neq i}}^{N}\left[\int_{\text{strip i}} I_{ij}(s)g(s,s')ds + \int_{\text{strip j}} I_{jj}(s)g(s,s')ds + \sum_{\substack{k=1\\ k\neq j}}^{N}\int_{\text{strip j}} I_{jk}(s)g(s,s')ds\right] = 0 \tag{3.16}$$

when s' is on i.

where I_{ij} is the current induced on strip i due to strip j, $(j \neq i)$ and I_{jk} is the current induced on strip j due to a strip k, $(k \neq j)$. Since s' is on i, g in the first integral of (3.16) is much greater than that in second and third integral and further $I_{jj} >> I_{jk}$. Thus an iterative procedure can be established by solving

$$\sum_{\substack{j=1 \\ j\neq i}}^{n} \left[\int_{\text{strip } i} I_{ij}^{(1)}(s)g(s,s')ds + \int_{\text{strip } j} I_{jj}(s)g(s,s')ds \right] = 0 \qquad \text{for } s' \text{ on } i \tag{3.17}$$

Equation (3.17) represents an independent linear integral equation and there are in total n similar equations obtainable by putting i = 1, 2, 3, ... n.

Thus the set of n simultaneous integral equations represented by Equation (3.11) have been reduced to n independent equations for each order of the solution, a typical one of which is given by Equation (3.17).

Since Equation (3.17) is linear and $I_{ij}^{(1)}$ represents the current induced in strip i due to I_{jj} we get

$$\int_{\text{strip } i} I_{ij}(s)g(s,s')ds + \int_{\text{strip } j} I_{jj}(s)g(s,s')ds = 0 \qquad \text{for all } j \neq i \tag{3.18}$$

Equation (3.18) can be solved if I_{jj} is known. In that case it represents the integral equation of the current distribution on a strip i due to a known source distribution I_{jj} on strip j. Further by definition I_{jj} is the current induced on strip j due to a plane wave incident on it. Hence Equation (3.15) represents the integral equation for I_{jj}.

Thus the problem has been reduced to the solution of Equation (3.15) and using the value of I_{jj} there from, to solve Equation (3.18). Equation (3.18) can be solved if the two dimensional Greens function i.e. the current I_{ij} on strip i due to a filament source of unit strength is known.

Thus Equation (3.15) is a special case of Equation (3.18). The rigorous solution of both of these equations leads to a series solution involving Mathieu functions. There are also various approximate solutions of sufficient accuracy for the two above equations and these have been discussed in the next chapter.

Once I_{ii} and $I_{ij}^{(1)}$ have been evaluated by solving the above equations, the current distribution on all the strips can be determined and putting the values of $I_i(s)$ in

$$\frac{k^2}{i\omega\epsilon} \sum_{i=1}^{n} \int_{\text{strip } i} I_i(s)g(s,s')ds = E(s) \qquad (3.19)$$

the field at any point s can be calculated.

4. BRIEF SURVEY OF PREVIOUS WORK ON THE DIFFRACTION BY A STRIP OR A SLIT

This has been the object of investigation by several authors. There are at least two methods which lead to the exact solution, viz

(1) Method employing separable coordinates to solve the wave equation.

(2) Integral equation method.

4.1 Method Employing Separable Coordinate System

Morse and Rubenstein[20] obtained the solution of the problem of diffraction by a strip due to an incident plane wave using the separable coordinate systems. The result is obtained in terms of infinite series of Mathieu Functions. The summary of their work is given below.

Let a perfectly conducting elliptic cylinder be considered with its axis parallel to the electric vector E_{inc} of an incident plane wave whose direction of propagation makes an angle α with the major axis of the ellipse. In all discussions the time factor $e^{i\omega t}$ will not be written but understood.

Let the distance between the two focii of the ellipse be 2h. Using an elliptic cylindrical system of coordinates, we have,

$$x = h \cosh \xi \cos \eta, \quad y = h \sinh \xi \sin \eta \quad \text{and} \quad z = z$$

and the diffracting ellipse is defined by ξ_o. The wave equation

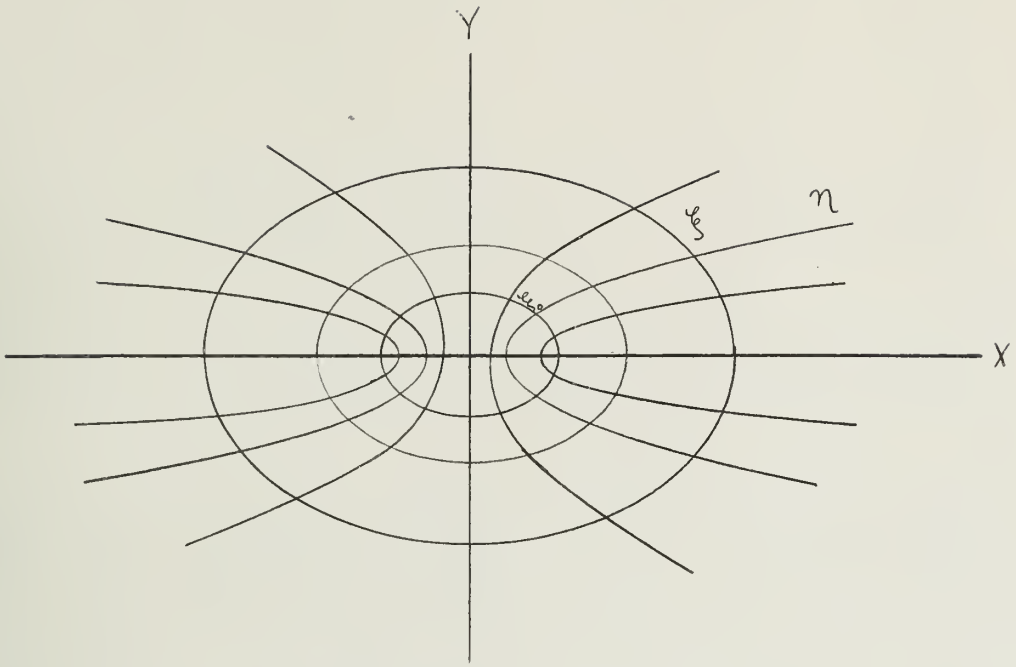

FIGURE 3

expressed in an elliptic cylindrical coordinate system is given by

$$\frac{\partial^2 E}{\partial \xi^2} + \frac{\partial^2 E}{\partial \eta^2} + \tfrac{1}{2} k^2 h^2 (\cosh 2\xi - \cos 2\eta)\, E = 0 \qquad (4.1)$$

Assuming a solution of the above in the form $\phi(\xi)\psi(\eta)$, (4.1) is reduced to

$$\frac{\partial^2 \phi}{\partial^2 \xi} + (s \cosh^2 \xi - b)\, \phi = 0 \qquad (4.2)$$

and

$$\frac{\xi^2 \psi}{\partial \eta^2} + (b - s \cos^2 \eta)\, \psi = 0 \qquad (4.3)$$

where b is the separation constant and $s = k^2h^2$. The solutions of (4.2) and (4.3) are given by

$$\text{and} \begin{cases} Se_r(s,ix) = \sum_{k=0}^{\infty} De_{2k+p}^{(r)} \cosh (2k+p)x & \text{(even solution)} \\ So_r(s,ix) = i \sum_{k=0}^{\infty} Do_{2k+p}^{(r)} \sinh (2k+p)n & \text{(odd solution)} \end{cases} \tag{4.4}$$

$$\begin{cases} Se_r(s,x) = \sum_{k=0}^{\infty} De_{2k+p}^{(r)} \cos (2k+p)x & \text{(even solution)} \\ So_r(s,x) = \sum_{k=0}^{\infty} Do_{2k+p}^{(r)} \sin (2k+p)n & \text{(odd solution)} \end{cases} \tag{4.5}$$

where $p = 0$ if r is even and $p = 1$ if r is odd.

and

$$Se_r(s,0) = 1 \quad \text{i.e.} \quad \sum_{k=0}^{\infty} De_{2k+p} = 1$$

using the boundary condition i.e. E_{tan} on the surface of the diffracting ellipse ξ_o must vanish, Morse and Rubenstien obtained the diffracted field given by

$$\frac{E_{Diff}}{E_{inc}} = -\sqrt{2\pi}\sum_{n=0}^{\infty}\left\{\frac{1}{N_{2n}}\frac{Je_{2n}(\xi_o)}{He^{(2)}_{2n}(\xi_o)}\cdot He^{(2)}_{2n}(\xi)\cdot Se_{2n}(\eta)Se_{2n}(\alpha)\right.$$

$$+\frac{1}{N'_{2n+2}}\frac{Jo_{2n+2}(\xi_o)}{Ho^{(2)}_{2n}(\xi_o)}Ho^{(2)}_{2n}(\xi)\ So_{2n+2}(\eta)\ So_{2n+2}(\alpha)$$

$$+j\left[\frac{1}{N_{2n+1}}\frac{Je_{2n+1}(\xi_o)}{He^{(2)}_{2n+1}(\xi_o)}He^{(2)}_{2n+1}(\xi)\ Se_{2n+1}(\eta)\ Se_{2n+1}(\alpha)\right. \tag{4.6}$$

$$\left.\left.+\frac{1}{N'_{n+1}}\frac{Jo_{2n+1}(\xi_o)}{Ho^{(2)}_{2n+1}(\xi_o)}Ho^{(2)}_{2n+1}(\xi)\ So_{2n+1}(\eta)\ So_{2n+1}(\alpha)\right]\right\}$$

where E_{Diff} is the diffracted field at any point $P(\xi,\eta)$ and E_{inc} is the incident field. When $\xi_o = 0$, the elliptic cylinder degenerates into a strip of width 2h and Equation (4.6) gives the scattered field due to a strip.

By using the relations $\text{curl}\ \bar{E} = -B$ and $I = \hat{n} \times \bar{H}$ where $\hat{n}$ is the outward normal unit vector to the strip, the current density at any point on the surface of the strip is found to be[21]

$$I = \frac{4E_{z_{inc}}}{|\omega\mu h \sin\eta|}\sqrt{\frac{\pi}{2}}\left\{\sum_{n=0}^{\infty}\frac{Se_{2n}(\eta)\ Se_{2n}(\alpha)}{N_{2n}\ He^{(2)}_{2n}(0)}+j\frac{Se_{2n+1}(\eta)\ Se_{2n+1}(\alpha)}{N_{2n+1}\ He^{(2)}_{2n+1}(0)}\right. \tag{4.7}$$

$$\left.+\sum_{n=0}^{\infty}\left[\frac{So_{2n+2}(\eta)\ So_{2n+2}(\alpha)}{N'_{2n+2}\ Ho^{(2)}_{2n+2}(o)}+j\frac{So_{2n+1}(\eta)\ So_{2n+1}(\alpha)}{N'_{2n+1}\ Ho^{(2)}_{2n+1}(o)}\right]\right\}$$

If the incident field instead of being plane is that due to a

filament parallel to the z axis with strength I_o located at a point $S(\xi_o,\eta_o)$, it can be shown that the Hertz potential at any point $P(\xi,\eta)$ is given by

$$\pi_z = \frac{I_o}{-i\omega\epsilon} \sum_{n=0}^{\infty} \left[\frac{He_n^{(2)}(\xi_o)\, ze_n(\xi)\, Se_n(\eta)\, Se_n(\eta_o)}{N_n\, He_n^{(2)}(o)} + \frac{Ho_n^{(2)}(\xi_o)}{N_n'\, Ho_n^{(2)}(o)}\, zo_n(\xi)\, So_n(\eta)\, So_n(\eta_o) \right] \tag{4.8}$$

for the region defined by $0 \leq \xi \leq \xi_o$. For the region defined by $\xi > \xi_o$ interchange ξ and ξ_o in Equation (4.8).

Further

$$ze_n(u) = Ne_n(u_1)\, Je_n(u) - Je_n(u_1)\, Ne_n(u) \tag{4.9}$$

$$zo_n(u) = No_n(u_1)\, Jo_n(u) - Jo_n(u_1)\, No_n(u) \tag{4.10}$$

$$Je_n(u) = \sqrt{\frac{\pi}{2(De_o)^2}} \sum_{r=0}^{\infty} (-1)^{r-\frac{n}{2}}\, De_{2r}\, J_r\left(\frac{khe^{-u}}{2}\right) \tag{4.11}$$

if n is even

$$Je_n(u) = \sqrt{\frac{\pi}{2(De_1)^2}} \sum_{r=0}^{\infty} (-1)^{r-\frac{n-1}{2}}\, De_{2r+1} \left[J_r\left(\frac{khe^{-u}}{2}\right) J_{r+1}\left(\frac{khe^{u}}{2}\right) + J_{r+1}\left(\frac{khe^{-u}}{2}\right) J_r\left(\frac{khe^{u}}{2}\right) \right] \tag{4.12}$$

if n is odd

$$Ne_n(u) = \sqrt{\frac{\pi}{2(De_o)^2}} \sum_{r=o}^{\infty} (-1)^{r-\frac{n}{2}} De_{2r} Y_r\left(\frac{khe^{u}}{2}\right) J_r\left(\frac{khe^{-u}}{2}\right) \qquad \text{if n is even}$$

$$= \sqrt{\frac{\pi}{2(De_1)^2}} \sum_{r=o}^{\infty} (-1)^{r-\frac{n-1}{2}} De_{2r+1}\left[J_r\left(\frac{khe^{-u}}{2}\right) Y_{r+1}\left(\frac{khe^{u}}{2}\right) + J_{r+1}\left(\frac{khe^{-u}}{2}\right) Y_r\left(\frac{khe^{u}}{2}\right) \right]$$

$$\text{if n is odd} \qquad (4.13)$$

$$Jo_n(u) = \sqrt{\frac{\pi}{2(Do_z)^2}} \sum_{r=1}^{\infty} (-1)^{r-\frac{n}{2}} Do_r\left[J_{r-1}\left(\frac{khe^{-u}}{2}\right) J_{r+1}\left(\frac{khe^{u}}{2}\right) - J_{r+1}\left(\frac{khe^{-u}}{2}\right) J_{r-1}\left(\frac{khe^{u}}{2}\right) \right]$$

$$\text{if n is even}$$

$$= \sqrt{\frac{\pi}{2(Do_1)^2}} \sum_{r=o}^{\infty} (-1)^{r-\frac{n-1}{2}} Do_{2r+1}\left[J_r\left(\frac{khe^{-u}}{2}\right) J_{r+1}\left(\frac{khe^{u}}{2}\right) - J_{r+1}\left(\frac{khe^{-u}}{2}\right) J_r\left(\frac{khe^{u}}{2}\right) \right]$$

$$\text{if n is odd} \qquad (4.14)$$

$$No_n = \sqrt{\frac{\pi}{2(D_o)^2}} \sum_{r=o}^{\infty} (-1)^{r-\frac{n}{2}} Do_{2r}\left[J_{r-1}\left(\frac{khe^{-u}}{2}\right) Y_{r+1}\left(\frac{khe^{u}}{2}\right) - J_{r+1}\left(\frac{khe^{-u}}{2}\right) Y_r\left(\frac{khe^{u}}{2}\right) \right]$$

$$\text{if n is even}$$

$$= \sqrt{\frac{\pi}{2(D_1)^2}} \sum_{r=o}^{\infty} (-1)^{r-\frac{n-1}{2}} Do_{2r+1}\left[J_r\left(\frac{khe^{-u}}{2}\right) Y_{r+1}\left(\frac{khe^{u}}{2}\right) - J_{r+1}\left(\frac{khe^{-u}}{2}\right) Y_r\left(\frac{khe^{u}}{2}\right) \right]$$

$$\text{if n is odd} \qquad (4.15)$$

$$He_n^{(2)}(u) = Je_n(u) - i\, Ne_n(u) \qquad (4.16)$$

$$Ho_n^{(2)}(u) = Jo_n(u) - i\, No_n(u) \qquad (4.17)$$

$$N_n = \pi\left[2\,(De_o)^2 + (De_2)^2 + \ldots \right] \qquad \text{if n is even}$$

$$= \pi \sum_{r=o}^{\infty} (De_{2r+1})^2 \qquad \text{if n is odd.} \qquad (4.18)$$

From Equation (4.8) and (4.9) the current induced on the surface of the strip can be obtained as

$$I = -I_o \sum_{n=o}^{\infty} \frac{He_n^{(2)}(\xi_o)Se_n(\eta)Se_n(\eta_o)}{N_n He_n^{(2)}(o)} - \frac{Ho_\eta^{(2)}(\xi_o)Se_n(\eta)So_n(\eta)}{N_n' Ho_n^{(2)}(o)} \qquad (4.19)$$

4.2 Integral Equation Method

Schwarzchild[30] solved the diffraction problem due to a slit in a plane infinite screen which is complementary to a strip. His results, obtained in a different way by Baker and Copson[2], are indicated below.

Let the screen and slit occupy the plane $x = 0$ in rectangular cartesian coordinates. The edges of the slit of width 2h coincide with lines $x = 0$, $y = 0$ and $x = 0$, $y = -2h$. Let the incident electric vector E_{inc} be polarized parallel to the z axis and the normal to the wave front, i,e. direction of propagation make an angle α with the positive x-axis. Then H_y is the only nonvanishing component of the magnetic field tangential to the screen and a current of density $I_z(y,\alpha)$ flows on the screen in the direction of the z axis. The total E field at any point (x_o, y_o) is then given by

$$E_z(x_o,y_o) = e^{ik(x_o \cos\alpha + y_o \sin\alpha)} - \frac{kz_o}{4}\left\{\int_{-\infty}^{-2h} + \int_{o}^{\infty}\right\} I_{z(y,\alpha)} H_o^{(2)}(kr)dy \qquad (4.20)$$

where

$$r = \sqrt{x_o^2 + (y-y_o)^2} \qquad \text{and} \qquad z_o = \sqrt{\frac{\mu}{\epsilon}}$$

When the boundary condition, i,e. $E_z(x_o, y_o)$ is zero at all points on the

screen, is applied the following integral equation is obtained.

$$\left\{\int_{-\infty}^{-2h} + \int_{o}^{\infty}\right\} I_z(y,\alpha)\, H_o^{(2)}(k|y-y_o|)dy = \frac{4e^{-iky_o \sin\alpha}}{kz_o} \qquad (4.21)$$

for $y_o > 0$ and $y_o < -2h$.

Using Fox's Formula[7] and changing the variables, Equation (4.21) can be transformed into a pair of simultaneous integral equations of Wiener-Hopf type having solutions given by

$$\frac{z_o}{4} I_z(y,\alpha) = \psi(y,\alpha) - \frac{1}{\pi}\int_o^\infty \frac{z_o}{4} I_z(-y-2h,\alpha)\; e^{\frac{-ik(y+z+2h)}{z+y+2h}} \sqrt{\frac{z+2h}{y}}\, dz$$

and (4.22)

$$\frac{z_o}{4} I_z(-y-2h,\alpha) = e^{-i2kh \sin\alpha}\psi(y,-\alpha) - \frac{1}{\pi}\int_o^\infty \frac{z_o}{4} I_z(y,\alpha)\, \frac{e^{-ik(y+z+2h)}}{y+z+2h}\sqrt{\left(\frac{z+2h}{y}\right)}dz$$

where

$$\psi(y,\alpha) = \frac{\cos\alpha}{2} e^{iky \sin\alpha} - \frac{e^{i\frac{\pi}{4}}}{\sqrt{\pi}} \cos\alpha\, e^{iky \sin\alpha} F[\sqrt{2ky}\, \sin(\frac{\pi}{4} + \frac{\alpha}{2})]$$
$$+ \frac{e^{-i\frac{\pi}{4}}}{\sqrt{2\pi}} \frac{e^{-iky}}{\sqrt{ky}} \sin(\frac{\pi}{4} - \frac{\alpha}{2}) \qquad (4.23)$$

where F(u) is the Fresnel integral.

Equations (4.22) are exact and can be solved by successive approximations which yield a solution of the form

$$I_z(y,\alpha) = \sum_{n=0}^{\infty} I_{n_z}(y,\alpha) \qquad (4.24)$$

where

$$I_{n_z}(y,\alpha) = -\frac{1}{\pi}\int_0^\infty I_{n-1_z}(z,\alpha)\,\frac{e^{-ik(y+z+2h)}}{y+z+2h}\,\sqrt{\frac{z+2h}{y}}\,dz \quad \text{for } n \geq 1 \tag{4.25}$$

and

$$I_o(y,\alpha) = \psi(y,\alpha).$$

The series represented by Equation (4.24) has been proved by Schwarzchild[30] to be uniformly and absolutely convergent for all values of h greater than zero if k is real.

Schwarzchild evaluated the first term of the series of Equation (4.24) which physically corresponds to considering Sommerfeld's formula[29] for two half planes considered separately for the slit and neglecting the diffraction by each half plane of the field scattered by the other. Solutions of the same problem in series form in increasing power of the ratio of slit width to wavelength have been obtained by Sommerfeld,[29] and Bouwkamp. These solutions are particularly effective when the slit is relatively narrow.

The results obtainable from the solution in Mathieu functions have their use restricted to the availability of appropriate Mathieu function tables. Further these functions converge very slowly for large arguments. Thus when the strip width is small conpared to wavelength the Mathieu function solutions are very useful. The same is true for Sommerfeld's method in which the rate of convergence of the series depends on the narrowness of the strip or slit.

The integral equation method employed by Schwarzchild[30] on the other hand is good for very wide strips in which case the convergence is extremely fast. In fact with strips or slits, large compared to wavelength, even the first term of the series as obtained by Schwarzchild corresponding to the first order approximation gives very satisfactory results.

For slits and strips not large compared to the wavelength, Karp and Russek[13] and Millar[19] have obtained approximate solutions. Their solutions are very suitable when the width of the slit is neither narrow enough for Sommerfeld's series solution nor wide enough to use the first term of Schwarzchild's series solution.

4.2.1 Approximate Solution by Karp and Russek[13]

The solution obtained by Karp and Russek has, as the first term, the term calculated by Schwarzchild from the exact series solution and a correction term which accounts for the interaction between the two edges of the half planes forming the slit. The effect of the mutual interaction between the two edges are accounted for by lumping these effects in the form of two fictitious filament sources at the two edges of the slit and then determining the strength of these two filaments.

The effectiveness of the solution arises from the fact that the strength of the fictitious line sources at the edges of the slit which are used for representing the effect of diffraction due to the half planes can be obtained in terms of simple trigonometric functions and Fresnel integrals.

4.2.2 Asymptotic Solution by Millar[19]

H. F. Millar obtained an asymptotic representation for each term of the series solution of the integral equations given by Equation (4.22) in terms of the inverse powers of kh. He has shown that each term of the series of Equation (4.24) gives rise to an asymptotic expansion whose leading term is of the order $(2kh)^{-\frac{1}{2}}$ compared to that of the preceding term. The asymptotic expansion of the series solution to any finite order in inverse powers of (2kh) can therefore be obtained by considering a finite number of terms of the series.

Millar has calculated a few higher order terms of the asymptotic expansion. The calculation becomes very involved as the order of term is larger. He has calculated the tramsmission coefficients taking different number of terms of the asymptotic series and comparing them to those obtained by Skavlem.[31] A study of this table reveals that for some moderate values of 2kb (e g. 10 i.e. of width of about 1.6λ) the best result is obtained when only the first term of the expansion is considered. It, therefore, seems reasonable to expect a satisfactory result even if only the first term of the series solution is used for widths larger or equal to one wavelength.

4.2.3 Approximation by Moullin[21]

Moullin and Phillips have computed the current distribution on strips of different widths for incident plane waves at different angles from the Mathieu function solution given by Equation (4.7) and compared numerically to that near the edge of a half plane, for the same incident plane wave. They found that the difference between the two becomes very

small for strips over $\lambda/2$ wide. Therefore they concluded that the current distribution near the edge of a strip is sensibly independent of the presence of the other edge i.e. the coupling between the edges is very small if the strip is at least one half wavelength wide. Hence they approximated the current distribution over an isolated strip by that which would appear if the strip were a part of an infinite plane with two filament sources located at the two edges of the strip. Moullin[22] also reached the same conclusion for a cylindrical wave diffracted by a strip.

5. APPROXIMATION USED FOR THE SOLUTION OF THE DIFFRACTION PROBLEM OF A ZONED MIRROR

It has already been shown that the density of current induced on the surface of a ribbon due to a plane wave incident at an angle α with the E vector parallel to the edge of the ribbon, in elliptic cylindrical coordinates defined by ξ and η is given exactly by

$$I(\eta) = 4\sqrt{\frac{\pi}{2}}\,\frac{E_{inc}}{|\omega\mu h \sin\eta|}\sum_{n=o}^{\infty}\frac{Se_{2n}(\eta)Se_{2n}(\alpha)}{N_{2n}He^{(2)}_{2n}(o)} + j\,\frac{Se_{2n+1}(\eta)\,Se_{2n+1}(\alpha)}{N_{2n+1}He^{(2)}_{2n+1}(o)} \tag{5.1}$$

$$+\sum_{n=o}^{\infty}\frac{Se_{2n+2}(\eta)So_{2n+2}(\alpha)}{N'_{2n+2}Ho^{(2)}_{2n+2}(o)} + j\,\frac{So_{2n+1}(\eta)So_{2n+1}(\alpha)}{N'_{2n+1}Ho^{(2)}_{2n+1}(o)}$$

$S = k^2h^2$, 2h being the width of the ribbon and η determining the location of a point on the ribbon.

In order to determine $I(\eta)$, the Mathieu functions Se_n, He_n and the constants N_n have to be computed for each of the ribbon widths 2h. This can be easily accomplished when s i.e. k^2h^2 is small, since the Fourier expansion of the Mathieu function series converge rapidly under that condition. However when s is large, (corresponding to a strip a few wavelengths wide) as is the case for some strips in the present problem, the usefulness of the Mathieu function series is lost because the convergence of the series is extremely slow. The other difficulties involved in the computation of this function with large s have been discussed in the appendix. It has been shown there that the computation of current density across the surface of a wide ribbon using Mathieu function solution

Equation (5.1) is not only involved and impractical, the accuracy obtainable is not the same for all values of η and, in fact, it is quite low when η approaches $\pi/2$.

On the other hand a physical argument indicates that as the strip becomes very wide, the solution for each half of the strip should approach that of a half plane which is readily obtainable in terms of Fresnel Integrals.

Millar, Karp and Russek, and Moullin and Phillips in one way or another obtained solutions along this approach. They extablished their theory by demonstrating numerically the small difference between the approximate and exact solutions for a certain set of parameters for which the latter is available, without going into a general treatment of the error involved in the approximation. In fact the first order term of the solution obtained by all of them is the same as that obtained by Schwarzchild which is sufficiently accurate for strips of the order of a wavelength wide.

5.1 Approximation for the Current Distribution across an Isolated Strip Due to an Incident Plane Wave

As discussed in the last section, for a strip of width no less than a wavelength, the first order Schwarzchild's solution, namely the Sommerfeld's half plane solution furnishes a satisfactory answer to the problem. The current distribution across a strip can therefore, for the present purpose, be approximated in the following way.

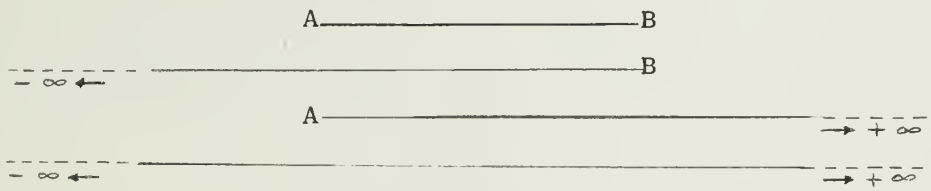

FIGURE 4

Let the strip AB have a current distribution across its surface given by I (Figure 4). We then assume

$$I = \begin{cases} I_{h_A} + I_{h_B} - I_\infty & \text{on the strip} \\ = 0 & \text{outside the strip} \end{cases}$$

where I_{h_A} is the current distribution across a half plane extending from A to ∞.

I_{h_B} is that current distribution across a half plane extended from B to $-\infty$ and I_∞ is the current distribution across an infinite plane.

All these current distributions I_{h_A}, I_{h_B} and I_∞ are known exactly in terms of Fresnel Integrals and simple functions. Thus I can be easily computed if this approximation is used. With this approximation it is noted that current across the half plane with edge at B and that across the infinite plane are nearly equal at points far off from the edge B. Hence if AB is large, the current distribution near the edge A of the strip will approximately be that due to the half plane with its edge at A. The same is also true near the edge B of the strip AB. While at the middle of the strip, since $I_{h_A} \approx I_{h_B} \approx I_\infty$, the current is approximately I_∞. This agrees closely with the conclusions of Moullin and Phillips.

The error involved in the above approximation with regard to matching the boundary condition at the surface of the strip has been calculated and found to be very small. Further the computation from the asymptotic expansions of the exact solution as discussed in the appendix are both involved and inaccurate. Thus the above approximation probably does not yield results inferior to that one could obtain from the exact solution

by asymptotic expansion.

Evaluation of I_{h_A}

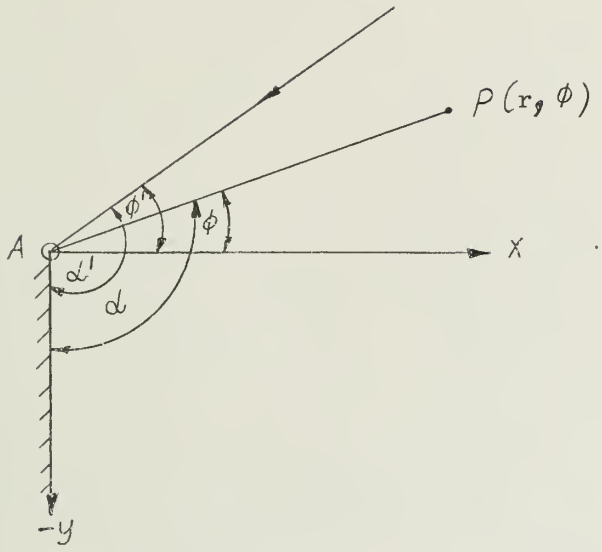

FIGURE 5

Consider an incident plane wave given by $E_z = e^{ikr \cos(\phi-\phi')} = u_o(r,\phi;\phi')$ with its E vector parallel to the edge of the half plane defined by the lower half of y-z plane. r,ϕ are the coordinates of the point of observation P, and ϕ' is the direction of the incident wave, all measured from the origin A as shown in Figure 5. The total E field is given by Sommerfeld's half plane solution viz

$$E_z(r,\phi;\phi') = u(r,\phi;\phi') - u(r,\phi;3\pi-\phi) \tag{5.3}$$

where

$$u = \frac{e^{i\frac{\pi}{4}}}{\sqrt{\pi}} u_o(r,\phi;\phi') \int_{-\infty}^{T} e^{-i\lambda 2} d\lambda \qquad \text{and} \qquad T = \sqrt{2kr} \cos\frac{\phi-\phi'}{2} \tag{5.4}$$

Therefore

$$E_z = \frac{e^{i\frac{\pi}{4}}}{\sqrt{\pi}} \left[e^{ikr\cos(\phi-\phi')} \int_{-\infty}^{\sqrt{2kr}\cos\frac{\phi-\phi'}{2}} e^{-i\lambda^2} d\lambda - e^{ikr\cos(\phi-3\pi+\phi')} \int_{-\infty}^{\sqrt{2kr}\cos\frac{\phi-3\pi+\phi'}{2}} e^{-i\lambda^2} d\lambda \right] \quad (5.5)$$

If the angles are measured from the half plane, then

$$\alpha = \frac{\pi}{2} + \phi \qquad \text{and} \qquad \alpha' = \frac{\pi}{2} + \phi'$$

and

$$E_z = \frac{e^{i\frac{\pi}{4}}}{\sqrt{\pi}} \left[e^{ikr\cos(\alpha-\alpha')} \int_{-\infty}^{\sqrt{2kr}\cos\frac{\alpha-\alpha'}{2}} e^{-i\lambda^2} d\lambda - e^{ikr\cos(\alpha+\alpha')} \int_{-\infty}^{\sqrt{2kr}\cos\frac{\alpha+\alpha'}{2}} e^{-i\lambda^2} d\lambda \right] \quad (5.6)$$

Using the relation $\bar{H} = -\frac{1}{i\omega\mu} \operatorname{curl} \bar{E}$, the magnetic field is obtained. On the surface of the strip, the surface current density induced due to the incident electromagnetic wave is given by the discontinuity of the magnetic field i.e.

$$i = \hat{x} \times \left[H_{tan}\Big|_{\alpha=0} - H_{tan}\Big|_{\alpha=2\pi} \right]$$

$$H_{tan} = \hat{y} \frac{1}{i\omega\mu} \frac{\partial E_z}{\partial x}$$

$$\therefore I_{h_A} = \hat{x}\times\hat{y} \frac{1}{i\omega\mu} \left[\frac{\partial E_z}{\partial x}\Big|_{\alpha=0} - \frac{\partial E_z}{\partial x}\Big|_{\alpha=2\pi} \right]$$

from (5.5)

$$\frac{\partial E_z}{\partial x} = -\frac{e^{i\frac{\pi}{4}}}{\sqrt{\pi}}\frac{1}{r}\left[\sqrt{\frac{kr}{2}}\left(\sin\frac{\alpha-\alpha'}{2} - \sin\frac{\alpha+\alpha'}{2}\right)e^{-ikr}\right.$$

$$\left. + ikr\left\{e^{ikr\cos(\alpha-\alpha')}\sin(\alpha-\alpha')\int_{-\infty}^{T_1} e^{-i\lambda 2}d\lambda - e^{-ikr\cos(\alpha+\alpha')}\sin(\alpha+\alpha')\int_{-\infty}^{T_2} e^{-i\lambda 2}d\lambda\right\}\right]$$

where

$$T_1 = \sqrt{2kr}\cos\frac{\alpha-\alpha'}{2} \qquad \text{and} \qquad T_2 = \sqrt{2kr}\cos\frac{\alpha+\alpha'}{2}$$

It therefore follows that

$$I_{h_A} = \frac{2e^{i\frac{\pi}{4}}}{\sqrt{\pi}\omega\mu}\left\{k\sin\alpha' e^{ikr\cos\alpha'}\int_{-\sqrt{2kr}\cos\frac{\alpha'}{2}}^{\sqrt{2kr}\cos\frac{\alpha'}{2}} e^{-i\lambda 2}d\lambda - i\sqrt{\frac{2k}{r}}\sin\frac{\alpha'}{2}e^{-ikr}\right\}\hat{x}\times\hat{y} \tag{5.7}$$

$I_{hA'}$ which flows parallel to the edge of the half plane has its phase referred to A. Now consider

$$\int_{-\sqrt{2kr}\cos\frac{\alpha'}{2}}^{\sqrt{2kr}\cos\frac{\alpha'}{2}} e^{-i\lambda 2}d\lambda = 2\int_{o}^{\sqrt{2kr}\cos\frac{\alpha'}{2}} e^{-i\lambda 2}d\lambda$$

Substituting $\lambda^2 = \frac{\pi}{2}t^2$ we get

$$\int_{o}^{\sqrt{2kr}\cos\frac{\alpha'}{2}} e^{-i\lambda^2}d\lambda = \sqrt{\frac{\pi}{2}}\int_{o}^{2\sqrt{\frac{kr}{\pi}}\cos\frac{\alpha'}{2}} e^{-i\frac{\pi}{2}t^2}dt = \sqrt{\frac{\pi}{2}}\left[C_A - iS_A\right]$$

where

$$C_A = \int_o^u \cos \frac{\pi}{2} t^2 dt \qquad \text{and} \qquad S_A = \int_o^u \sin \frac{\pi}{2} t^2 dt$$

and

$$u = 2 \sqrt{\frac{kr}{\pi}} \cos \frac{\alpha'}{2}$$

Using the above we get

$$I_{h_A} = \frac{2}{\eta}\Big[\sin \alpha' \Big\{(C_A+S_A)\cos(kr \cos \alpha')-(C_A-S_A)\sin(kr \cos \alpha')\Big\} + \frac{1}{\sqrt{\pi kr}} \sin \frac{\alpha'}{2}$$

$$(\cos kr - \sin kr)\Big]$$

$$+ \frac{2i}{\eta}\Big[\sin \alpha' \Big\{(C_A+S_A)\sin(kr \cos \alpha')+(C_A-S_A)\cos(kr \cos \alpha')\Big\} - \frac{1}{\sqrt{\pi kr}} \sin \frac{\alpha'}{2}$$

$$(\cos kr + \sin kr)\Big] \qquad (5.8)$$

I_{h_B} is obtained by substituting $(\pi-\alpha')$ for α' and r' for r in Equation (5.8), since $(r', \pi-\alpha)$ is the observation point referred to B. Thus

$$I_{h_B} = \frac{2}{\eta}\Big[\sin \alpha' \Big\{(C_B+S_B)\cos(kr' \cos \alpha')+(C_B-S_B)\sin(kr \cos \alpha')\Big\} + \frac{1}{\sqrt{\pi kr}} \frac{\cos \alpha'}{2}$$

$$(\cos kr' - \sin kr')\Big]$$

$$+ \frac{2i}{\eta}\Big[\sin \alpha' \ (C_B-S_A) \cos(kr' \cos \alpha)-(C_B+S_B)\sin(kr' \cos \alpha') \ - \frac{1}{\sqrt{\pi kr}} \cos \frac{\alpha'}{2}$$

$$(\sin kr' + \cos kr')\Big] \qquad (5.9)$$

where

$$C_B = \int_o^V \cos \frac{\pi}{2} t^2 \, dt, \quad S_B = \int_o^V \sin \frac{\pi}{2} t^2 \, dt \text{ and } V = 2 \sqrt{\frac{kr}{\pi}} \sin \frac{\alpha'}{2}$$

The phase of I_{h_B} is referred to the point B. I_∞ can be calculated in a similar way. It turns out that

$$I_\infty = \frac{2k}{\omega\mu} \sin \alpha' e^{ikr \cos \alpha} \tag{5.10}$$

where r is the distance of the point of observation from the edge A and the phase of I_∞ is referred to A. Thus it has been possible to evaluate in terms of Fresnel Integrals and simple trigonometric functions, $I(=I_{h_A} + I_{h_B} - I_\infty)$, the current distribution at any point on the surface of a strip due to a plane wave, incident at an angle $\frac{\pi}{2} - \alpha'$. This expression does not take into account the proximity of other strips. Thus the current I is what has been called I_{ii}, the self induced current of the strip i, previously.

5.2 Evaluation of the Mutually Induced Current

The effect of the incident wave on an assembly of strips is to induce a self current in each of the strips. The proximity of the strips will influence the current distribution on the other strips, i.e. there will be a current induced in each strip due to the scattered field of other strips, which may be called "mutually induced current." Thus the resultant current distribution in each strip is the sum of the "self" and "mutual" currents.

The mutually induced current can be found by successive iteration as discussed previously. In order to evaluate the "mutual" current on any strip due to another strip in its neighborhood consider a strip AB and a filament source of strength I located at S. The current induced on AB due to the source at S can be evaluated exactly in terms of infinite

summation of products of Mathieu functions as given by Equation (4.19) of the previous chapter. However the limitation of this solution discussed there applies to this case as well. We, therefore, seek an approximate solution suitable for numerical computation. Following the case of "self current," the current distribution across AB can also be approximated by the sum of the current distributions on the two half planes with edges at A and B less by the current distribution on a doubly infinite plane each under the influence of the filament source at S, as before.

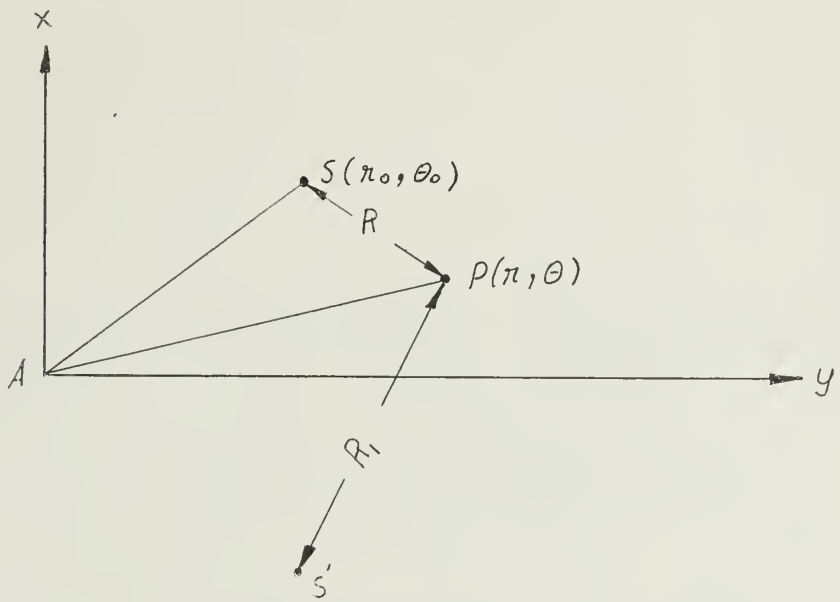

FIGURE 6

The part due to infinite plane can be obtained simply by the image method. The part due to the half plane can be obtained in two alternative forms: the series solution involving Bessel functions and the integral expression. Now consider the second form first. We know that the field at any point P due to a source of strength I at S in presence of a half

plane with edge at A (Figure 6) is given by[18]

$$E_z = \frac{i\omega\mu I}{4\pi}\left\{\int_{-\infty}^{\xi_0} e^{-ikR\cosh\xi}\,d\xi - \int_{-\infty}^{\xi_1} e^{-ikR_1\cosh\xi}\,d\xi\right\} \qquad (5.11)$$

where

$$\begin{cases} \sinh\xi_0 = 2\dfrac{\sqrt{rr_o}}{R}\cos\dfrac{\theta-\theta_o}{2} & \text{and} \qquad \sinh\xi_1 = 2\dfrac{\sqrt{rr_o}}{R_1}\cos\dfrac{\theta+\theta_1}{2} \\ R = \sqrt{r^2 + r_o^2 - 2rr_o\cos(\theta-\theta_o)} & \text{and} \quad R_1 = \sqrt{r^2 + r_o^2 - 2rr_o\cos(\theta+\theta_o)} \end{cases}$$

From the relation $-z\bar{H} = \text{curl}\ \bar{E}$ where $z = i\omega\mu$, the tangential component of the magnetic field due to E_z is

$$H_{tan} = \frac{i}{\omega\mu}\frac{\partial E_z}{r\partial\theta}$$

Now

$$\frac{\partial}{\partial\theta}\int_{-\infty}^{\xi_0} e^{-ikR\cosh\xi}\,d\xi = e^{-ikR\cosh\xi_0}\frac{d\xi_0}{d\theta} + \int_{-\infty}^{\xi_0}\frac{\partial}{\partial\theta}\left[e^{-ikR\cosh\xi}\right]d\xi$$

$$= -\sqrt{\frac{rr_o}{R^2}}\,(r+r_o)\sin\frac{\theta-\theta_o}{2}\,e^{-ik(r+r_o)}$$

$$-\frac{ikrr_o}{R}\sin(\theta-\theta_o)\int_{-\infty}^{\xi_o}\cosh\xi\; e^{ikR\cosh\xi}\,d\xi$$

$$\therefore H_{tan} = \frac{i}{\omega\mu r} \cdot \frac{\partial E_z}{\partial \theta}$$

$$= -\frac{I}{4\pi}\left[-\sqrt{\frac{r_o}{r}}\cdot \frac{(r+r_o)}{R^2} \sin\frac{\theta-\theta_o}{2}\, e^{-ik(r+r_o)} - \frac{ikr_0}{R}\sin(\theta-\theta_o) \int_{-\infty}^{\xi_0} \cosh\xi\, e^{-ikR\cosh\xi}\, d\xi \right.$$

$$\left. + \sqrt{\frac{r_o}{r}}\frac{(r+r_o)}{R_1^2}\sin\frac{\theta+\theta_o}{2}\, e^{-ik(r+r_o)} + \frac{ikr_o}{R_1}\sin(\theta+\theta_o) \int_{-\infty}^{\xi_1} \cosh\xi\, e^{-ikR_1\cosh\xi}\, d\xi \right]$$

Hence

$$H_{tan}\Big|_{\theta=0} = -\frac{I}{2\pi}\left[\sqrt{\frac{r_o}{r}}\frac{(r+r_o)}{R^2}\sin\frac{\theta_o}{2}\, e^{-ik(r+r_o)} - \frac{ikr_o}{R}\sin\theta_o \int_{-\infty}^{\frac{2\sqrt{rr_o}}{R}\cos\frac{\theta}{2}} e^{-ikR\sqrt{z^2+1}}\, dz \right]$$

and

$$H_{tan}\Big|_{\theta=2\pi} = \frac{I}{2\pi}\left[\sqrt{\frac{r_o}{r}}\frac{(r+r_o)}{R^2}\sin\frac{\theta_o}{2}\, e^{-ik(r+r_o)} - \frac{ikr_o}{R}\sin\theta_o \int_{-\infty}^{\frac{-2\sqrt{rr_o}}{R}\cos\frac{\theta}{2}} e^{-ikR\sqrt{z^2+1}}\, dz \right]$$

by change of variable $\sinh\xi = z$.

The density of the current induced on the surface of the half plane with edge A due to E_z is given by

$$I'_{h_A} = \hat{x} \times \left[H_{tan_o} - H_{tan_{2\pi}} \right]$$

$$I_{12} = \int_{CD} I' d\ell \tag{5.16}$$

where $d\ell$ is an elementary length of CD and I' is the Green's function for the induced current at a typical point on strip (1) due to the current at another typical point on strip (2) as given above.

The alternate form of the solution may be obtained for the induced current I'_{h_A} and I'_{h_B} by method of separable variables in cylindrical coordinates as discussed in Chapter 3. They are[23]

$$I_{h'_A} = \frac{I}{2r} (A+i\ C) \tag{5.17}$$

$$I_{h'_B} = \frac{I}{2r'} (A'+i\ C') \tag{5.18}$$

where

$$A = \sum_{n=0}^{\infty} (-1)^n (2n+1) Y_{n+\frac{1}{2}}(2\pi r) J_{n+\frac{1}{2}}(2\pi R) \cos \frac{2n+1}{2} \alpha_o \tag{5.19}$$

and

$$C = \sum_{n=0}^{\infty} (-1)^n (2n+1) J_{n+\frac{1}{2}}(2\pi r) J_{n+\frac{1}{2}}(2\pi R) \cos \frac{2n+1}{2} \alpha_o \tag{5.20}$$

where $\alpha_o = \pi - \theta_o$ when $R > r$ interchange r and R in A and C. Similarly for $I_{h'_B}$, A' and C' are obtained by replacing r, R by r' and R' respectively where r' and R' refer to B as the origin i.e. for the half plane extending from B to $-\infty$. With this formula, one of the double integrations required by the other method is avoided by taking summation instead. Either of the two will give the value of the "mutual current" correct to the first order.

5.3 Investigation of the Error Due to Assumed Current Distribution

From the discussion in the previous chapter it is clear that with the assumed current distribution across a strip the scattered field at any point will not be exactly the same as would be obtained from the exact current distribution. It is therefore necessary to estimate the change caused by the assumed distribution over the exact one so far as the scattered field is concerned. In order to estimate this we need to know the field produced by the exact current distribution which, in turn, implies that we must know the exact current distribution. However, in this section an expression has been obtained by which it is possible to estimate the effect of the assumed current distribution on the tangential E field over the surface of the strip. The total tangential E field on the surface of the strip with the exact current distribution must be zero. The total tangential E field on the surface of the strip with assumed current distribution will therefore provide an estimate of the closeness of the assumed current distribution to the exact one.

Let the exact current distribution at any point x' on the strip AB be given by $I_s(x')$. Then the field at any point $P(r,\theta)$ due to the current distribution $I_s(x')$ on the strip AB is given by

$$\frac{-k^2}{4\omega\epsilon} \int_{-h}^{h} I_s(x') H_o^{(2)}[k|r-x'|]dx' = E_z(r,\theta) \qquad (5.21)$$

When the point of observation P is on the surface of the strip AB, the the total tangential E field on the surface being zero, we have the integral equation for I_s given by

$$-\frac{k^2}{4\omega\epsilon}\int_{-h}^{h} I_s(x')\, H_o^{(2)}(k|x-x'|)\, dx' = -E_{inc}(x) \quad \text{for } -h \leq x \leq h. \qquad (5.22)$$

The assumed current distribution $I(x')$ will, in general, not satisfy the above integral equation. Suppose $I(x')$ satisfies a slightly different integral equation

$$-\frac{k^2}{4\omega\epsilon}\int_{-h}^{h} I(x')\, H_o^{(2)}(k|x-x'|)\, dx = -[E_{inc}(x) + \Delta E(x)]$$

$$\text{for } -h \leq x \leq h \qquad (5.23)$$

where $\Delta E(x)$ is the amount by which the right hand side of (5.23) differs from that of Equation (5.22). Combining Equations (5.22) and (5.23) we get

$$\frac{k^2}{4\omega\epsilon}\int_{-h}^{h} (I_s(x') - I(x'))\, H_o^{(2)}(k|x-x'|)\, dx = \Delta E.$$

Thus ΔE indicates the error committed in the boundary condition by taking the assumed current distribution $I(x')$ for the problem of the strip. Although $I_s(x')$, the exact current distribution is an unknown function, the left hand quantity can still be found due to the fact that $I(x')$ consists of half plane and whole plane solutions which satisfy certain equations.

As stated before $I_{h_A}(x')$, $I_{h_B}(x')$, and $I_\infty(x')$ are solutions of half plane and whole plane problems, and they satisfy the following equations.

$$-\frac{k^2}{4\omega\epsilon}\int_{-\infty}^{h} I_{h_B}(x')\, H_o^{(2)}[k|x-x'|]\, dx' = -E_{inc} \quad \text{for } -\infty \leq x \leq h \qquad (5.25)$$

$$-\frac{k^2}{4\omega\epsilon}\int_{-h}^{\infty} I_{h_A}(x')H_o^{(2)}[k|x-x'|]dx' = -E_{inc} \quad \text{for} \quad -h \le x \le \infty \tag{5.26}$$

and

$$-\frac{k^2}{4\omega\epsilon}\int_{-\infty}^{\infty} I_{\infty}(x')H_o^{(2)}[k|x-x'|]dx = -E_{inc} \quad \text{for} \quad -\infty \le x \le \infty \tag{5.27}$$

Thus from the above we obtain

$$-\frac{k^2}{4\omega\epsilon}\left[\int_{-\infty}^{h} I_{h_B}(x)H_o^{(2)}(k|x-x'|)dx' + \int_{-h}^{\infty} I_{h_A}(x')H_o^{(2)}(k|x-x'|)\,dx'\right.$$

$$\left. - \int_{-\infty}^{\infty} I_{\infty}(x')\,H_o^{(2)}(k|x-x'|)dx' = -E_{inc} \right] \quad \text{for} \quad -h \le x \le h. \tag{5.28}$$

Thus from Equation (5.24) and (5.28)

$$\frac{k^2}{4\omega\epsilon}\int_{-h}^{h}[I_s(x') - I(x')]\,H_o^{(2)}(k|x-x'|)dx = \Delta E_{(x)}$$

$$= \frac{k^2}{4\omega\epsilon}\left\{\int_{-\infty}^{-h}[I_{h_B}(x') - I_{\infty}(x')[H_o^{(2)}[k|x-x'|]dx'\right.$$

$$\left. + \int_{h}^{\infty}[I_{h_A}(x') - I_{\infty}(x')]H_o^{(2)}[k|x-x'|]dx'\right\} \tag{5.29}$$

$$\text{for } -h \le x \le h.$$

The above equation states that the contributions due to $I_{h_B}(x')$ for $x' \le h$, $I_{h_A}(x')$ for $h \le x' \le \infty$ and $I_{\infty}(x')$ for x', $-\infty \le x' \le \infty$ satisfy the boundary conditions of the problem exactly. It is interesting to note that then

$\triangle E$ i.e. the mismatch in the boundary condition is due to the fact that only parts of these current $I_{h_A}(x')$, $I_{h_B}(x')$ and $I_\infty(x')$ in the finite region AB have been taken into account for the approximate current distribution $I(x')$. Thus it is obvious that $\triangle E$ is the contribution of those parts of $I_{h_A}(x')$, $I_{h_B}(x')$ and $I_\infty(x')$ which have been excluded for approximating $I_s(x')$ as given by the Equation (5.29).

Since both $I_{h_A}(x')$ and $I_{h_B}(x')$ tend to $I_\infty(x')$ for x' sufficiently away from the edge, when the width of the strip is comparable to a wavelength, both $I_{h_A}(x') - I_\infty(x')$ and $I_{h_B}(x') - I_\infty(x')$ are very small within the range of integration as given by the right hand side of the Equation (5.29). It is therefore expected that $\triangle E$ will be a very small quantity especially when h is very large.

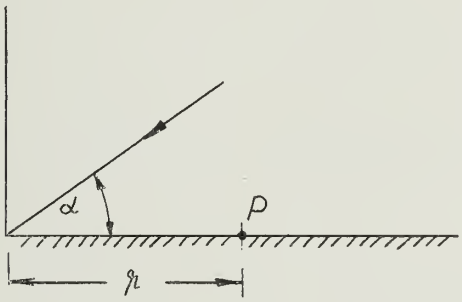

FIGURE 7

As discussed before I_{h_A} and I_{h_B} are of the form

$$I_{\text{half plane}} = \frac{2e^{j\frac{\pi}{4}}}{\omega\mu\sqrt{\pi}} \left[k \sin\alpha \, e^{ikr\cos\alpha} \int_{-\sqrt{2kr}\cos\frac{\alpha}{2}}^{\sqrt{2kr}\cos\frac{\alpha}{2}} e^{-\lambda^2} d\lambda - i\sqrt{\frac{2k}{\pi}}\sin\frac{\alpha}{2} e^{-ikr} \right. \tag{5.30}$$

When the angle $\alpha \neq \pi$ and $\sqrt{2kr}\cos\frac{\alpha}{2} >> 1$, $\int_{-\sqrt{2kr}\cos\frac{\alpha}{2}}^{\sqrt{2kr}\cos\frac{\alpha}{2}} e^{-i\lambda^2} d\lambda$ can

be expanded asymptotically as follows: Let $a = 2kr\cos\alpha/2$ and

$B = \sqrt{2/\pi}\,A$. Then

$$\int_{-A}^{A} e^{-i\lambda^2} d\lambda = \sqrt{\frac{\pi}{2}} \int_{-B}^{B} e^{-i\frac{\pi}{2}t^2} dt = \sqrt{2\pi} \int_{o}^{B} e^{-i\frac{\pi}{2}t^2} dt$$

Since Fresnel integrals are odd functions

$$= \sqrt{\frac{\pi}{2}} \left[(1-i) + i\frac{2}{\pi B} e^{-i\frac{\pi}{2}B^2} - 2\,\frac{e^{-i\frac{\pi}{2}B^2}}{\pi^2 B^3} + 0\left(\frac{1}{B^5}\right) \right]$$

$$= \sqrt{\frac{\pi}{2}} \left[(1-i) + e^{-i2kr\cos^2\frac{\alpha}{2}} \left(\frac{i}{\sqrt{2kr}\cos\frac{\alpha}{2}} - \frac{1}{4kr\cos^3\frac{\alpha}{2}\sqrt{\pi kr}} \right.\right.$$

$$\left.\left. + 0\left(\frac{1}{kr}\right)^{\frac{5}{2}} \right] \right.$$

Therefore

$$I_{\text{half plane}} \simeq \frac{2e^{i\frac{\pi}{4}}}{\omega\mu\sqrt{\pi}} \left[k\sin\alpha\sqrt{\frac{\pi}{2}}(1-i)e^{ikr\cos\alpha} + k\sin\alpha\sqrt{\frac{\pi}{2}}\,e^{-ikr} \right.$$

$$\left. \left(\frac{i}{\sqrt{\pi kr}\cos\frac{\alpha}{2}} - \frac{1}{4kr\cos^3\frac{\alpha}{2}\cdot\sqrt{\pi kr}} \right) - i\sqrt{\frac{2k}{r}}\sin\frac{\alpha}{2}\,e^{-ikr} \right]$$

$$= \frac{2k}{\omega\mu}\sin\alpha\, e^{ikr\cos\alpha} - \frac{e^{i\frac{\pi}{4}}}{\omega\mu} \frac{k\sin\frac{\alpha}{2}\,e^{-ikr}}{\sqrt{2\pi kr}\,kr\cos^2\frac{\alpha}{2}} + 0\left(\frac{1}{kr}\right)^{\frac{5}{2}} \tag{5.31}$$

The current induced on the surface of an infinite plane under the same

condition is given by

$$I_{\infty} = \frac{2}{\omega\mu} k\sin\alpha\, e^{ikr\cos\alpha}$$

Therefore

$$I_{half} - I_{\infty} = - \frac{e^{i\frac{\pi}{4}}}{\omega\mu} \frac{k \sin\frac{\alpha}{2}\, e^{-ikr}}{\sqrt{2\pi}\,(kr)^{\frac{3}{2}} \cos^2\frac{\alpha}{2}}$$

$$= - \frac{e^{i\frac{\pi}{4}}}{\sqrt{2\pi}\eta} \cdot \frac{\sin\frac{\alpha}{2}}{\cos^2\frac{\alpha}{2}} \frac{e^{-ikr}}{(kr)^{\frac{3}{2}}} \qquad \text{where } \eta = \sqrt{\frac{\mu}{\epsilon}} \tag{5.32}$$

Here it may be noted that the phase is referred to the edge of the half plane and that the magnitude is proportional to $(kr)^{3/2}$.

Since r is given by $(h-x')$ for $I_{h_B}(x')$ and by $(h+x')$ for $I_{h_A}(x')$, within the range of integration, r is always greater than 2h.

Hence the asymptotic expansion is justified for $I_{h_B}(x')$ if $\alpha \neq \pi$ and $\sqrt{4kh}\cos\alpha/2 >> 1$, and for $I_{h_A}(x')$ if $\alpha \neq 0$ and $\sqrt{4kh}\sin\alpha/2 >> 1$.

$$\begin{cases} I_{h_B}(x') - I_{\infty}(x') \simeq - \dfrac{e^{i\frac{\pi}{4}}}{\sqrt{2\pi}\eta} \dfrac{\sin\frac{\alpha}{2}}{\cos^2\frac{\alpha}{2}} \dfrac{e^{-ik(h-x')}}{[k(h-x')]^{3/2}}\, e^{ikh\cos\alpha} \\ I_{h_A}(x') - I_{\infty}(x') \simeq - \dfrac{e^{i\frac{\pi}{4}}}{\sqrt{2\pi}\eta} \dfrac{\cos\frac{\alpha}{2}}{\sin^2\frac{\alpha}{2}} \dfrac{e^{-ik(h+x')}}{[k(h+x')]^{3/2}}\, e^{-ikh\cos\alpha} \end{cases} \tag{5.33}$$

Therefore

$$\Delta E = - \frac{k^2}{4\omega\epsilon\eta} \frac{e^{i\frac{\pi}{4}}}{\sqrt{2\pi}} \left[\int_{-\infty}^{-h} \frac{\sin\frac{\alpha}{2}}{\cos^2\frac{\alpha}{2}} \frac{e^{-ik(h-x'-h\cos\alpha)}}{[k(h-x')]^{3/2}} H_o^{(2)}[k|x-x'|]dx \right.$$

$$\left. + \int_{h}^{\infty} \frac{\cos\frac{\alpha}{2}}{\sin^2\frac{\alpha}{2}} \frac{e^{-ik(h+x'+h\cos\alpha)}}{[k(h+x')]^{3/2}} H_o^{(2)}[k|x-x'|]dx' \right]$$

$$\Delta E = \frac{k^2}{4\omega\epsilon\eta} \cdot \frac{e^{i\frac{\pi}{4}}}{\sqrt{2\pi}} \left[\int_h^\infty \frac{\sin\frac{\alpha}{2}}{\cos^2\frac{\alpha}{2}} \frac{e^{-ik(h+x'-h\cos\alpha)}}{[k(h+x')]^{3/2}} H_o^{(2)}[k(x+x')]dx' \right.$$

$$\left. + \int_h^\infty \frac{\cos\frac{\alpha}{2}}{\sin^2\frac{\alpha}{2}} \frac{e^{-ik(h+x'+h\cos\alpha)}}{[k(h+x')]^{3/2}} H_o^{(2)}[k(x'-x)]dx \right] \qquad (5.34)$$

Using the integral representation of Hankel Function given by

$$H_o^{(2)}(x) = \frac{2}{\pi i} \int_1^\infty \frac{e^{-ixt}}{\sqrt{t^2-1}} dt$$

we obtain from Equation (5.34)

$$\Delta E = -\frac{k^2}{4\omega\epsilon\eta} \frac{e^{i\frac{\pi}{4}}}{\sqrt{2\pi}} \cdot \frac{2}{\pi i} \left[\frac{\sin\frac{\alpha}{2}}{\cos^2\frac{\alpha}{2}} \int_h^\infty \int_1^\infty \frac{e^{-ik(h+x'-h\cos\alpha) - ik(x+x')t}}{[k(h+x')]^{3/2}\sqrt{t^2-1}} dt\,dx \right.$$

$$\left. + \frac{\cos\frac{\alpha}{2}}{\sin^2\frac{\alpha}{2}} \int_h^\infty \int_1^\infty \frac{e^{-ik(h+x'+h\cos\alpha) - ik(x'-x)t}}{[k(h+x')]^{3/2}\sqrt{t^2-1}} dt\,dx' \right] \qquad (5.35)$$

Now consider

$$\int_h^\infty \int_1^\infty \frac{e^{-ik(h+x') - ik(x'\pm x)t}}{[k(h+x')]^{3/2}\sqrt{t^2-1}} dt\,dx'$$

$$= e^{-ikh} \int_1^\infty \frac{e^{\mp ikxt}}{\sqrt{t^2-1}} dt \int_h^\infty \frac{e^{-ik(1+t)x'}}{[k(h+x')]^{3/2}} dx'$$

by changing the order of integration.

But

$$\int_h^\infty \frac{e^{-ik(1+t)x'}}{[k(h+x')]^{3/2}}\,dx' \approx -\frac{2}{k}\,e^{-ikh(1+t)} \sum_{r=1}^{\infty} (i)^r \frac{\Gamma(r+\frac{1}{2})}{(1+t)^r (2kh)^{r+\frac{1}{2}}}$$

by integration by parts when $kh >> 1$.

$$\therefore \int_h^\infty \int_1^\infty \frac{e^{-ik(h+x')-ik(x'\pm x)t}}{[k(h+x')]^{3/2}\sqrt{t^2-1}}\,dt\,dx' \approx -\frac{2}{k}\,e^{-2ikh} \sum_{r=1}^{\infty} (i)^r \frac{\Gamma(r+\frac{1}{2})}{(2kh)^{r+\frac{1}{2}}} \int_1^\infty \frac{e^{-ik(h\pm x)t}}{(1+t)^r\sqrt{t^2-1}}\,dt \tag{5.36}$$

But

$$\int_1^\infty \frac{e^{-ik(h\pm x)t}}{(1+t)^r\sqrt{t^2-1}} = e^{-ik(h\pm x)} \int_0^\infty \frac{e^{-ik(h\pm x)z}}{(2+z)^{n+\frac{1}{2}}\sqrt{z}}\,dz$$

by change of variable.

When the point of observation is such that $k(h \pm x)$ is sufficiently large to permit asymptotic expansion,

$$\int_0^\infty \frac{e^{-ik(h\pm x)z}}{(2+z)^{n+\frac{1}{2}}\sqrt{z}}\,dz$$

can be evaluated asymptotically. If $h \pm x = 0$, the above can be evaluated exactly, while in general, if $k(x \pm h)$ is not large enough to permit asymptotic expansion, the upper bound of the above can be determined. Thus the following three cases will be considered.

Case I. The point of observation is at or near the center of the strip so that $k(h \pm x)$ is sufficiently large.

Consider

$$\int_C \frac{e^{-ik(h\pm x)z}}{(2+z)^{n+\frac{1}{2}}\sqrt{z}}\,dz$$

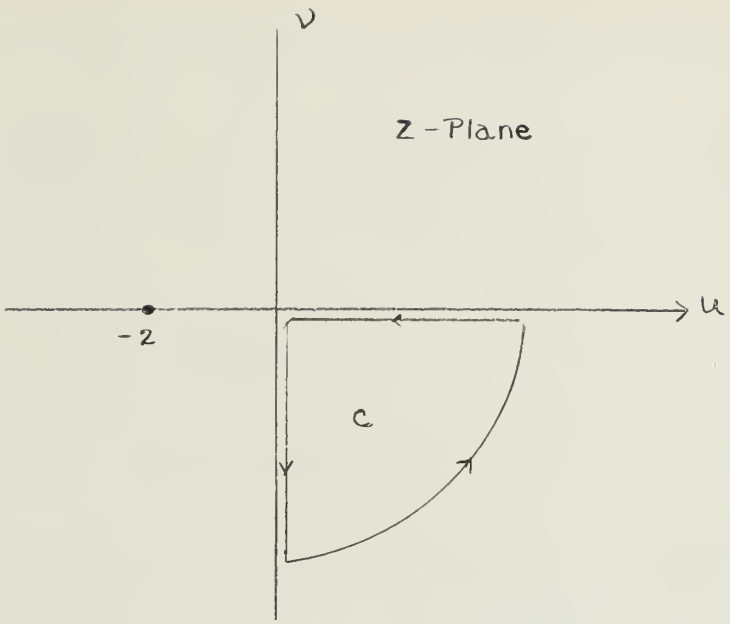

FIGURE 8

taken around the contour C in the complex z plane as shown in Figure 8, in which the branch points are at -2 and 0. Let a branch cut be made along the real axis from u = 0 to u = ∞ and to u = -2 and let the branch of $\sqrt{z}$ be chosen in which the value of $\sqrt{z}$ is $i|z|^{\frac{1}{2}}$ when z is real and negative. The integrand is analytic along the contour C as shown in Figure 8 and hence the value of the integral around the path is zero. The integral around the large circle tends to zero when the radius of the arc tends to infinity. The integral around the small circle also goes to zero as the radius of the small one tends to zero.

Hence

$$\int_0^\infty \frac{e^{-ik(h\pm x)z}}{(2+z)^{r+\frac{1}{2}}\sqrt{z}}\,dz = e^{-i\frac{\pi}{4}} \int_0^\infty \frac{e^{-k(h\pm x)v}}{(2-iv)^{r+\frac{1}{2}}\sqrt{v}}\,dv$$

which by Watson's lemma can be expanded asymptotically and is given by

$$\int_0^\infty \frac{e^{-ik(h\pm x)z}}{(2+z)^{r+\frac{1}{2}}\sqrt{z}}\,dz \simeq e^{-i\frac{\pi}{4}} \sum_{m=0}^{\infty} \frac{\Gamma(m+\frac{1}{2})a_{rm}}{[k(h\pm x)]^{m+\frac{1}{2}}}, \quad \text{with } h \pm x > 0 \tag{5.37}$$

where a_{rm} is defined by

$$\sum_{m=0}^{\infty} a_{rm}\,\nu^m = (2-i\nu)^{-(r+\frac{1}{2})} \tag{5.38}$$

To sum up the result, for $x \approx 0$, such that $k(h \pm x) > 1$,

$$\Delta E \simeq -\frac{e^{-i3kh}}{\pi\sqrt{2\pi}}\left[\frac{\sin\frac{\alpha}{2}}{\cos^2\frac{\alpha}{2}} e^{-ik(x-h\cos\alpha)} \sum_{r=1}^{\infty}(i)^r \frac{\Gamma(r+\frac{1}{2})}{(2kh)^{r+\frac{1}{2}}} \sum_{m=0}^{\infty} \frac{\Gamma(m+\frac{1}{2})a_{rm}}{[k(h+x)]^{m+\frac{1}{2}}}\right.$$

$$\left. + \frac{\cos\frac{\alpha}{2}}{\sin^2\frac{\alpha}{2}} e^{ik(x-h\cos\alpha)} \sum_{r=1}^{\infty}(i)^r \frac{\Gamma(r+\frac{1}{2})}{(2kh)^{r+\frac{1}{2}}} \sum_{m=0}^{\infty} \frac{\Gamma(m+\frac{1}{2})a_{rm}}{[k(h-x)]^{m+\frac{1}{2}}}\right]$$

It may be noted that since in the expression for current along a half plane as given by Equation (5.31) is accurate to the order of $(kr)^{-\frac{5}{2}}$, the above equation, (5.39), will yield results accurate up to the same order. However, by considering terms involving higher powers of $(\frac{1}{kr})$ in Equation (5.31), Equation (5.39) may be made to yield results accurate up to any higher order of $(\frac{1}{kr})$.

Case II: The point of observation is at the edge i.e. $x = \pm h$.

In this case

$$\int_1^\infty \frac{e^{-ik(h\pm x)t}}{(1+t)^r\sqrt{t^2-1}}\,dt = \int_1^\infty \frac{dt}{(1+t)^r\sqrt{t^2-1}} = \frac{1}{2^r}\frac{(r-1)!}{\Gamma(r+\frac{1}{2})}$$

$$\frac{\Gamma(r+\frac{1}{2})}{(2kh)^{r+\frac{1}{2}}} \sum_{m=0}^{\infty} \frac{\Gamma(m+\frac{1}{2})a_{rm}}{(2kh)^{m+\frac{1}{2}}}$$

$$\frac{r-1)!}{2kh)^{r+\frac{1}{2}}} \Bigg] \qquad (5.40)$$

$$(i)^{r} \frac{(r-1)!}{2^{r}(2kh)^{r+\frac{1}{2}}}$$

$$\sum_{m=0}^{\infty} \frac{\Gamma(m+\frac{1}{2})a_{rm}}{(2kh)^{m+\frac{1}{2}}} \Bigg] \qquad (5.41)$$

edges say B, i.e.

ge enough to justify

in terms of $k(h-x)$. Then the result obtained in Case 1 for the second term in the right hand side of Equation (5.39) is not valid. However, in this case an upper bound of ΔE can be obtained as follows:

$$\int_{1}^{\infty} \frac{e^{-ik(h-x)t}}{\sqrt{t^2-1}\ (1+t)^{r}}\, dt \leq \int_{1}^{\infty} \frac{dt}{(1+t)^{r}\sqrt{t^2-1}} = \frac{1}{2^{r}} \frac{(r-1)!}{\Gamma(r+\frac{1}{2})} \qquad (5.42)$$

Therefore

$$\Delta E_{\text{at } x=h} = -\frac{1}{\pi\sqrt{2\pi}}\left[\frac{\sin\frac{\alpha}{2}}{\cos^2\frac{\alpha}{2}}\, e^{-ikh(4-\cos\alpha)} \sum_{r=1}^{\infty} (i)^r \frac{\Gamma(r+\frac{1}{2})}{(2kh)^{r+\frac{1}{2}}} \sum_{m=0}^{\infty} \frac{\Gamma(m+\frac{1}{2})a_{rm}}{(2kh)^{m+\frac{1}{2}}}\right.$$

$$\left. + e^{i\frac{\pi}{4}} \frac{\cos\frac{\alpha}{2}}{\sin^2\frac{\alpha}{2}}\, e^{-ikh(2+\cos\alpha)} \sum_{r=1}^{\infty} (i)^r \frac{(r-1)!}{2^r (2kh)^{r+\frac{1}{2}}}\right] \tag{5.40}$$

while

$$\Delta E_{\text{at } x=-h} = -\frac{1}{\pi\sqrt{2\pi}}\left[\frac{\sin\frac{\alpha}{2}}{\cos^2\frac{\alpha}{2}}\, e^{-i\left\{kh(2-\cos\alpha)-\frac{\pi}{4}\right\}} \sum_{r=1}^{\infty} (i)^r \frac{(r-1)!}{2^r (2kh)^{r+\frac{1}{2}}}\right.$$

$$\left. + \frac{\cos\frac{\alpha}{2}}{\sin^2\frac{\alpha}{2}}\, e^{-ikh(4+\cos\alpha)} \sum_{r=1}^{\infty} (i)^r \frac{\Gamma(r+\frac{1}{2})}{(2kh)^{r+\frac{1}{2}}} \sum_{m=0}^{\infty} \frac{\Gamma(m+\frac{1}{2})a_{rm}}{(2kh)^{m+\frac{1}{2}}}\right] \tag{5.41}$$

Case III: The observation point is near one of the edges say B, i.e. h and x are of the same order and k(h-x) is not large enough to justify asymptotic expansion of

$$\int_0^{\infty} \frac{e^{-k(h-x)\nu}}{(2-i\nu)^{r+\frac{1}{2}}\sqrt{\nu}}\, d\nu$$

in terms of k(h-x). Then the result obtained in Case I for the second term in the right hand side of Equation (5.39) is not valid. However, in this case an upper bound of ΔE can be obtained as follows:

$$\int_1^{\infty} \frac{e^{-ik(h-x)t}}{\sqrt{t^2-1}\,(1+t)^r}\, dt \le \int_1^{\infty} \frac{dt}{(1+t)^r\sqrt{t^2-1}} < \frac{1}{2^r}\,\frac{(r-1)!}{\Gamma(r+\frac{1}{2})} \tag{5.42}$$

Now

$$\int_h^\infty \int_1^\infty \frac{e^{-kl(h+x')-ik(x'-x)t}}{[k(h+x')]^{3/2}\sqrt{t^2-1}}\,dt\,dx' \simeq -\frac{2}{k}e^{-2ikh}\sum_{r=1}^{\infty}(i)^r\frac{\Gamma(r+\frac{1}{2})}{(2kh)^{r+\frac{1}{2}}}\int_1^\infty \frac{e^{-ik(h-x)t}}{(1+t)^r\sqrt{t^2-1}}\,dt$$

$$= -\frac{2}{k}e^{-2ikh}\left\{\sum_{r=1}^{\infty}(-1)^r\frac{\Gamma(2r+\frac{1}{2})}{(2kh)^{2r+\frac{1}{2}}}\int_1^\infty \frac{e^{-ik(h-x)t}}{(1+t)^{2r}\sqrt{t^2-1}}\,dt + \sum_{r=0}^{\infty}(i)^{2r+1}\frac{\Gamma(2r+3/2)}{(2kh)^{2r+3/2}}\int_1^\infty \frac{e^{-ik(h-x)t}\,dt}{(1+t)^{2r+1}\sqrt{t^2-1}}\right\}$$

$$\leq -\frac{2}{k}e^{-2ikh}\left\{\sum_{r=1}^{\infty}\frac{(2r-1)!}{(2kh)^{2r+\frac{1}{2}}}\frac{1}{(2)^{2r}} + i\sum_{r=0}^{\infty}\frac{2r}{(2)^{2r+1}(2kh)^{2r+3/2}}\right\}$$

Therefore

$$\Delta E \leq -\frac{1}{\pi\sqrt{2\pi}}\left[e^{-ik\{h(3-\cos\alpha)+x\}}\frac{\sin\frac{\alpha}{2}}{\cos^2\frac{\alpha}{2}}\sum_{r=1}^{\infty}(i)^r\frac{\Gamma(r+\frac{1}{2})}{(2kh)^{r+\frac{1}{2}}}\sum_{m=0}^{\infty}\frac{\Gamma(m+\frac{1}{2})a_{rm}}{[k(h+x)]^{m+\frac{1}{2}}}\right.$$

$$\left. + e^{i\frac{\pi}{4}}\cdot e^{-ik\{h(3+\cos\alpha)-x\}}\frac{\cos\frac{\alpha}{2}}{\sin^2\frac{\alpha}{2}}\left\{\sum_{r=1}^{\infty}\frac{(2r-1)}{(2kh)^{2r+\frac{1}{2}}}\frac{1}{(2)^{2r}} + i\sum_{r=0}^{\infty}\frac{2r}{(2)^{2r+1}(2kh)^{2r+3}}\right\}\right] \qquad (5.43)$$

Similar results can be obtained for the observation point x near the other edge A, i.e., $x \approx -h$. In that case

$$\Delta E \leq -\frac{1}{\pi\sqrt{2\pi}}\left[e^{-ik\{h(3+\cos\alpha)-x\}}\frac{\cos\frac{\alpha}{2}}{\sin^2\frac{\alpha}{2}}\sum_{r=1}^{\infty}(i)^r\frac{\Gamma(r+\frac{1}{2})}{(2kh)^{r+\frac{1}{2}}}\sum_{m=0}^{\infty}\frac{\Gamma(m+\frac{1}{2})a_{rm}}{[k(h-x)]^{m+\frac{1}{2}}}\right.$$

$$\left. + e^{i\frac{\pi}{4}}\cdot e^{-ik\{h(3-\cos\alpha)+x\}}\frac{\sin\frac{\alpha}{2}}{\cos^2\frac{\alpha}{2}}\left\{\sum_{r=1}^{\infty}\frac{(2r-1)!}{(2kh)^{2r+\frac{1}{2}}}\frac{1}{(2)^{2r}} + i\sum_{r=0}^{\infty}\frac{2r!}{(2)^{2r+1}(2kh)^{2r+\frac{3}{2}}}\right\}\right]$$

It is interesting to note that the first term in all these asymptotic series involves at least $(\frac{1}{kh})^2$ and succeeding terms are of higher order in $(\frac{1}{kh})$. Thus if kh is sufficiently large, a good approximation can be obtained even if only the first few terms of the series are considered.

In a later section, ΔE expressed as $\frac{\Delta E}{E_{inc}} \times 100$ for various h and a have been computed and plotted in order to determine the extent of deviation from the boundary condition with assumed current distribution. It is found that this deviation is very small for the sizes of strips used in the construction of the zoned mirror in which the width of each zone is of the order of a wavelength or more. Thus the use of the approximate current distribution for the computation of the field of the zoned mirror assembly has been justified.

6. NUMERICAL COMPUTATIONS

For the purpose of computation the dimensions chosen are:

(a) $F = f/D = .556$ where F is the focal length and D is the diameter

(b) $f = 10\lambda$. of the aperture.

(c) Total number of Zones = 11.

Equations (5.8), (5.9) and (5.10) are used for computation of I_{ii} while Equation (5.16) is used for computation of coupled current I_{ij}. The expression for I used for the above are given by Equations (5.13), (5.14) and (5.15). Equations (5.15, (5.17) and (5.18) are not used because when the arguments of the Bessel functions of the two kinds approach each other, the convergence of the series given by Equation (5.19) becomes very slow and hence the number of terms of the series required for a certain accuracy becomes extremely large.

Once the current distribution across a given strip has been calculated from the above, the electric field at any point due to each strip is computed from Equation (3.19). In computing the field due to any strip, the asymptotic form of Hankel function is used. Since the geometry is such that the argument of the Hankel function in Equation (3.19) i.e., kr is much greater than unity.

The first zone is a smooth parabola of finite dimension. The rigorous solution for this is unknown. However, if the parabolic zone is replaced by a flat strip of the same aperture, it is possible to compute I_{ii}, I_{ij} and fields due to I_{ii} and $I_{ii} + I_{ij}$. It is found that not only was I_{ij} very small compared to I_{ii}, but the fields due to I_{ii} and $I_{ii} + I_{ij}$ were practically the same. Further, we can reasonably assume that I_{ij} of the first zone either as a flat strip or a smooth parabola should be of the same order of magnitude. Therefore we conclude that $I_{ii}+I_{ij}$ and I_{ii} produce almos the same field for a smooth parabola also. However, I_{ii}, the current induced

on a finite smooth parabola due to an incident plane wave is still unknown; but it is generally known that the physical optics solution for a finite parabola agrees very closely with experimental results. Further according

Table 1

Comparison of the contribution of the first zone (flat strip) to the image pattern (a) with physical optics solution (b) with edge effect.

Magnitude of the E Field		
y	Case (a)	Case (b)
0	1.29	1.28
-.2	1.27	1.26
-.4	1.22	1.21
-.6	1.14	1.14
-.8	1.05	1.05
-.9	1.01	1.01
-1.0	.97	.96

to the computation (Table 1) the physical optics solution for the corresponding flat strip does not differ significantly from that including the edge effect, since the strip is quite wide in terms of wavelengths (6.245 λ). Therefore it seems reasonable to use the physical optics solution for the smooth parabola representing the central zone. In other words, the significant contribution of the first strip is that due to the geometrical optics current regardless of whether the first zone is a flat strip or

a portion of a smooth parabola. However, this does not imply that the contribution due to the flat strip is the same as that due to an equivalent smooth parabola. This becomes clear if one observes that in the present case the geometrical path difference at the edge between the two is of the order of $\lambda/4$. The difference in over-all contribution is indicated in Figure 9 for normal incidence. It shows that in actual construction the first zone should not be approximated by a flat strip.

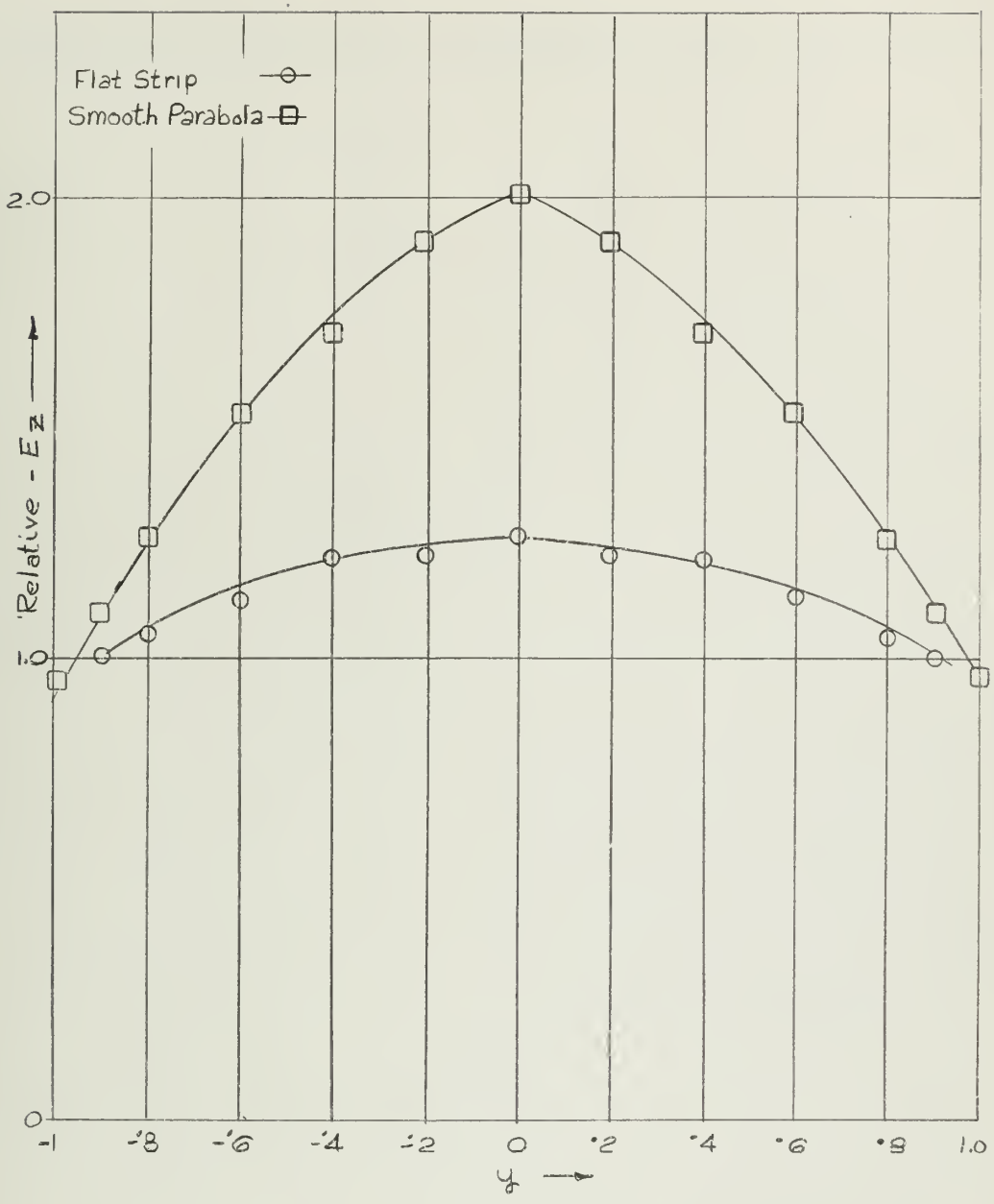

FIGURE 9 CONTRIBUTION OF IMAGE PATTERN ON THE FOCAL PLANE OF THE ZONED MIRROR DUE TO THE CENTRAL ZONE ONLY FOR NORMAL INCIDENCE

7. DISCUSSION OF RESULTS

7.1 Error in the Satisfaction of the Boundary Condition Due to the Approximation of the Current Distribution on the Strip

The magnitude of the error in the satisfaction of the boundary condition, $|\Delta E|$, on the surface of an isolated strip due to the approximate current distribution, expressed in percentage of incident electric field, is plotted as a function of the observation point on the strip in Figure 10 for strip widths of 2λ, λ, $.75\lambda$ and $0 \quad .5\lambda$ with normal incidence and in Figure 11, $|\Delta E|$ is plotted for a strip of width λ for incident angles of 0^{o}, 15^{o}, 25^{o} and 45^{o}. The graph shows that $|\Delta E|$ varies from point to point across the strip. The average of $|\Delta E|$, however, increases if the strip width decreases or for a given width if the angle of incidence increases. For the dimensions of the strips used in the zoned mirror the average $|\Delta E|$ is less than about 0.5% for normal incidence; and about 2.0% for oblique incidence. It is therefore clear that the half plane current distribution is a very close approximation of the exact distribution. It is doubtful whether much greater accuracy could be achieved by using the exact solution, due to the difficulty of computation as discussed in great detail in the appendix.

7.2 Current Distribution (I_{ii} and I_{ij})

The surface current density I_{ii} on an isolated strip due to an incident plane wave and the first order surface current density I_{ij} induced on the strip due to the presence of other strips have been plotted for different configurations of the strips and different angles of incidence in Figures 12 to 17. The curves of I_{ii} show the correct singularity at the two edges as expected since they are half-plane solutions. The current drops sharply to a value well below that at

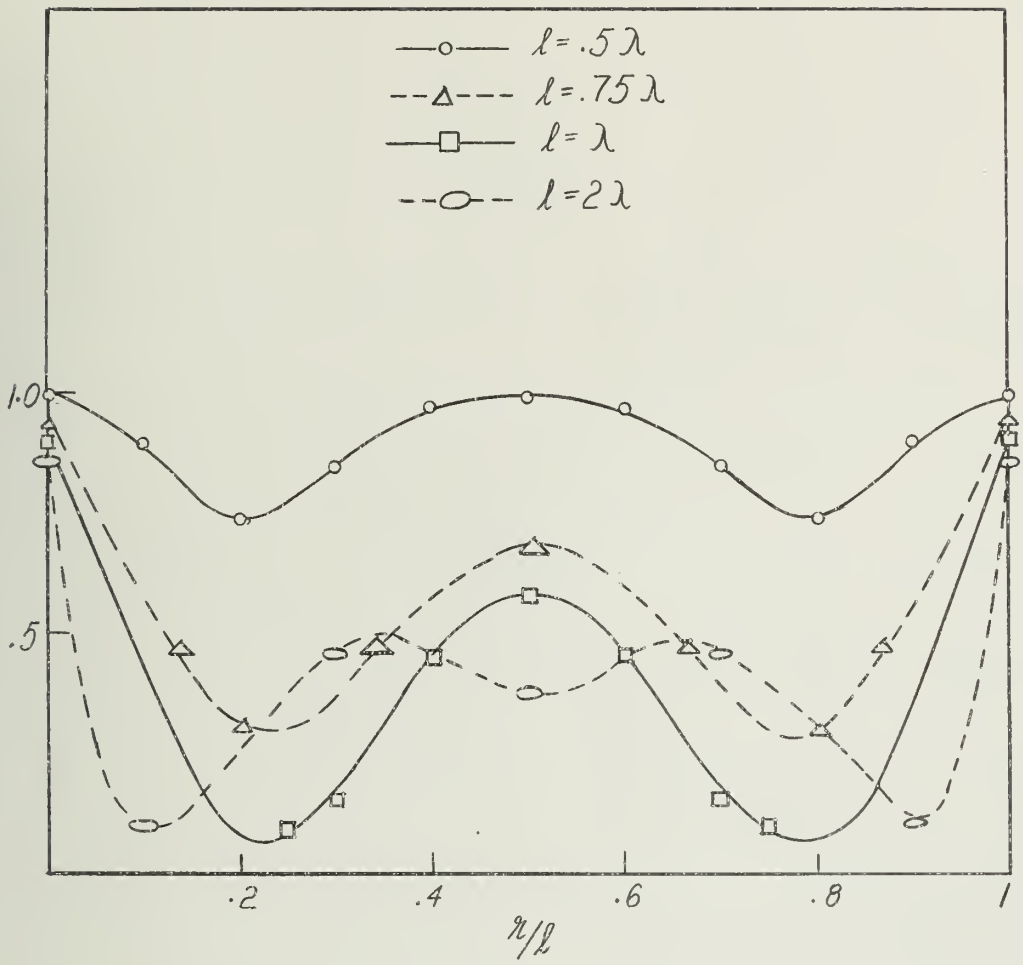

FIGURE 10 $|\Delta E|$ IN PERCENT OF INCIDENT FIELD VS POINT OF OBSERVATION ANGLE OF INCIDENCE $\alpha = 0$

Angle of Incidence

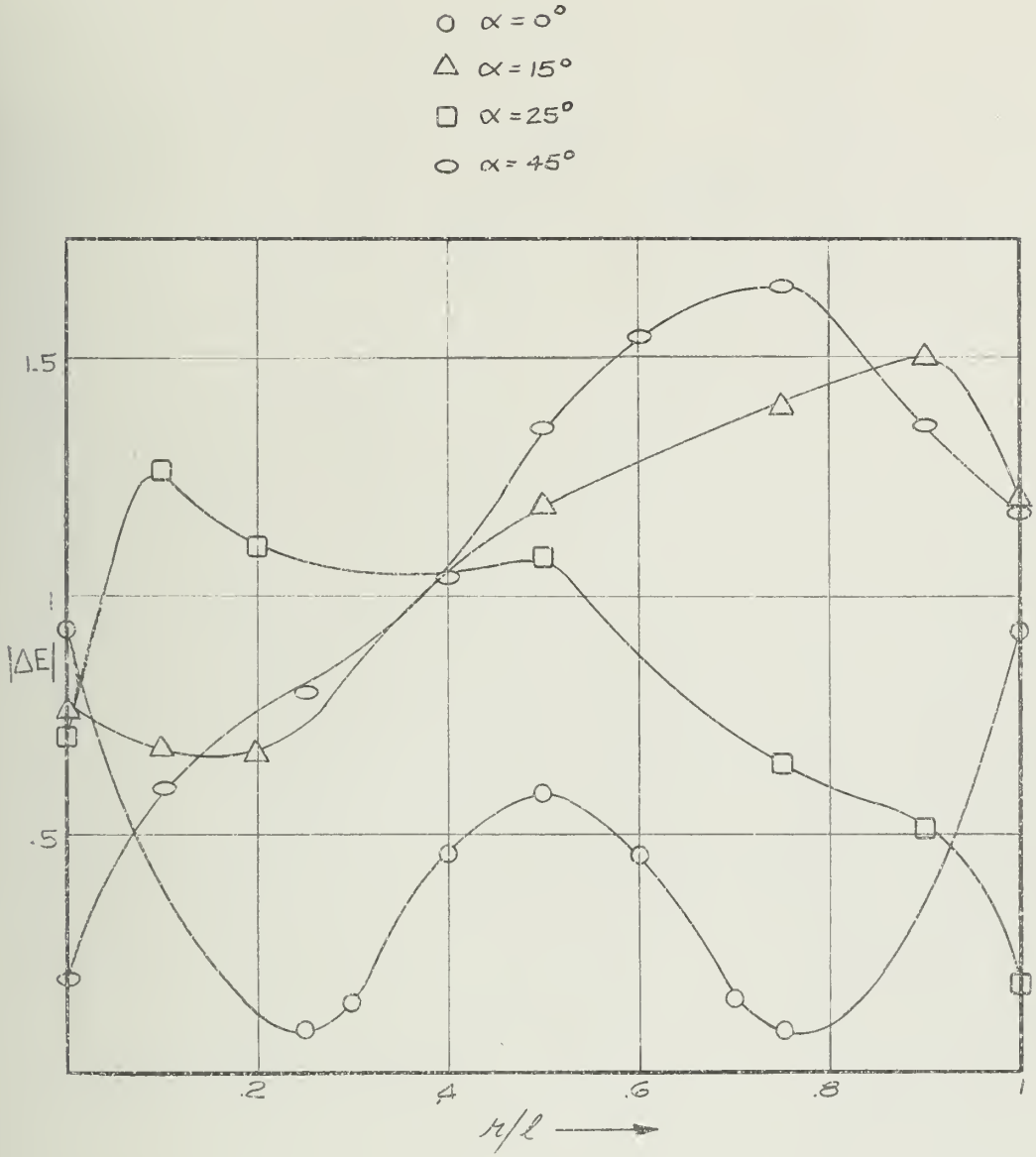

FIGURE 11 |Δ E| IN PERCENT OF INCIDENT FIELD VS POINT OF OBSERVATION (STRIP WIDTH = 1λ).

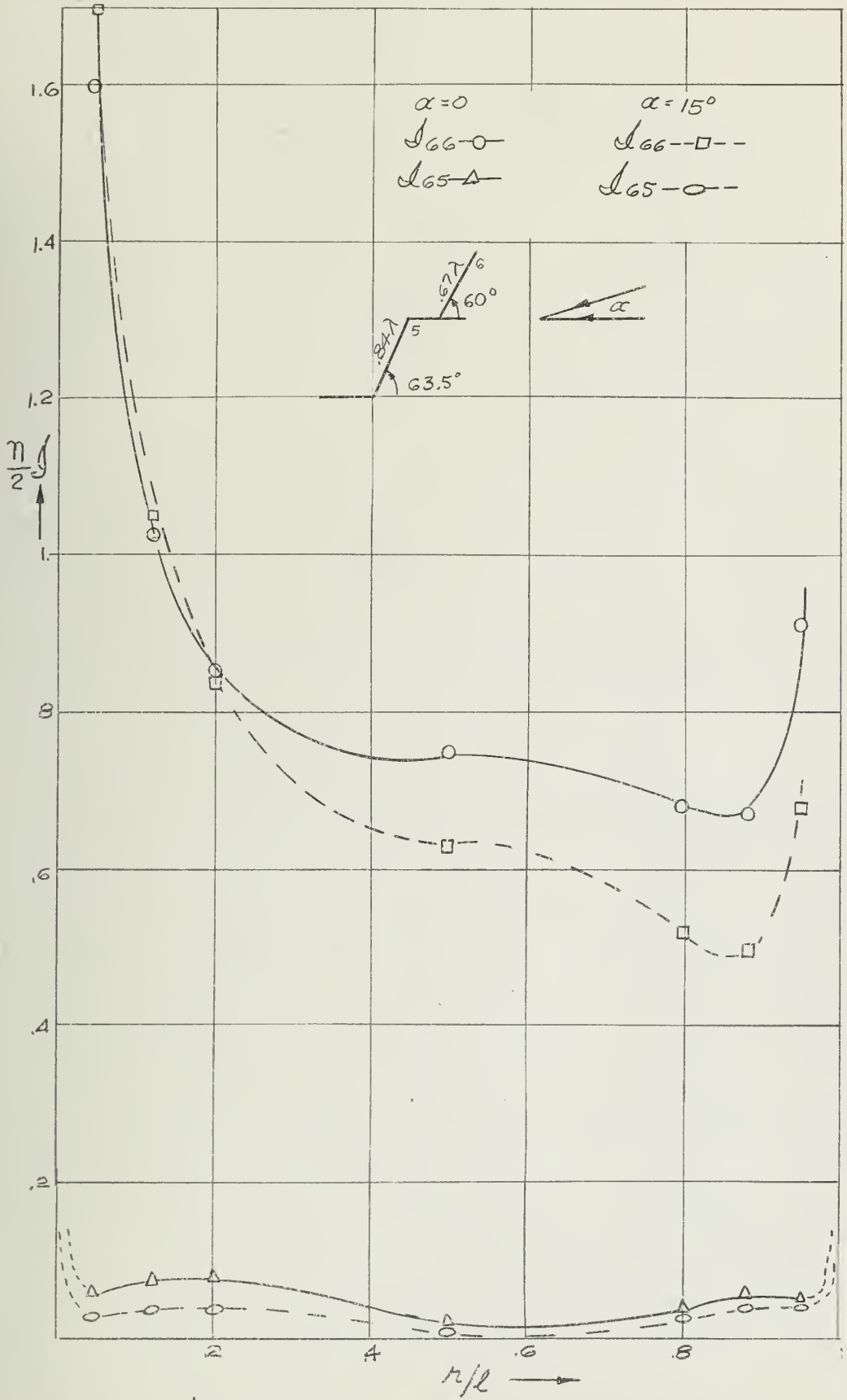

FIGURE 12 'SELF CURRENT' AND 'MUTUAL' CURRENT ON STRIP 6

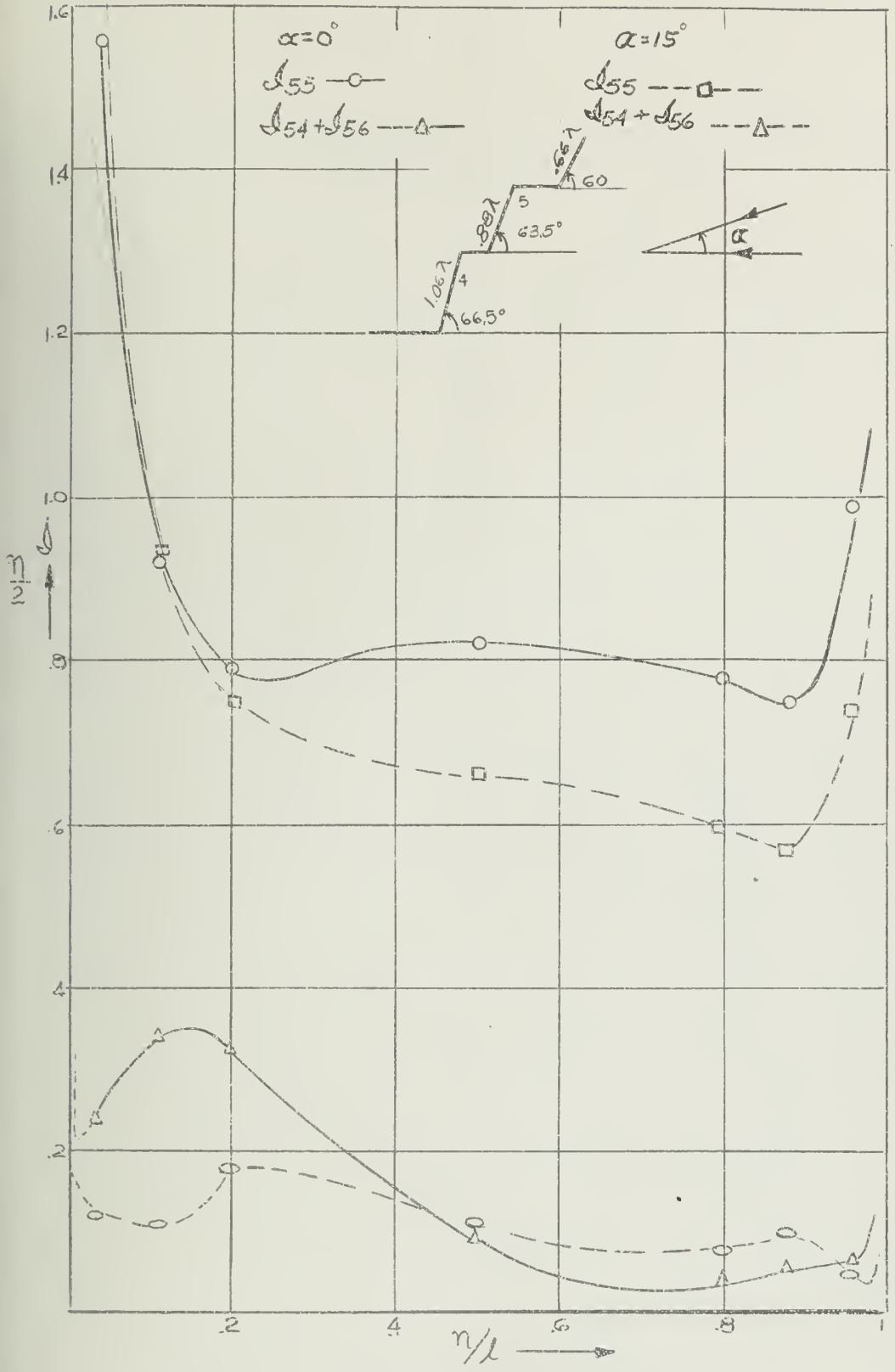

FIGURE 13 SELF AND MUTUAL CURRENT ON STRIP 5

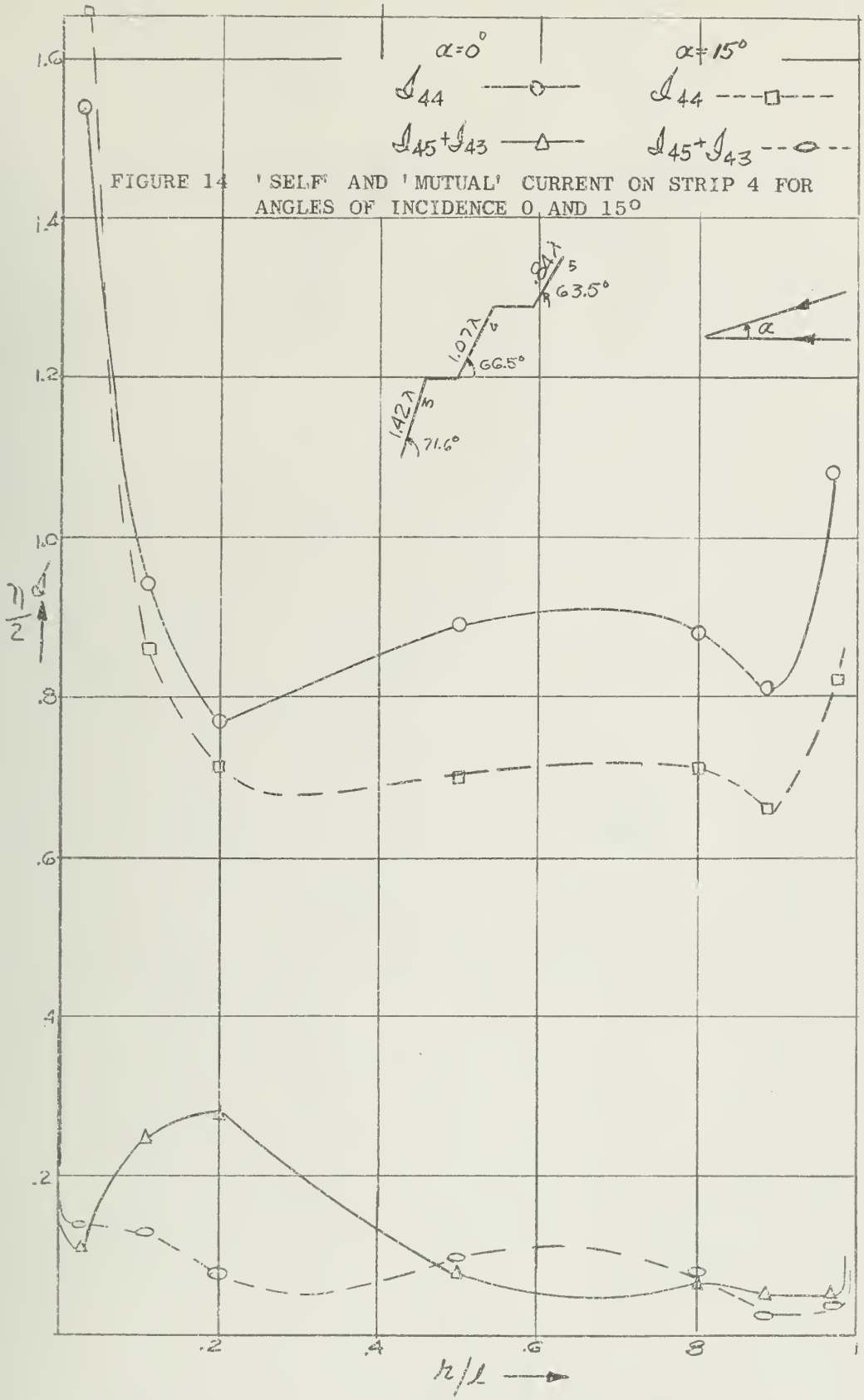

FIGURE 14 'SELF' AND 'MUTUAL' CURRENT ON STRIP 4 FOR ANGLES OF INCIDENCE 0 AND 15°

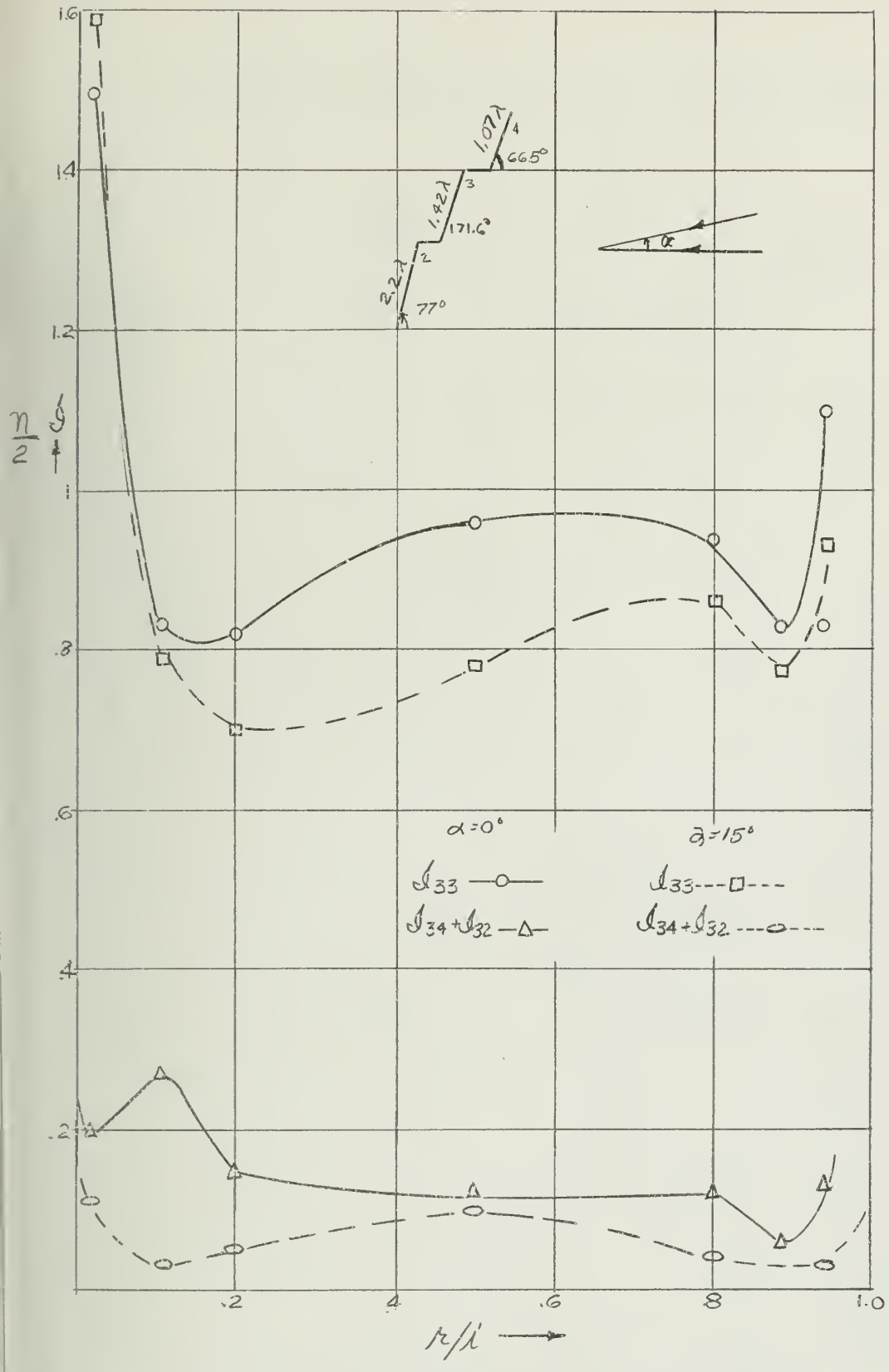

FIGURE 15 'SELF' AND 'MUTUAL' CURRENT ON STRIP 3
for $\alpha = 0$ and 15°

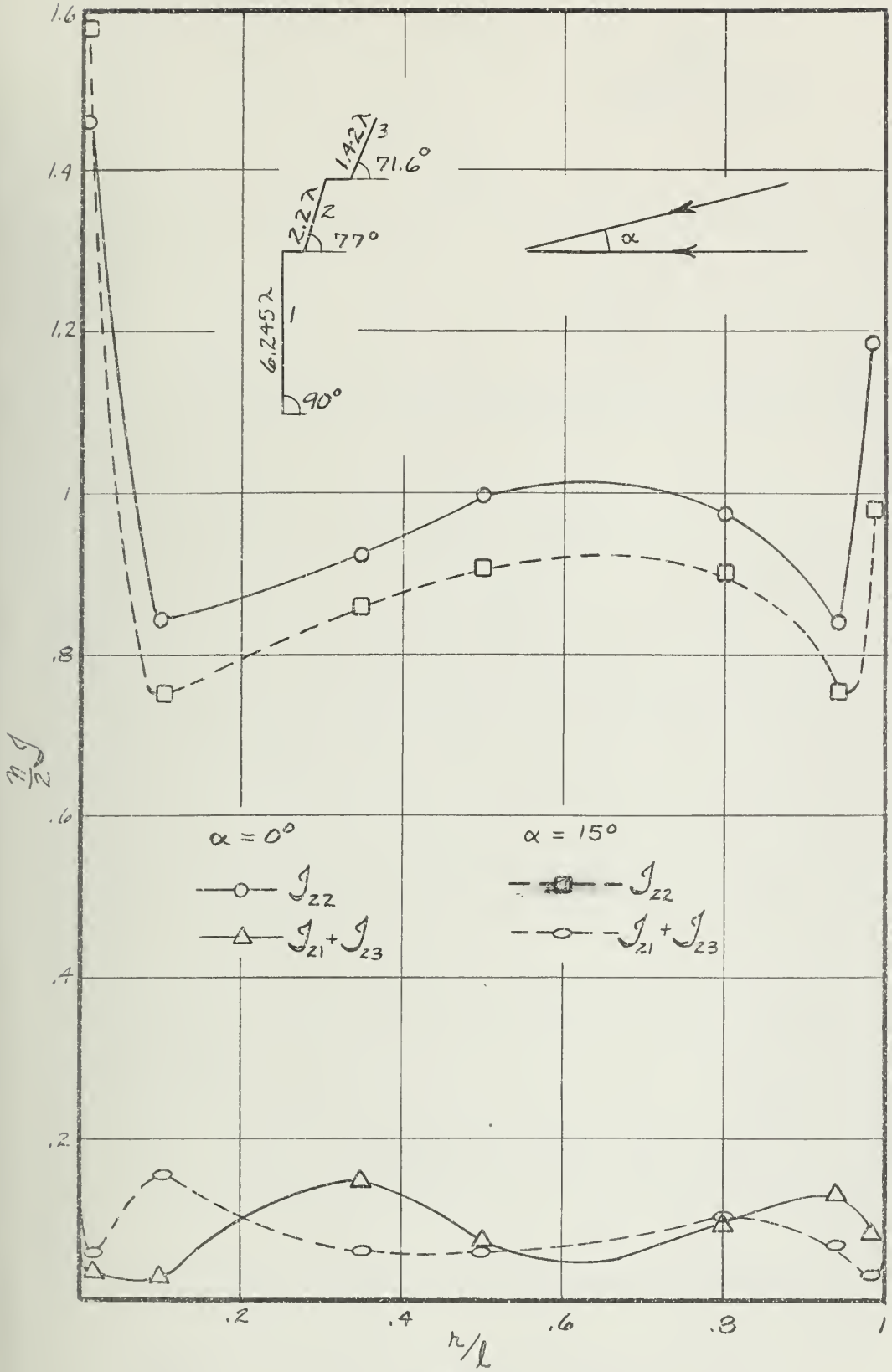

FIGURE 16 'SELF' AND 'MUTUAL' CURRENT ON STRIP 2

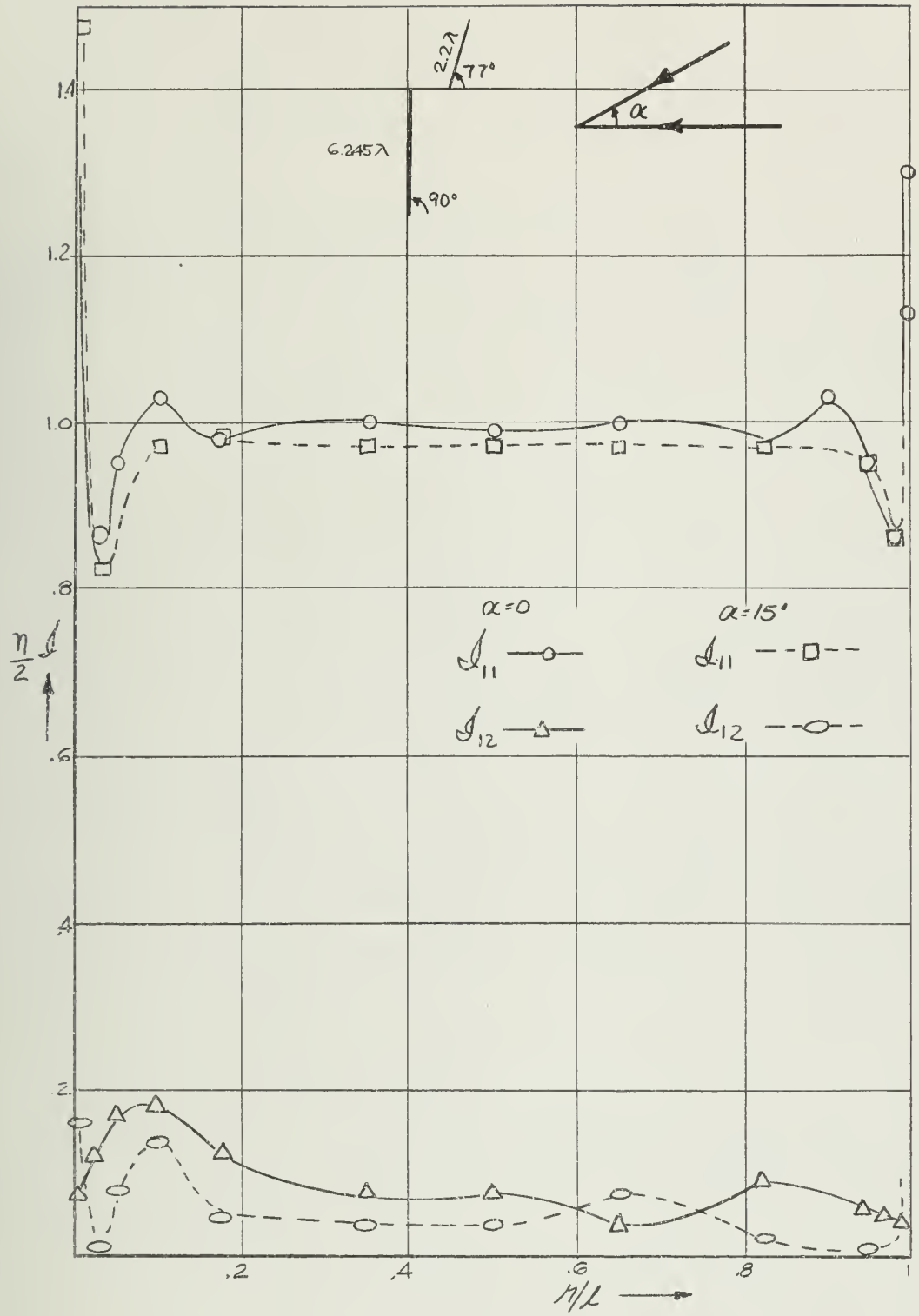

FIGURE 17 SELF AND MUTUAL CURRENT ON STRIP 1

the middle as the point of observation is moved away from the edge. It then increases again approaching the geometrical optics value near the middle. The rate of decrease is reduced as the angle of incidence is increased.

The first order coupled current distribution I_{ij} also has similar singularities at the two edges as evident from Equation (5.13). This current distribution varies with the size of the adjacent strips, their relative inclination and their distance from the strip under consideration. In general I_{ij} is in the order of 10% of I_{ii}. Hence the second order coupled current will be in the order of 1% of I_{ii}. Thus, although it is possible to obtain the second order solution in the present iteration procedure, it seems to be insignificant and it is probably within the error introduced by substituting the exact solution of an isolated strip by half plane solution in actual computation as explained before.

7.3 Image Patterns

To demonstrate the difference in performance with various orders of approximation, the image pattern of the zoned mirror has been studied with the following current distributions on the strips due to a plane wave at various incident angles:

(1) The geometrical optics current distribution i.e. the current distribution on the strip which is obtained as if it were a part of an infinite plane. In this case the effects of both the edges and coupling between strips are neglected.

(2) A current distribution which takes into account the edge effect but ignores the effect of coupling between strips i.e. the zero order solution of the integral equation given by Equation (3.15).

(3) A current distribution which considers both the edge effect and the first order coupling between adjacent strips as given by Equation (3.17)

All computations are done by ILLIAC, the electronic high speed computer at the University of Illinois. The time required for computing an image pattern with one angle of incidence for three different current approximations is roughly given below:

(a) Case 1 14 minutes

(b) Case 2 16 minutes

(c) Case 3 1 hour

For comparative study, the image pattern of an equivalent smooth parabola i.e. a smooth parabola with the same focal length and aperture area as the zoned mirror, is also computed. These are all shown in Figures 18 to 23.

With normal incidence, the maximum intensity due to a smooth parabola and Case 1 of the above, are almost identical, while Cases 2 and 3 yield almost the same value, which is about four percent less than that of a smooth parabola. Thus the edge effect reduces the gain slightly.

The secondary maxima occur at the same positions for the smooth parabola as for the Case 1 and Case 3 of the zoned mirror while for Case 2 they are slightly displaced. The value of the secondary maxima is the largest with the smooth parabola while for Cases 1, 2 and 3 of the zoned mirror they are the same, having a value approximately 60 percent of that of the smooth parabola.

As the angle of incidence is changed from normal, the maximum intensity falls off rapidly for the smooth parabola. Case 1 also shows a drop while for Cases 2 and 3 the drop is very small until the angle of incidence exceeds 15^{o}. The locations of the primary and secondary maxima for all

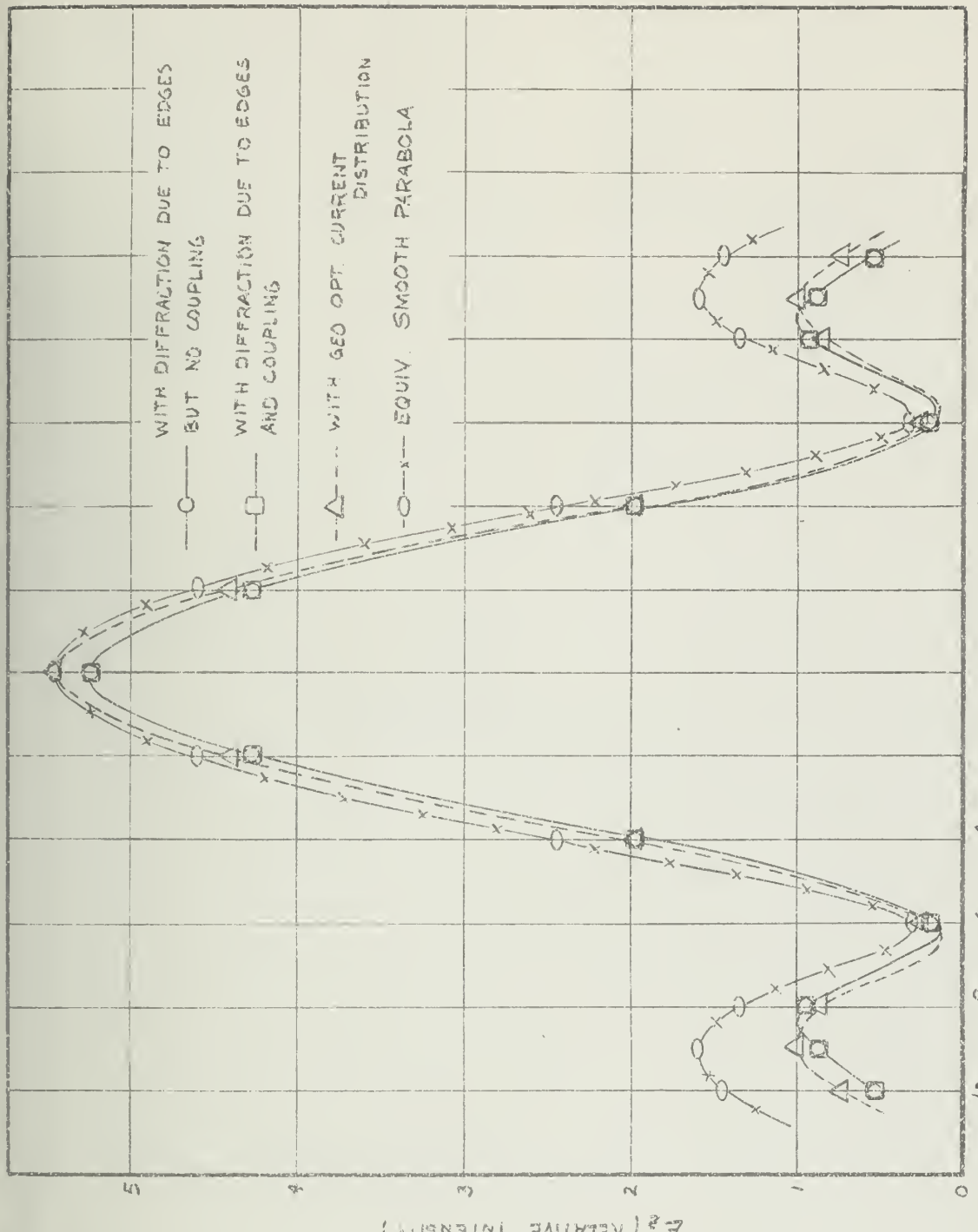

FIGURE 18 IMAGE PATTERN ON THE FOCAL PLANE FOR $\alpha = 0$

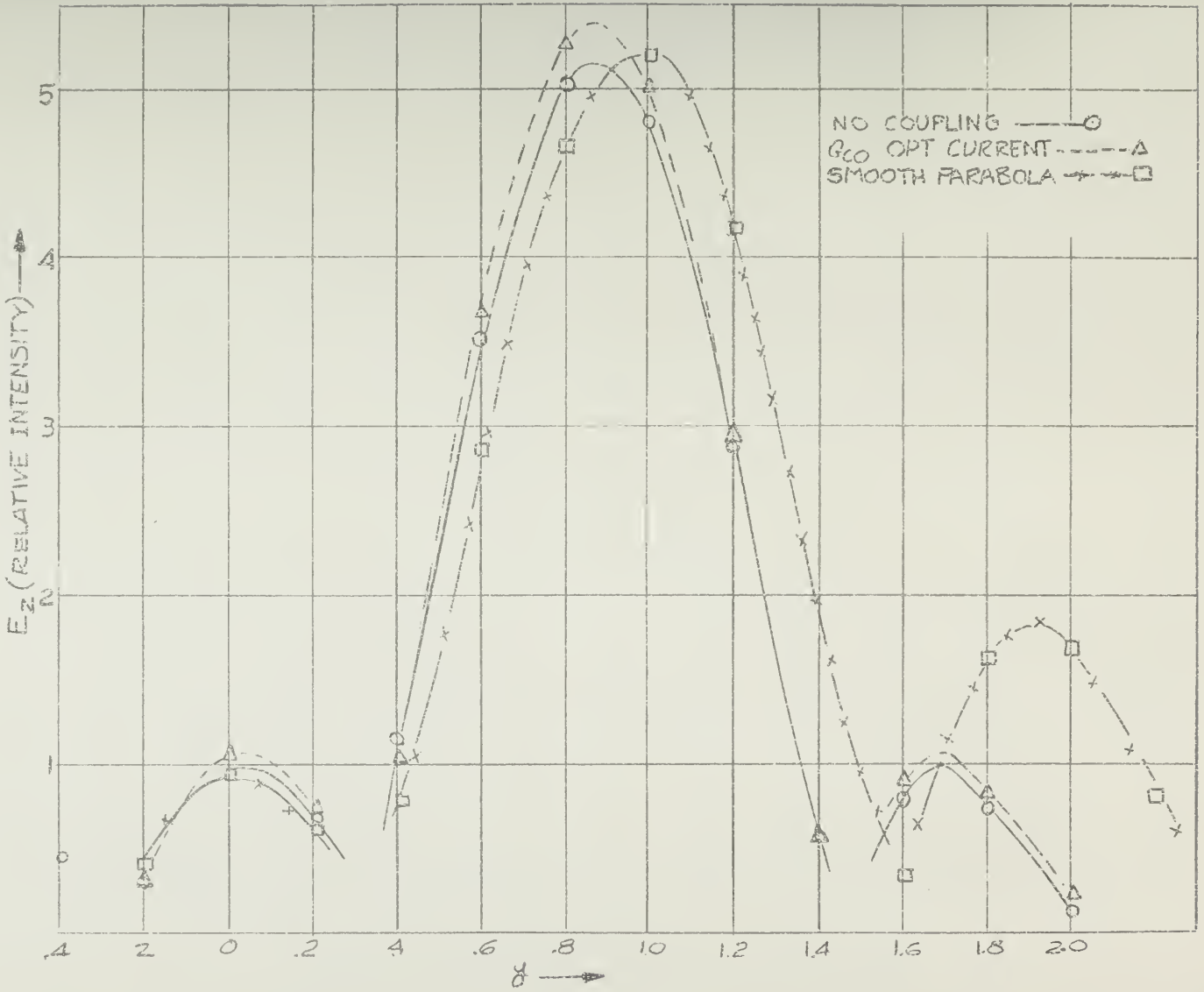

FIGURE 19 IMAGE PATTERN ON THE FOCAL PLANE, $\alpha = 5^{\circ}$

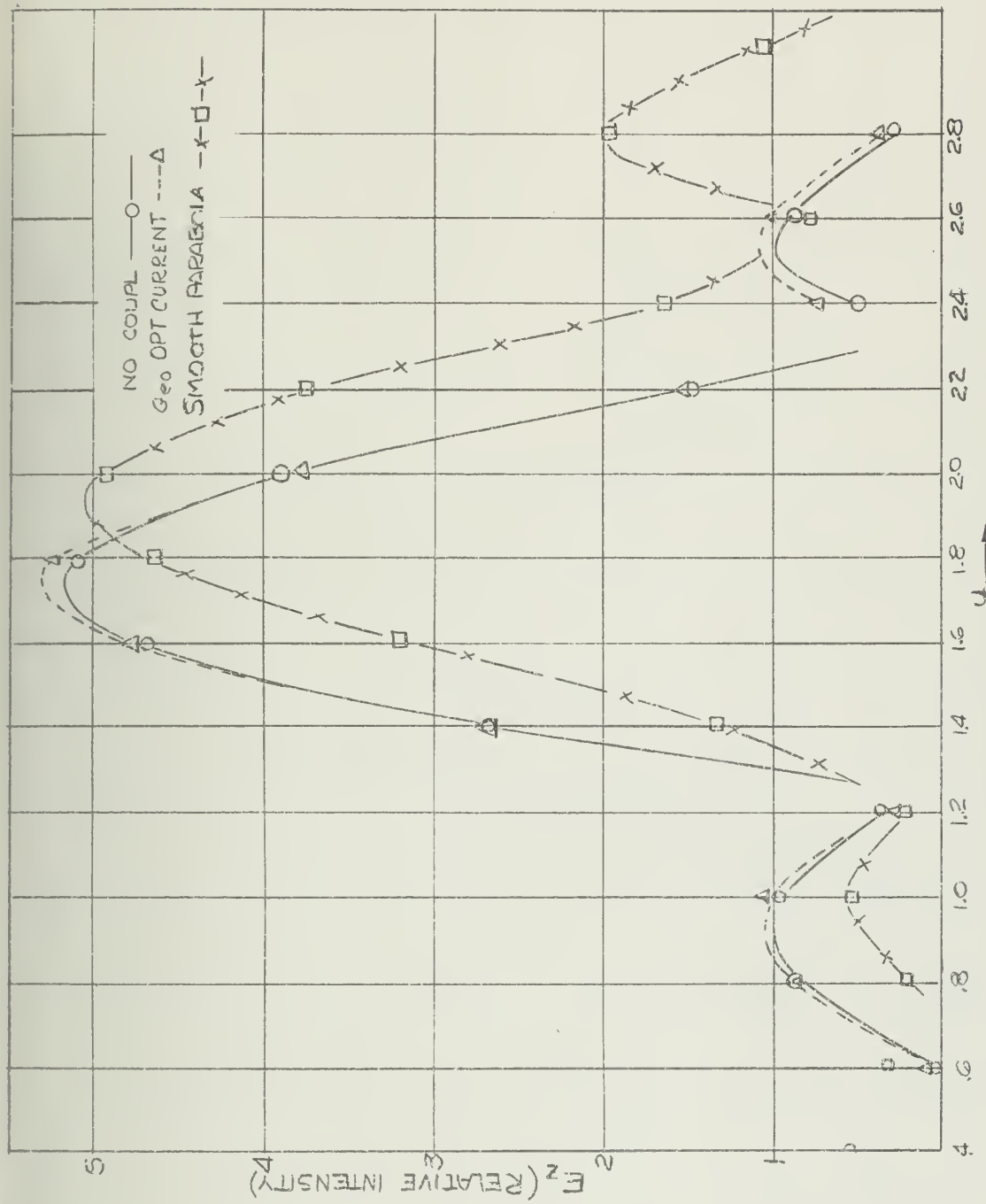

FIGURE 20 IMAGE PATTERN ON THE FOCAL PLANE $\alpha = 10^{\circ}$

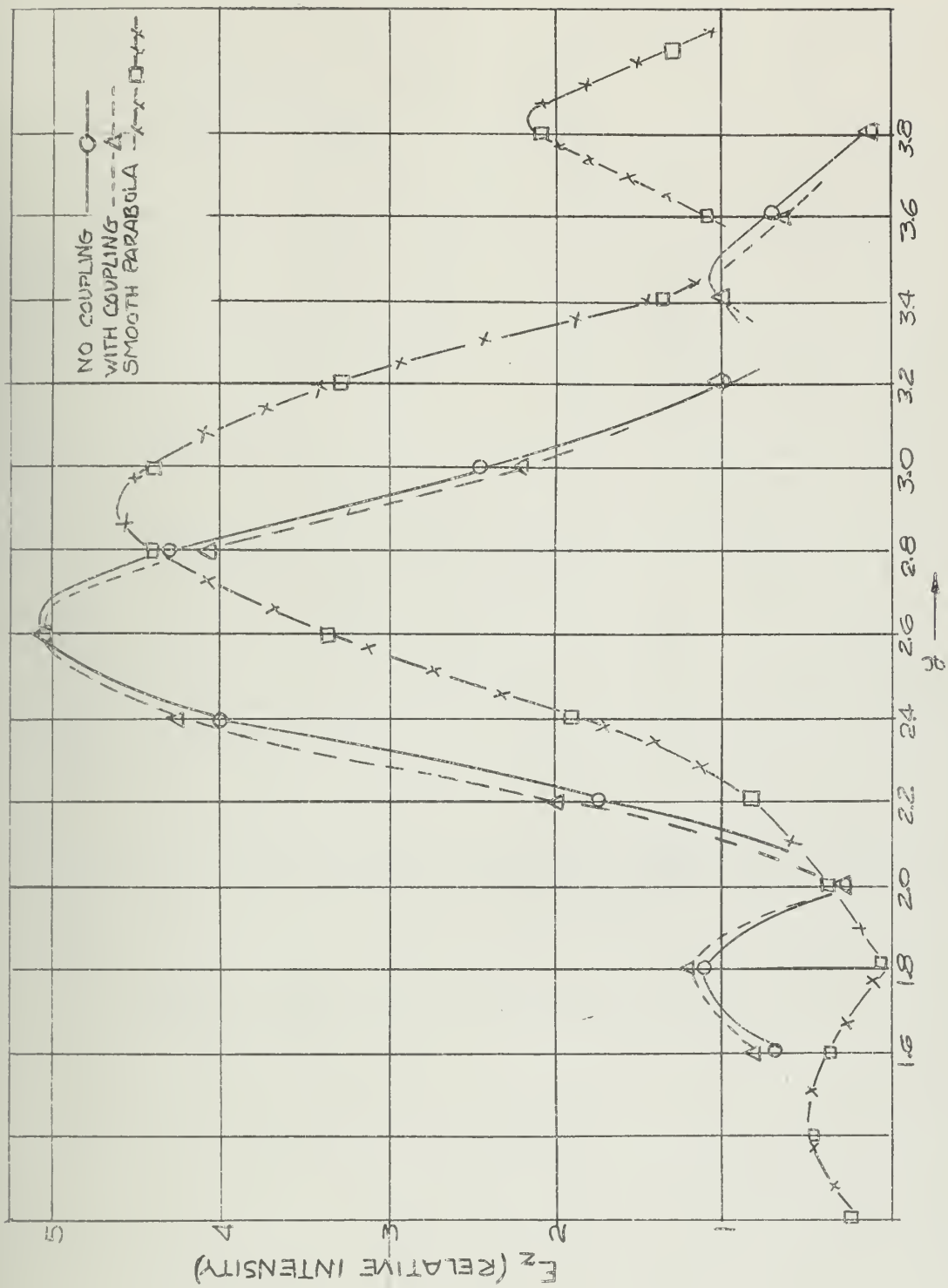

FIGURE 21 IMAGE PATTERN ON THE FOCAL PLANE $\alpha = 15^{o}$

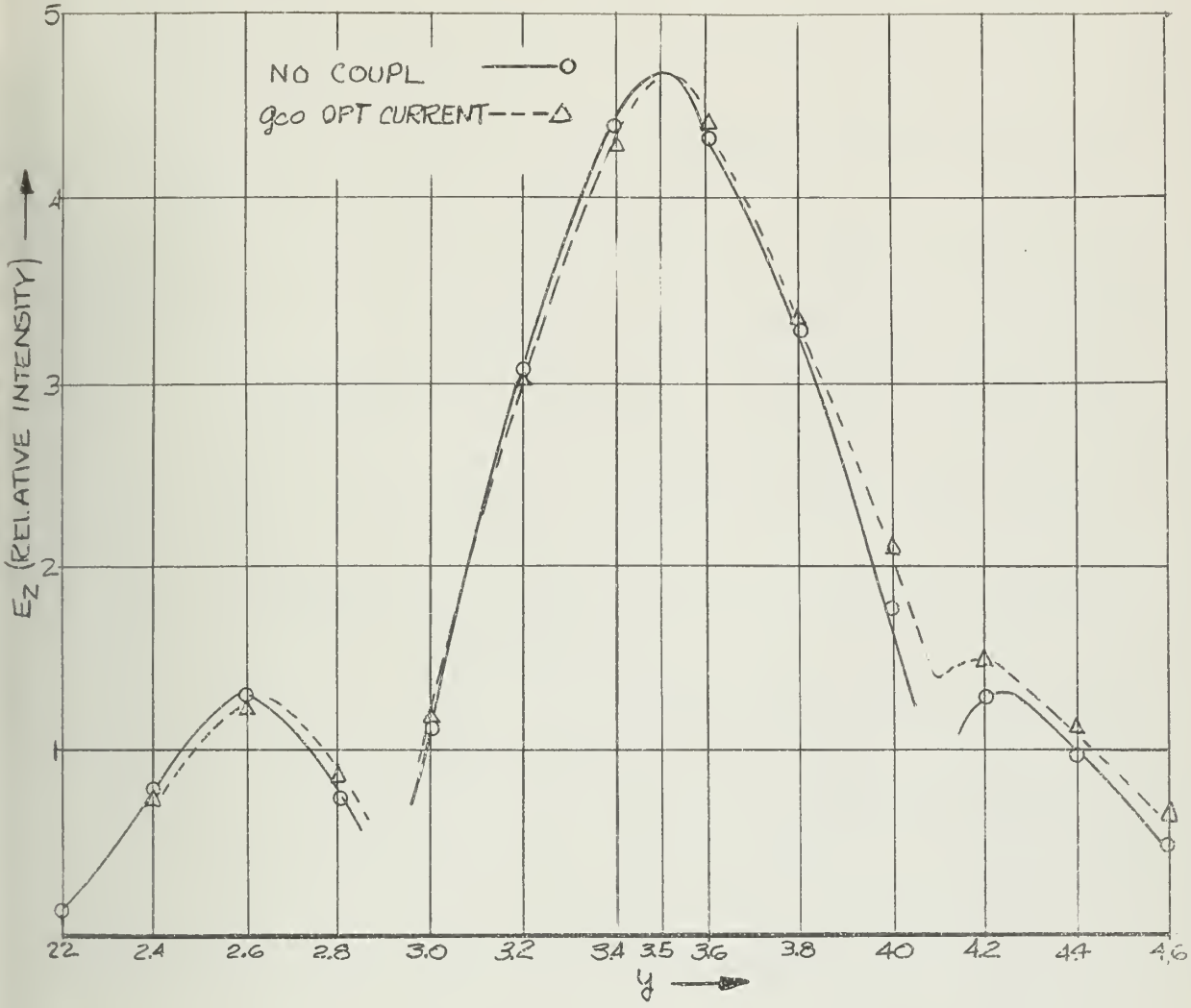

FIGURE 22 IMAGE PATTERN ON THE FOCAL PLANE $\alpha = 20^{\circ}$

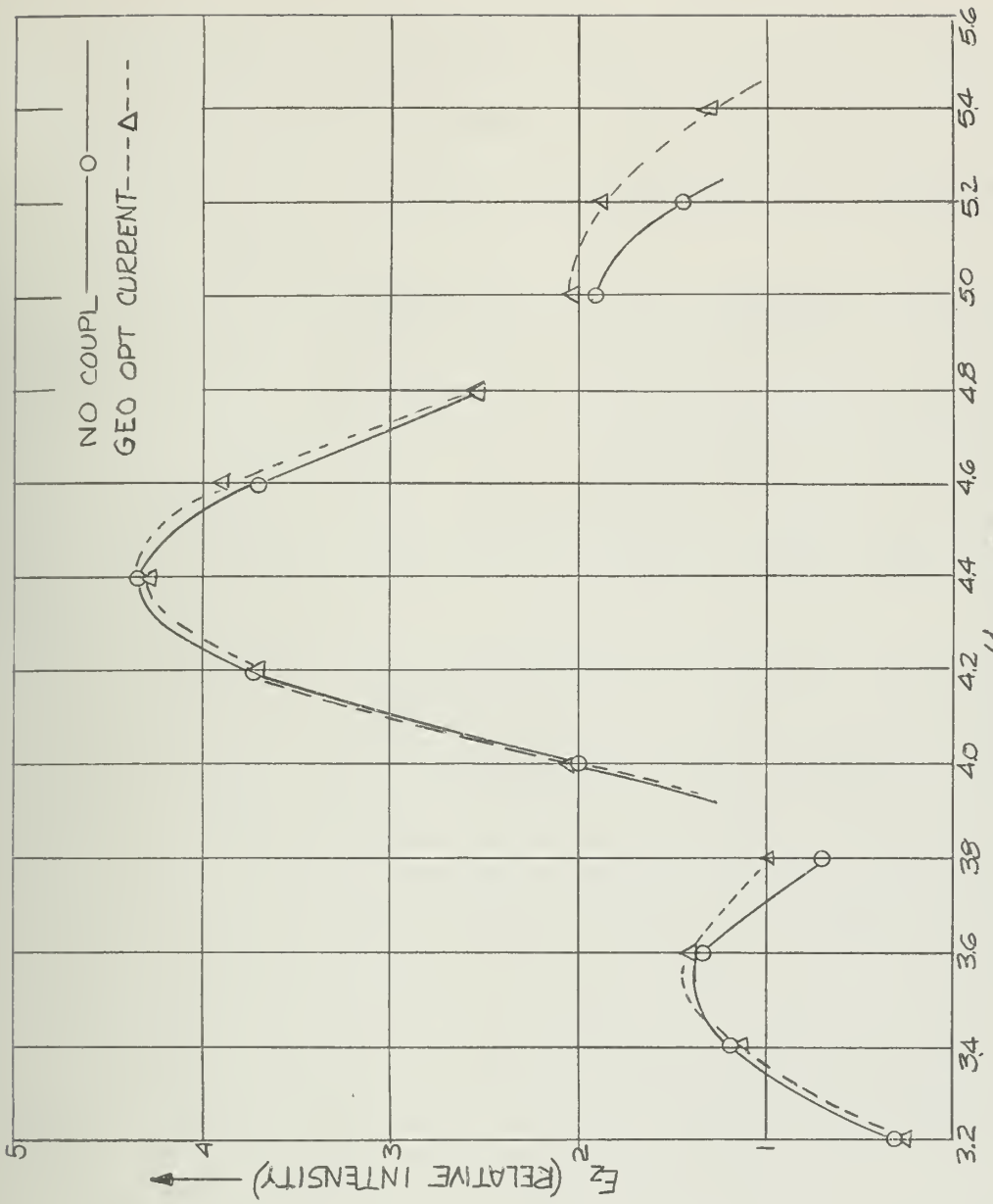

FIGURE 23 IMAGE PATTERN ON THE FOCAL PLANE $\alpha = 25^{\circ}$

the three cases of the zoned mirror remain the same while those of the smooth parabola change considerably. The sharpness of the intensity distribution curves (i.e., the focussing ability) for the smooth parabola drops off considerably.

The ratio of the magnitude of the two secondary maxima for the three cases of the zoned mirror remain constant and equal to unity up to an incident angle of about 20^{o}, while it changes rapidly for a smooth parabola as the angle of incidence is changed, e.g., a change in the angle of incidence from 0 to 15^{o} changes the ratio from 1 to 4.25. (See later in Figure 26).

The absolute value of the secondary maximum for the zoned mirror shows a slight increase as the angle of incidence is changed from normal. The secondary maxima for Case 1 deviate more and more from those of Cases 2 and 3 as the angle of incidence is increased and with an incident angle of 20^{o}, the two secondary maxima for Case 1 give a ratio of 1.2 as against 1.01 for Case 2.

The fact that the intensity distributions of the electric field for Cases 2 and 3 are very nearly the same, indicates that the contribution of the coupled current to the field is negligible.

These results indicate an important fact that the coupling effect between strips can be ignored without sacrificing the accuracy. It may also be remarked that the coupling effect which is the result of the first order iteration, is the most time consuming step in the computation as indicated in the beginning of this section.

Though there is some difference between Case 1 and Case 2 particularly for oblique incidence, the physical optics solution as given by Case 1

yields a reasonably good approximation (though at less accuracy) even with 22 discontinuities due to the edges in the present system. The simplification of computation is, however, considerable.

It is interesting to note that the two secondary maxima on either side of the principal are more symmetrical for Cases 2 and 3 than for Case 1 indicating that the effect of the edges seems to reduce the "coma".

According to parageometrical optics the focal plane is actually not the best image surface. Accordingly an image pattern is obtained, as shown in Figure 24, in a plane (for simplicity of computation only a plane surface is considered) passing through the best image point and perpendicular to the focal axis, for 15^{o} incident angle. It show that the gain is slightly higher but the minor lobes become large and more asymmetric.

7.4 Radiation Patterns

The curves in Figures 25, 26, 27, 28, 29 and 30, which are derived with the aid of the reciprocity theorem from the intensity distribution curves discussed before, show the important and interesting properties of the zoned mirror as an antenna in comparison with a smooth parabola, with isotropic feed. It is clear from Figure 25, that for a zoned mirror the deflection of the beam of the radiation pattern from the axis is proportional to the displacement of the feed, while it is not so for the smooth parabola. For the same scan angle, a larger displacement of the feed is required for the smooth parabola than for a zoned mirror and this difference in displacement increases as the scan angle is increased. Figure 26 shows the maximum field intensity on the focal plane for various angles of incidence while Figure 27 shows the variation of the directive gain against the scan angle. The gain of the zoned mirror is substantially constant.

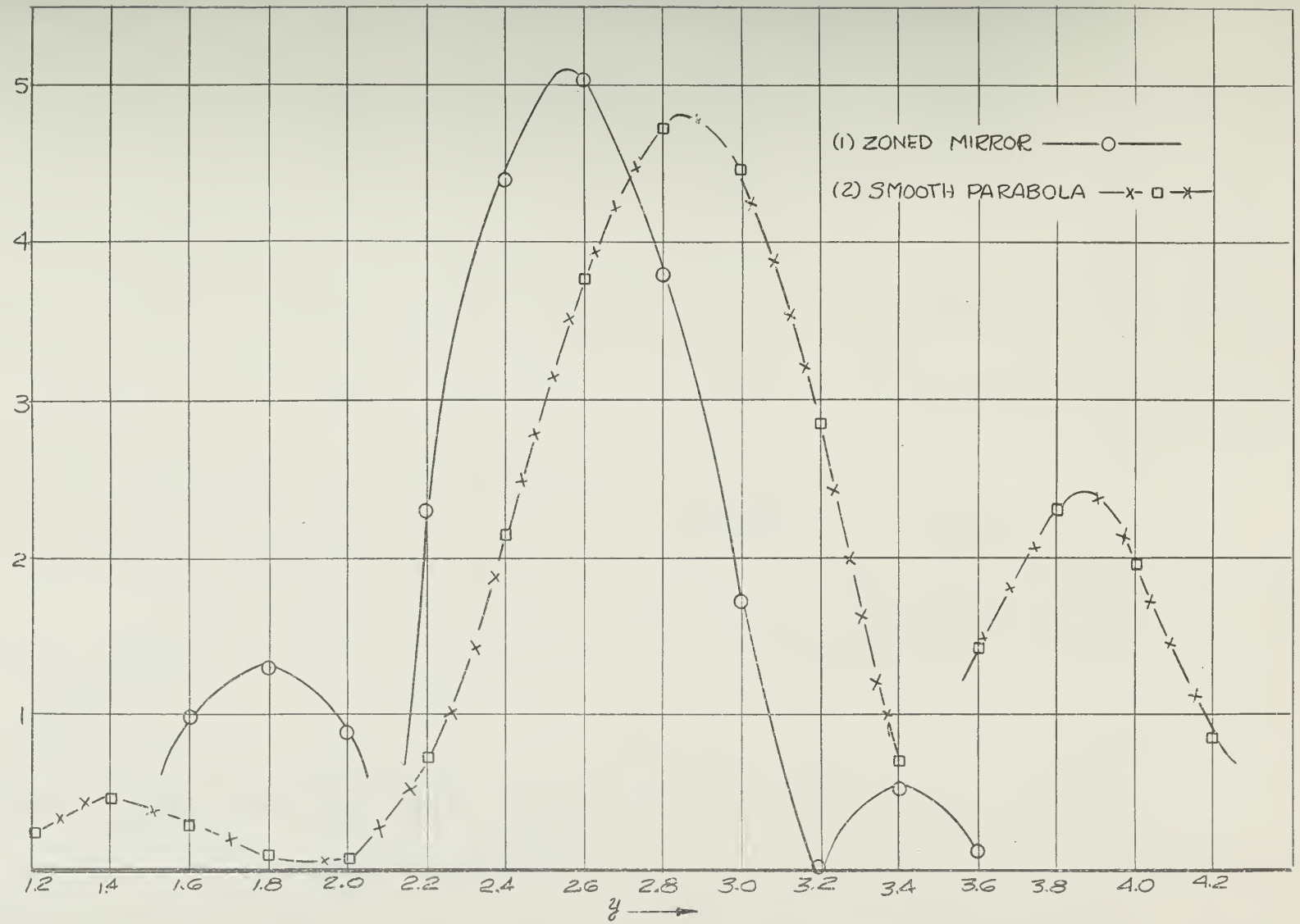

FIGURE 24 IMAGE PATTERN ON THE PLANE OF THE BEST IMAGE POINT (x = 9,67) $a = 15^{o}$

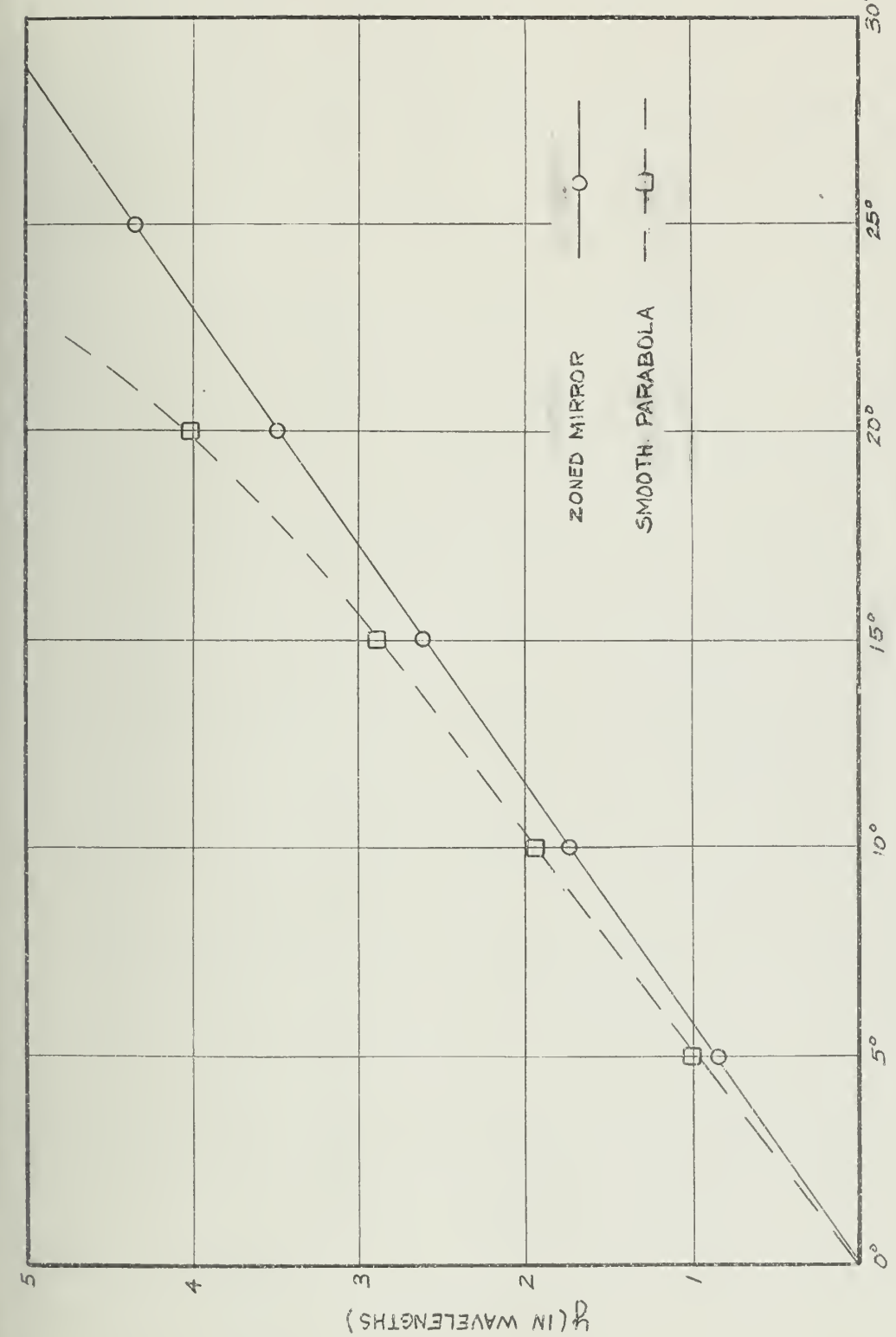

FIGURE 25 THE RELATION BETWEEN THE POSITION OF OFF AXIS FEED AND THE BEAM DEFLECTION ANGLE α

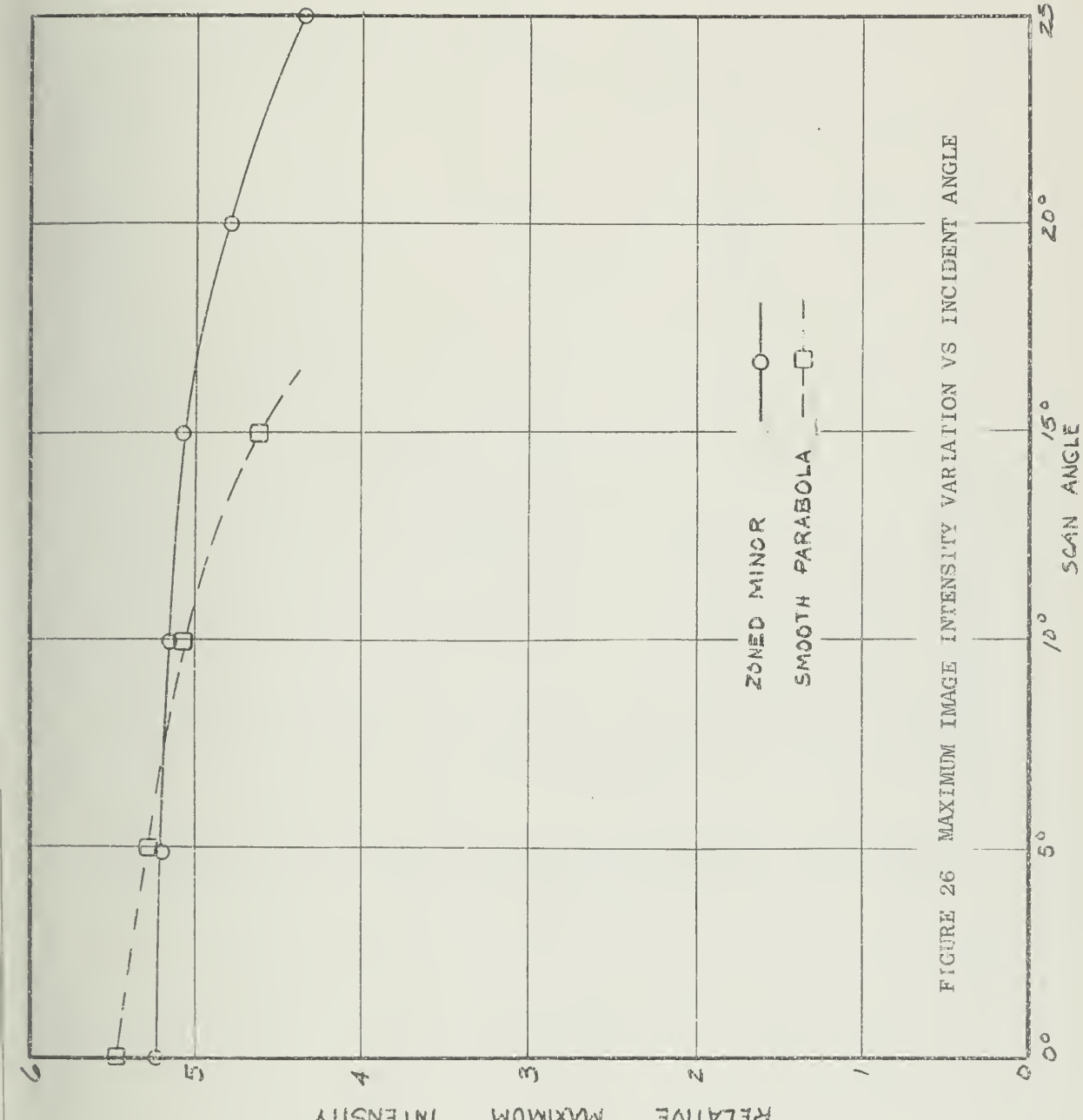

FIGURE 26 MAXIMUM IMAGE INTENSITY VARIATION VS INCIDENT ANGLE

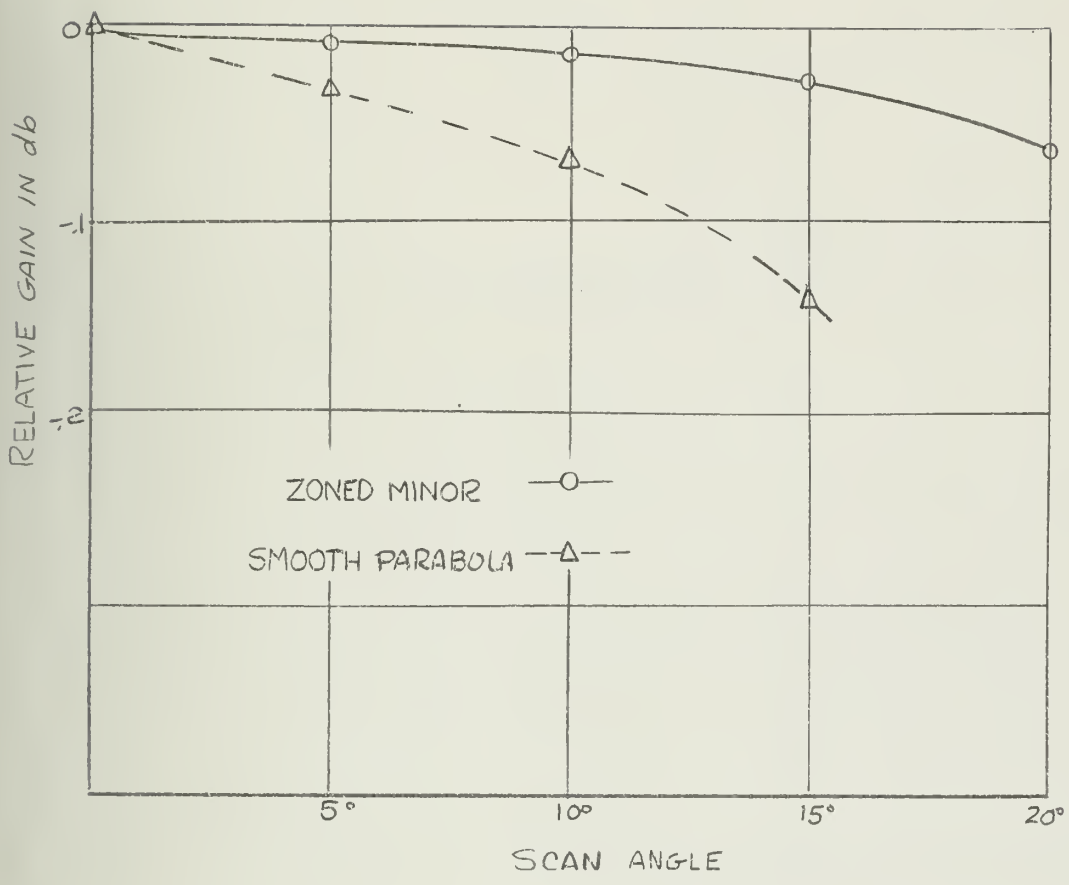

FIGURE 27 RELATIVE GAIN OF THE RADIATION PATTERN VS SCAN ANGLE

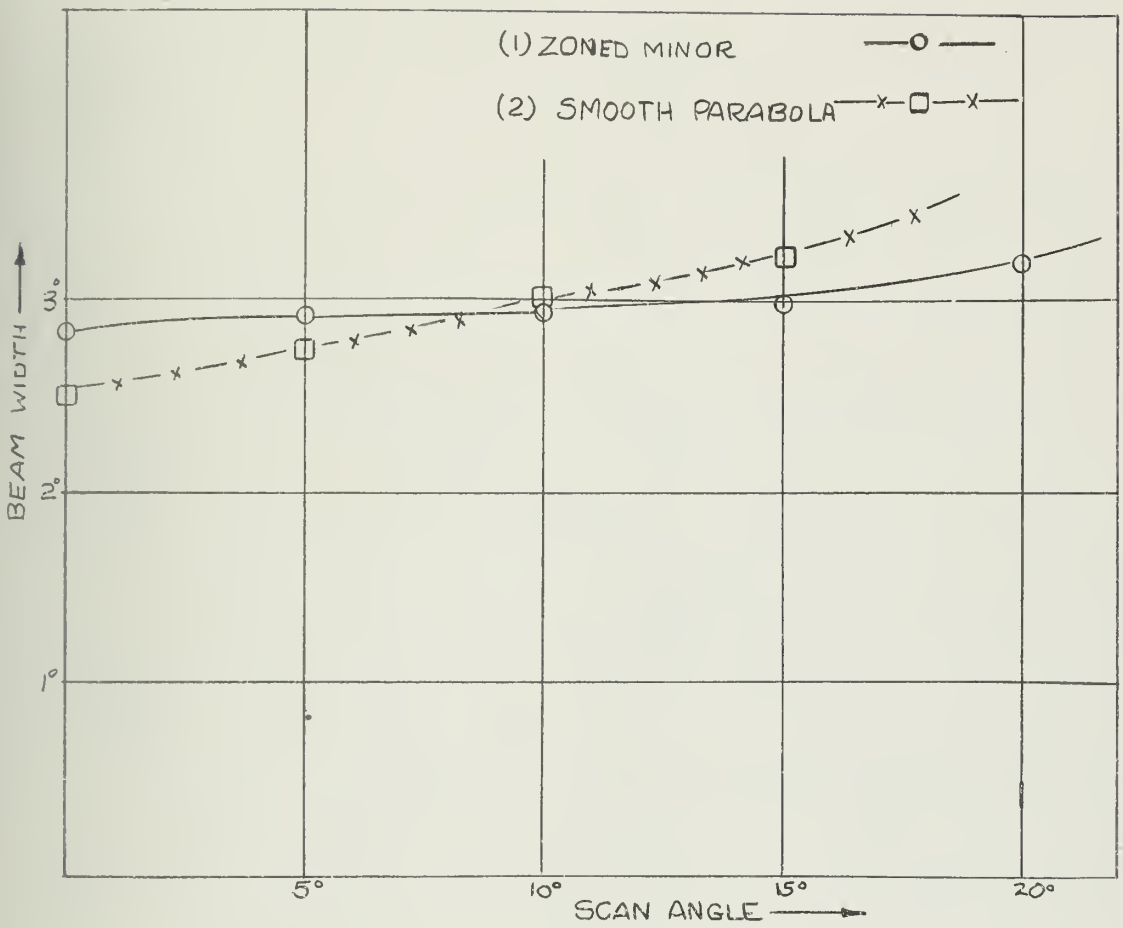

FIGURE 28 BEAM WIDTH OF THE RADIATION PATTERN VS SCAN ANGLE

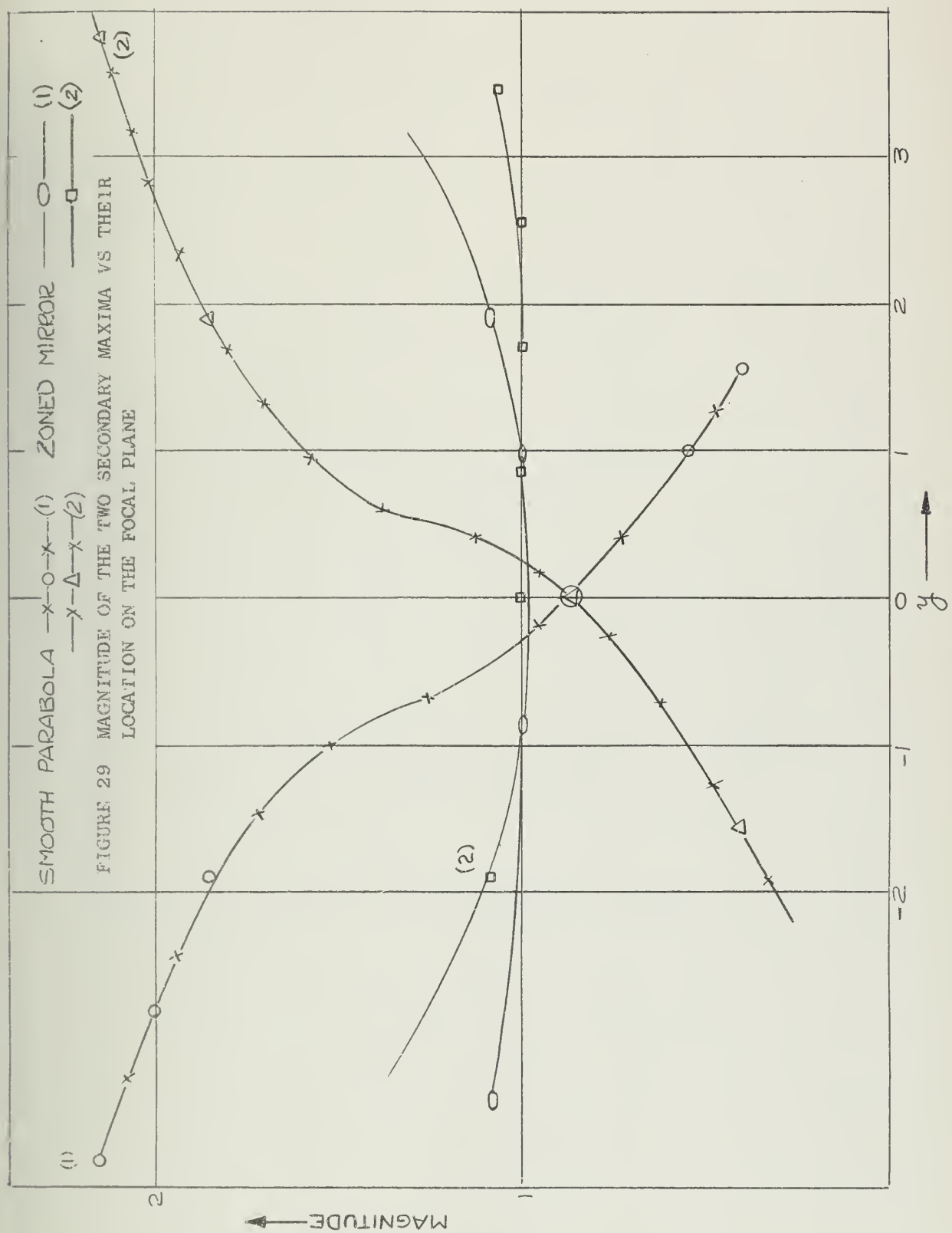

FIGURE 29 MAGNITUDE OF THE TWO SECONDARY MAXIMA VS THEIR LOCATION ON THE FOCAL PLANE

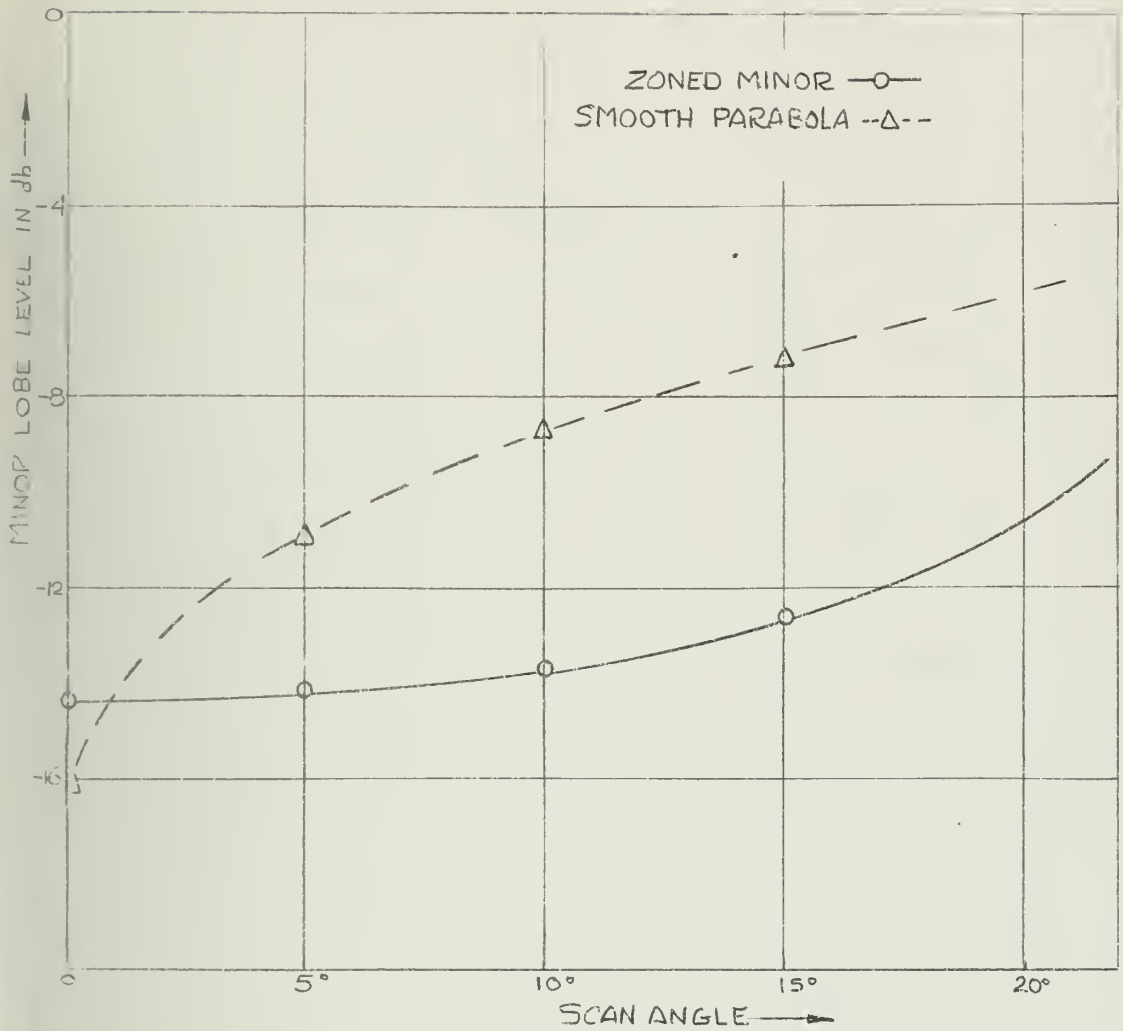

FIGURE 30 MINOR LOBE LEVEL AT THE RADIATION PATTERN VS SCAN ANGLE

For a 15^{o} scan angle, the loss in gain is only 0.27 db as referred to the on focus feed case, while for a parabola the loss is 1.36 db.

Figure 28 shows that the change in beam width for 0^{o} to 15^{o} scan angle is roughly 30% for the smooth parabola against 5% for the zoned mirror. Figure 29 is a plot of the magnitude of the first two secondary maxima of the image pattern against their positions in the focal plane. In Figure 30, a plot of minor lobe level of the radiation pattern against the scan angle, it may be noted that the minor lobe level is smaller for the smooth parabola than that of the zoned mirror for the on focus feed case, the figures being -16.14 db and -14.43 db respectively. This is expected since the zoned mirror having reflecting strips at a constant distance from the focus, is uniformly illuminated while the smooth parabola is not. The minor lobe level of the radiation pattern goes up rapidly as the offsetting of the feed is increased for the smooth parabola whereas it increases very slowly for the zoned mirror. For example, as the scan angle varies from 0^{o} to 15^{o} the minor lobe level is raised by 9.03 db for the smooth parabola and only 1.95 db for the zoned mirror. At 15^{o} scan angle the minor lobe level is only -7.2 db for the smooth parabola and -12.6 db for the zoned mirror.

A more interesting result so far as the coma correction is concerned, is shown in Figure 31. It is seen therefrom that the ratio of the first two secondary maxima, (a function of coma aberration) is substantially constant for a zoned mirror in contrast with that for a smooth parabola. It clearly indicates that the zoned mirror like the one considered is very effective in the reduction of the coma aberration.

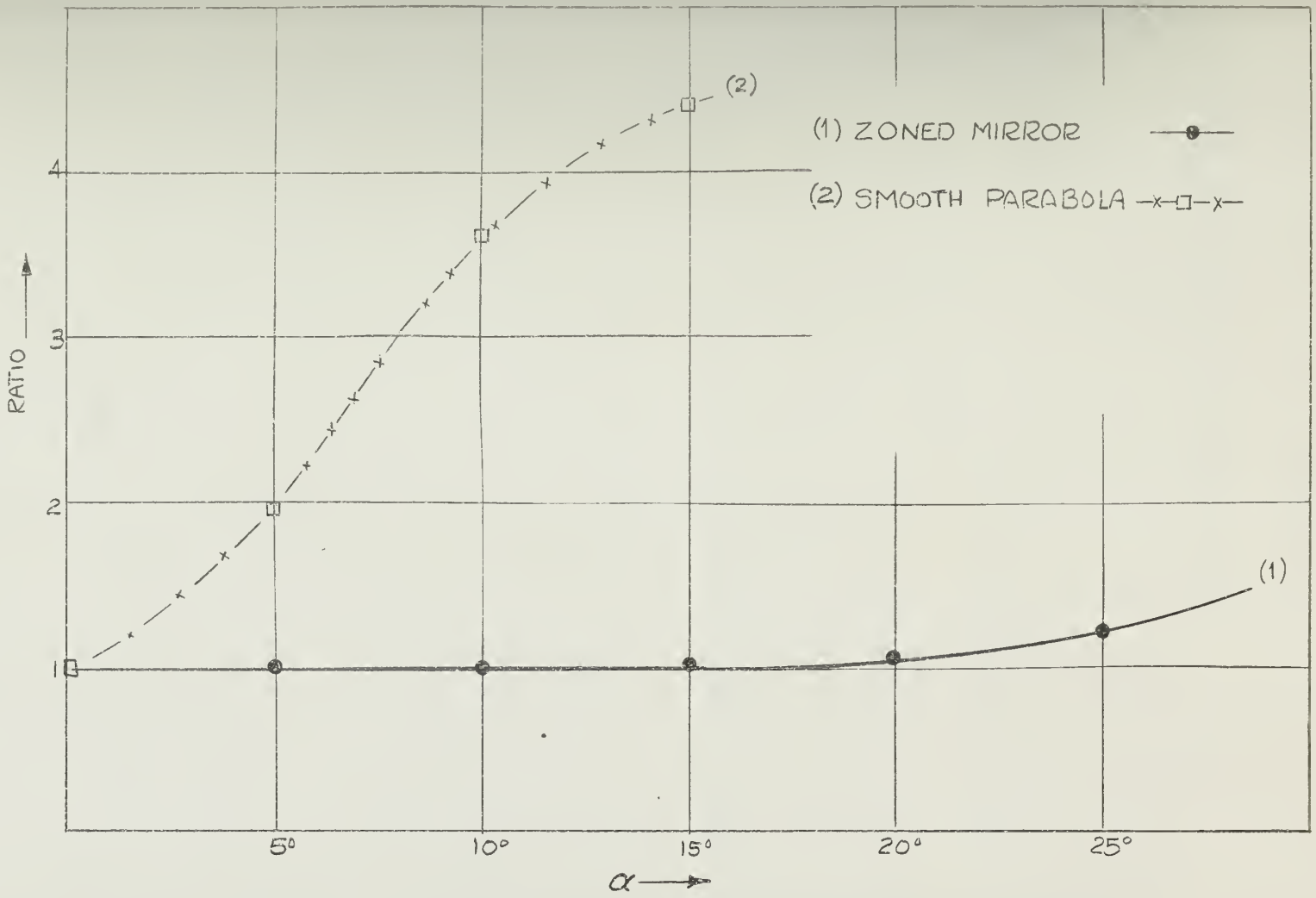

FIGURE 31 RATIO OF THE FIRST TWO SECONDARY MAXIMA VS SCAN ANGLE

8. CONCLUSIONS

8.1 The Approximate Current Distribution

A study of the $|\triangle E|$ curves reveals that the approximate solution is very close to the exact one. Because of the ease of computation, it has more practical value than the exact solution. The computation for the exact solution may be extremely difficult if not impossible.

8.2 The Technique of Analysis

In spite of a large number of discontinuities in the structure, the generally used physical optics solution offers a sufficiently accurate result. This method is simple and straightforward. For higher accuracy the edge effect should be considered but the coupling effect seems to be of less importance.

In view of the fact that the contribution of the edge effect is only a higher order correction to the physical optics solution, it is expected that the computation of this contribution may be obtained simply by replacing each edge by a line source of proper intensity in which case the calculations involving Fresnel integrals can be avoided.

8.3 The Performance of the Zoned Mirror

The effectiveness of a coma-correlated zoned mirror has been the object of controversy for some time. The present investigation, made on a two-dimensional cylindrical zoned mirror which is free from astigmatism, enables us to evaluate its effectiveness in correction of "coma" particularly for a system with a small value of f/D (the smallest F-number of this system is 1/2), and uniform illumination, without complications due to other aberrations.

A comparison with the performance of an equivalent smooth parabola has indicated that the zoned mirror with small F-number and unifrom illumination has a performance much superior to that of a smooth parabola in the reduction of the "coma" aberration. The beam width, gain and minor lobe level of the radiation pattern and also the ratio of the two first minor lobe levels of the image distribution in the focal plane (a function of coma aberration) are relatively constant with a zoned mirror for a scan angle up to 25^{o}, while for a smooth parabola the ratio of the first minor lobe level increases drastically. Further coma correction seems to be possible by positioning the zones slightly off the coma circle such that the third order and the fifth order coma partially cancel each other.

8.4 Suggestions for Future Investigation

A detailed numerical study of the performance of zoned mirror with $f/D \approx 1/2$ but with different values of f/λ followed by experimental investigation is suggested. Since the zoned mirror is a frequency sensitive device, it will be interesting to evaluate its chromatic aberration by studying the reduction in gain and variation in minor lobes as the operating frequency changes.

BIBLIOGRAPHY

1. Bouwkamp, C.J., Reports in Progress of Physics, Vol XVIII, 1954.

2. Baker, B. B., and Copson, E. T., The Mathematical Theory of Huygens Principle, Clarendon Press, Oxford, 1950.

3. Braunbeck, W., "Neue Näherungsmethode für die Begung am ebenen shirm" Zeitschrift für Physik. Vol 127, 1949-50.

4. Blanch, G., and Rhodes, I., "Tables of Characteristic Values of Mathieu Equation for Large Values of the Parameter," Journal of the Washington Academy of Sciences, Vol 46, No. 6, June 1955.

5. Erdelyi, A, and Papas, C.H., "Diffraction by a Strip," Technical Report No. 1, California Institute of Technology, November 1953.

6. Fock, V.A., "New Methods in Diffraction Theory," Phil Mag Vol 39, 1948.

7. Fox, E.N., "Diffraction of Sound Pulses by an Infinitely Long Strip" Phil Trans. Royal Soc. A, Vol 241, 1948.

8. Goldstein, S., "Mathieu Functions" Cambridge Phil Soc Trans, Vol 23, 1927.

9. Goldstein, S., "On the Asymptotic Expansion of Characteristic Numbers of Mathieu Equation", Proc. Roy. Soc. Edin., Vol. 49, 1929.

10. Hadlock, R.K., "Diffraction Patterns at the Plane of a Slit in a Reflecting Screen," Journal of Applied Physics, Vol. 29, 1958.

11. Hamilton, W.R., "On Some Results of the View of a Characteristic Function in Optics," Brit. Ass. report, 1833.

12. Ince, E.L., "Researches into the Characteristic Numbers of the Mathieu Equation," Proc. Roy. Soc. Edin., Vol. 46, 1925-26 and Vol. 47, 1927.

13. Karp, S.N. and Russek, A, "Diffraction by a Wide Slit," Journal of Applied Physics, Vol 27, No. 8, August 1956.

14. Kellar, J.B., "Diffraction by an Aperture," Journal of Applied Physics, Vol. 28, No. 4, April 1957.

15. Kellar, J.B., "A Geometrical Theory of Diffraction," Research Report No. EM-115, New York Univ, July 1958. "General Theory of Diffraction," Proc. of the Symposium on Microwave Optics, McGill University, 1953.

16. Levy, Bertram, "Diffraction by an Elliptic Cylinder" Research Report No. EM-121, New York Univ., December 1958.

17. McLachlan, N.W., Theory and Application of Mathieu Function, Oxford Press, 1947.

18. McDonald, H.M., Electromagnetism, G Bell and Sons, London, 1934.

19. Millar, R.F., "Diffraction by a Wide Slit and Complementary Strip," Ph.D. Dissertation, Cambridge University, 1957.

20. Morse, P.M., and Rubenstein, P.J., "Diffraction of Waves by Ribbons and Slots," Physical Review, Vol 54, December 1938.

21. Moullin, E.B. and Phillips, P.M. "On the Current Induced in a Conducting Ribbon by the Incidence of a Plane Electromagnetic Wave," Proc. IEE, Vol 99, Part IV, No. 3, 1952.

22. Moullin, E.B., "On the Current Induced in a Conducting Ribbon by a Current Filament Parallel to It." Proc. IEE 1953, Monograph No 71 R

23. Moullin, E.B., Radio Aerials, Clarendon Press, Oxford, 1949.

24. National Bureau of Standards, "Tables Relating to Mathieu Functions," Columbia Univ. Press, 1951.

25. Nijboer, B.R., "Diffraction Theory of Aberrations," Ph.D. Dissertation, Univ. of Groningen, 1942.

26. Plonsey, R., "Diffraction by Cylindrical Reflectors," Proc IEE Monograph No. 281 R, January 1958.

27. Ronchi, A L. and Toraldo di Francia, G., "An Application of Parageometrical Optics to the Design of a Microwave Mirror," Trans IRE Antenna and Propagation No. 1, Vol AP-6, January 1958.

28. Ramsay, J. F. and Jackson, J.A.C., "Wide angle Scanning Performance of Mirror Aerials," Marcom Review, Vol 19, No. 122, 1956.

29. Sommerfeld, A., Optics, Academic Press, 1954.

30. Schwarzchild, K.,"Die Bungung und Polarisation des Lichts durch einen Spalt," Math. Ann. Vol 55, 1901.

31. Skavlem, S., "On the Differention of Scaler Plane Waves by a Slit of Infinite Length," Arch Math Maturvid, Vol 51, 1951.

32. Terman, E.F., Electronics and Radio Engineers, McGraw Hill Book Co, 1955

33. Toraldo di Francia, G., "Parageometrical Optics", J. Opt. Soc. Vol 40, 1950.

34. Watson, G.N., Theory of Bessel Functions, Cambridge University Press, 1944.

APPENDIX A

DISCUSSION ON THE DIFFICULTIES OF EXACT SOLUTION FOR NUMERICAL COMPUTATION FOR WIDE STRIPS

It has already been indicated that the exact solution of the above problem is obtained in terms of Fourier series expansion of various Mathieu functions as given by Equations (5.1).

(a) The Fourier expansion of se(s,x) i,e

$$se_n(s,x) = \sum_{k=0}^{\infty} De_{2k+p} \cos (2k+p)x, \quad \text{where } p = 0 \text{ if } n \text{ is even}, \; p = 1 \text{ if } n \text{ is odd} \tag{A.1}$$

is no longer useful for computation when s is sufficiently large. It can be shown from the asymptotic behavior of the coefficients De_{2k+p}, that they are extremely large, even though $Se_n(s,x)$ is small. For example with large s, we have, asymptotically,[24]

$$De_0(s) \approx e^{\sqrt{s}}/2s^{1/4}\sqrt{\pi} \quad \text{and} \quad |De_2(s)/De_0(s)| \approx 2 \tag{A.2}$$

based upon a normalization which requires that

$$\sum_{k=0}^{\infty} De_{2k+p} = 1$$

For s = 2500 corresponding to h approximately equal to 8λ it would be necessary to know the coefficients up to 22 significant figures before the normalization condition is satisfied up to two significant figures. The same difficulty will arise for functions of higher orders. This

difficulty can not be avoided by using a different normalization. For the ratio $Se_0(s,\pi/2) \Big/ Se_0(s,0)$ is independent of the normalization and unless the coefficients were computed with extreme accuracy, the order of the magnitude of the function would remain undetermined over a large part of the S-x plane. For example, Goldstein[8] obtained 22 coefficients for S = 6400 for five decimal places for computing the function ce(s,x) which is proportional[12] to $Se_0(s,x)$. But although $ce(s,\pi/2)$ can be readily determined from his coefficients, the latter yield merely ce(s,x) = 0 for $x \leqslant 55^o$. Thus with trigonometric series, the individual terms are too large and too slowly convergent to be of any use for computational purposes when s is large. The asymptotic expansion seems to be the only feasible method for practical purposes under this condition.

The asymptotic expansion of the function $Se_n(s,x)$ is given by

$$Se_n(s,x) \approx \sigma_r[W_1\left\{P_0(x) - P_1(x)\right\} + W_2\left\{P_0(x) + P_1(x)\right\}] \text{ for } -\pi/2 \leqslant x \leqslant \pi/2 \tag{A.3}$$

where

$$W_1 = e^{\sqrt{s}\sin x}\frac{[\cos(\frac{n}{2}+\frac{\pi}{4})]^{2n+1}}{(\cos x)^{n+1}} \tag{A.4}$$

$$W_2 = e^{-\sqrt{s}\sin x}\frac{[\cos(\frac{n}{2}+\frac{\pi}{4})]^{2n+1}}{(\cos x)^{n+1}} \tag{A.5}$$

$$\sigma_n = \frac{2n^{-\frac{1}{2}}}{[1 + \frac{\nu}{4\sqrt{s}} + \frac{4\nu^2+3}{32s} + \frac{19\nu^2+59\nu}{256\, s^{3/2}} + \ldots]} \tag{A.6}$$

$$P_0(x) = 1 + \frac{\nu}{4\sqrt{s}\cos^2 x} + \frac{1}{s}\left[\frac{\nu^4 + 86\nu^2 + 105}{512\cos^4 x} - \frac{\nu^4 + 22\nu^2 + 57}{512\cos^2 x}\right] + \ldots \quad (A.7)$$

$$P_1(x) = \frac{(\nu^3 + 3)\sin x}{16\sqrt{s}\cos^2 x} + \frac{\sin x}{128s\cos^2 x}\left[\nu^3 + 3\nu + \frac{4\nu^3 + 44\nu}{\cos^2 x}\right] + \ldots \text{ and } \nu = 2n+1 \quad (A.8)$$

The above asynptotic expansion gives best results when x is very small. The accuracy falls off as x increases. It can be shown that for reliable results

$$\cos x \geq \frac{2\sqrt{\nu}}{s^{1/4}}. \quad (A.9)$$

Thus for a given s and x the order up to which the function can be evaluated asynptotically with reasonable accuracy is fixed. For example, with n = 0 i,e x = 1 and s = 2500, $Se_0(s,x)$ can be obtained satisfactorily up to a value of x given by

$$\cos x > \frac{2}{\sqrt{50}} \quad \text{i,e } x \approx 73^\circ 30'$$

For larger values of x the results obtained from the asymptotic series given by Equation (A.3) will not be satisfactory.

The expression given by Equation (A.3) fails altogether for $x = 90^\circ$. The above expression, however, can be extended in the following way[24] to be useful when $x = 90^\circ$.

Let $x = \frac{\pi}{2} - \rho$ be that value of n where the above asynptotic expansion gives accurate results. Now consider the Taylor expansion around $x = \frac{\pi}{2}$. Let $y_1(s,x)$ represent $Se_{2r}(s,x)$ and $y_2(s,x)$ represent $Se_{2r+1}(s,x)$.

Hence $y_1'(s,\pi/2) = y_2(s,\pi/2) = 0$ and $y_1(s,x)$, $y_2(s,x)$ are even and odd functions respectively of $\pi/2 - x$.

Let

$$y_1(s, \pi/2 - \rho) = y_1(s, \pi/2)\ T_1(s,\rho)$$

and

$$y_2(s, \pi/2 - \rho) = -y_2'(s,\pi/2)\ T_2(s,\rho)$$

where

$$T_1(s,\rho) = 1 + \left\{ \left[\frac{\rho^2 y_1''}{2!} + \frac{\rho^4 y_1^{(4)}}{4!} + \ldots + \frac{\rho^{2m} y_1^{(2m)}}{2m!}\right] y_1 \right\}_{x=\pi/2} \tag{A.10}$$

and

$$T_2(s,\rho) = \rho + \left\{ \left[\frac{\rho^3 y_2^{(3)}}{3!} + \ldots + \frac{\rho^{(2m+1)} y_2^{(2m+1)}}{(2m+1)}\right] y_2' \right\}_{x=\pi/2} \tag{A.11}$$

The derivatives of y_1 and y_2 can be obtained with the aid of

$$\frac{d^2y}{dx^2} + (b - s\cos^2 x)y = 0 \tag{A.12}$$

Then the ratios $\dfrac{y_1^{(2m)}}{y_1}$ and $\dfrac{y_2^{(2m+1)}}{y_2}$ for $x = \pi/2$ are known functions of and S and since the asymptotic expansion of b is given by

$$b = \nu\sqrt{s} - \frac{\nu^2 + 1}{8} - \frac{\nu^3 + 3\nu}{2^6\sqrt{s}} - \frac{5\nu^4 + 34\nu^2 + 9}{2^{10}s} + \ldots, \tag{A.13}$$

$T_1(s,\rho)$ and $T_2(s,\rho)$ can be determined. Therefore $y_1(s, \pi/2)$ can be calculated from the above expressions, only if $y_1(s, \frac{\pi}{2} - P)$, $y_2(s, \frac{\pi}{2} - \rho)$ can be calculated. Further, the computation of the successive derivatives become cumber-

some and the accuracy of the results obtained is less than for very small values of x.

(b) Evaluation of N_n:

By definition

$$N_n = \int_0^{2\pi} [Se_n(s,n)]^2 \, dx$$

Evaluation of N_n presents the same difficulty as that of $Se_n(s,x)$ since the asymptotic expression given before by Equation (A.3) is not valid over the entire range of x given by $0 \leqslant x \leqslant 2\pi$.

(c) Evaluation of $He_n^{(2)}(s,x)$:

$$He_{2n}^{(2)}(s,x) = Je_n(s,x) - j\, Ne_n(s,x) \tag{A.15}$$

The asymptotic expansions of Je_n and Ne_n are available and are given by

$$\frac{Je_r(s,x) \sim [F_0(x) \cos \varphi + F_1(x) \sin \varphi]}{s^{1/4} \sqrt{\cosh x}} \tag{A.16}$$

and

$$\frac{Ne_r(s,x) \sim [F_0(x) \sin \varphi - F_1(x) \cos \varphi]}{s^{1/4} \sqrt{\cosh x}} \tag{A.17}$$

where

$$\varphi = \sqrt{s} \sinh x - (2n + 1) \tan^{-1} (\tanh x) \tag{A.18}$$

and

$$F_0(x) = 1 + \frac{2}{4\sqrt{s}\cosh^2 x} + \frac{1}{s}\left[\frac{\nu^4+86\nu^2+105}{512\cosh^4 x} - \frac{\nu^4+22\nu^2+57}{512\cosh^2 x}\right]$$

$$+ \frac{1}{s^{3/2}}\left[\frac{-(\nu^5+14\nu^3+33\nu)}{2048\cosh^2 x} - \frac{2\nu^5+124\nu^3+1122\nu}{2048\cosh^6 x} + \frac{3\nu^5+29\nu^3+1627\nu}{2048\cosh^6 x}\right] + \ldots$$

(A.19)

$$F_1(x) = \frac{(\nu^2+3)\sinh x}{16\sqrt{s}\cosh^2 x} + \frac{\sinh x}{128s\cosh^2 x}\left[\nu^3 + 3\nu + \frac{4\nu^3 + 44\nu}{\cosh^2 x}\right]$$

$$+ \frac{\sinh x}{s^{3/2}}\left[\frac{5\nu^4+34\nu^2+9}{2048\cosh^4 x} - \frac{(\nu^6-47\nu^4+667\nu^2+2835)}{24576\cosh^4 x} + \frac{\nu^6+505\nu^4+12139\nu^2+10395}{24576\cosh^6 x}\right]$$

$$+ \ldots \qquad \text{(A.20)}$$

In this case, also, the accuracy of computation depends on the values of s, ν and x as in the case of $Se_n(s,x)$. Further, the asymptotic expansion for $Ne_n(s,x)$ is not valid when $x = 0$.

The possible way that the functions $He_n^{(2)}(s,0)$ can be computed are from the expansions of Je_n and Ne_n in the product of Bessels Functions given by

$$Je_{2n}(s,0) = (-1)^n \sqrt{\pi/2} \sum_{k=0}^{\infty} (-1)^k De_{2k} J_k\left(\frac{\sqrt{s}}{2}\right) J_k\left(\frac{\sqrt{s}}{2}\right) \qquad \text{(A.21)}$$

$$De_0$$

$$Je_{2n+1}(s,0) = (-1)^n \sqrt{\pi/2} \sum_{k=0}^{\infty} (-1)^k De_{2k+1}[2J_{k+1}(\sqrt{s/2})\ J_k(\sqrt{s/2})] \Big/ De_1 \qquad (A.22)$$

$$Ne_{2n}(s,0) = (-1)^n \sqrt{\pi/2} \sum_{k=0}^{\infty} (-1)^k De_{2k}\ J_k(\sqrt{s/2}) \Big/ De_0 \qquad (A.23)$$

$$Ne_{2n+1}(s,0) = (-1)^n \sqrt{\pi/2} \sum_{k=0}^{\infty} (-1)^k De_{2k+1}[Y_{k+1}(\sqrt{s/2})J_k(\sqrt{s/2})+Y_k(\sqrt{s/2})J_{k+1}(\sqrt{} \Big/ De_1 \qquad (A.24)$$

Calculations for the Image Pattern of a Smooth Parabola

Let aFb be the section of a smooth parabolic reflector (Figure 32) with 0 as focus and f as focal length. A plane wave polarized in the z direction is incident at an angle δ with the x axis. It is required to find the electric field on the line defined by x = 0.

Consider any point P(x,y) on the parabola. The path difference along incident wave propagation vector between P and F is given by

$$\begin{aligned} FQ' &= FS + SQ' = FS + QR = FQ \cos\delta + PQ \sin\delta \\ &= f \tan^2 \psi/2 \cos\delta + \rho \sin\psi \sin\delta \\ &= f \tan\psi/2\ (\tan\psi/2 \cos\delta + 2 \sin\delta), \text{ since } \rho = f \operatorname{Sec}^2\psi/2 \end{aligned}$$

$\therefore$ current induced at P due to the incident plane wave is given by

$$I(P) = \hat{z}\ \frac{2}{\eta} \cos(\psi/2 + \delta)\ e^{ikf(\cos\delta \tan^2\psi/2 + 2\sin\delta \tan\psi/2)} \cdot E_{inc} \qquad (A.25)$$

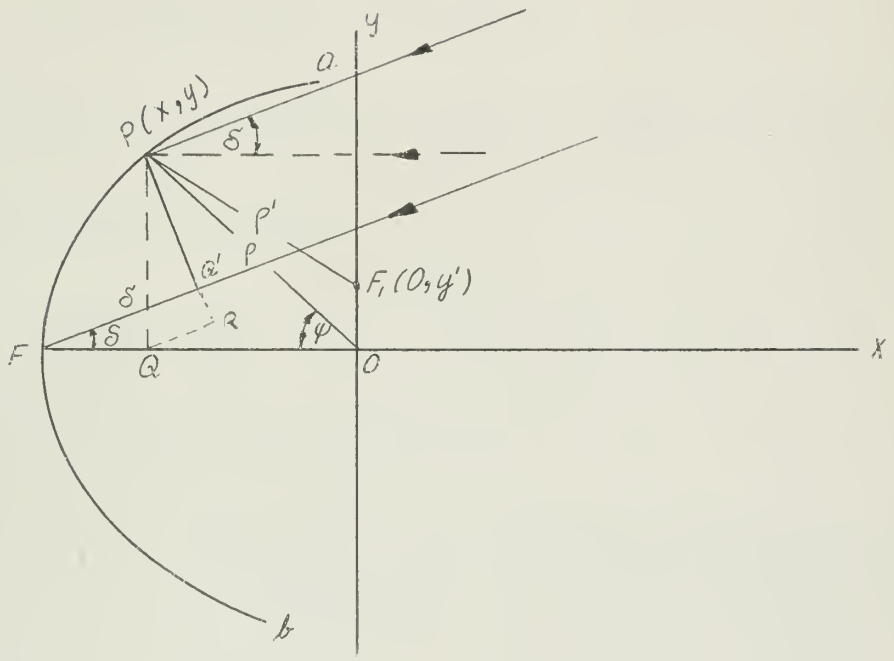

FIGURE 32

At F_1, the field due to P is given by

$$E_z(F_1) = \frac{i\,k^2}{4i\omega\epsilon}\, I(p)\; Ho^{(2)}[k\rho']$$

$$\simeq \frac{k^2}{4\omega\epsilon}\,\frac{2}{\pi}\cdot \cos^2(\psi/2 + \delta)\, e^{ikf(\cos\delta \tan^2\psi/2 + 2\sin\delta\tan\psi/2)}$$

$$\cdot\sqrt{\frac{2}{\pi}}\cdot\frac{e^{-i(k\rho' - \pi/4)}}{\sqrt{k\rho}}\cdot E_{inc} \qquad (A.26)$$

By using asymptotic expansion for $H_0^{(2)}[k\rho']$ and noting that $\rho' \sim \rho$ and $k\rho \gg 1$. Coordinates of P are given by

$$x_1 = f \tan^2 \psi/2, \quad y_1 = 2f \tan \psi/2$$

$\frac{dx_1}{dy} = f \tan \psi/2 \sec^2 \psi/2$ and $\frac{dy_1}{dx} = f \sec^2 \psi/2$. Hence a small length dS around P is given by

$$dS = \left(\frac{dx_1}{dx}\right)^2 + \left(\frac{dy_1}{dx}\right) \cdot d\psi = f \sec^3 \psi/2 \, d\psi$$

Field at F′due to the parabola is given by

$$E_z(F_1'') = f \, e^{i\pi/4} \int_{-\theta_1}^{\theta_1} \frac{\cos(\psi/2 + \delta)}{\cos^2 \psi/2} \, e^{-ik[\rho' - f \tan \psi/2 \cos\delta + 2 \sin\delta)]} \cdot d\psi.$$

where

$$\rho' = f^2 \sec^4 \psi/2 + y'^2 - 4fy' \tan \psi/2.$$

A Brief Discussion on Aberrations

An ideal optical system has a one to one correspondence and a linear relationship between an object and its image. The rays from a point source will converge to a point in the image space called its conjugate point or Gaussian image. In terms of geometrical optics the corresponding wavefront must be spherical in the image space. Any defect that will cause a deviation of the wavefront from the spherical surface is called the aberration of the system and will result in an imperfect image.

Consider a perfect optical system as shown in Figure 33 where the Gaussian image of a general object point P, is P′. Let P′ be the origin

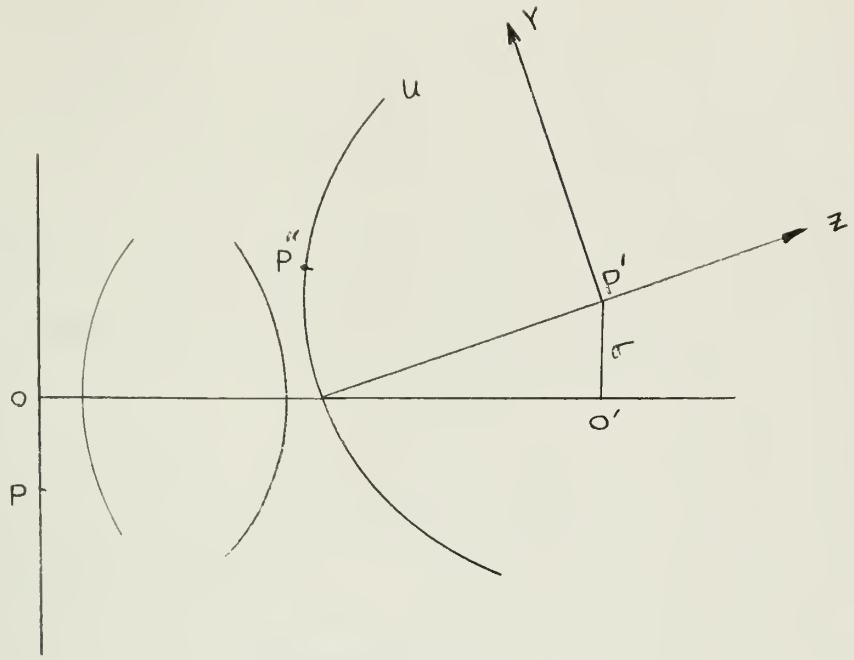

FIGURE 33

of the cartesian coordinates (x, y, z) where the z-axis passes through the center O'' of a portion of a spherical surface, representing the wavefront at the aperture in the image space, the center of the sphere being P' and radius R. Let $O'P'$, the displacement of the Gaussian image from the axis of the system be σ. Consider a point P'' on the wavefront which is uniquely described by two cartesian coordinates x'' and y'' or r and ϕ of the cylindrical coordinate system. Then

$$\frac{x''}{a} = r \cos \phi \quad \text{and} \quad \frac{y''}{a} = r \sin \phi \tag{A.28}$$

where a is the radius of the aperture.

For a perfect system, the wavefront in the image space is given by

$$x''^2 + y''^2 + z''^2 = R^2 \tag{A.29}$$

For a system with aberration, R will no longer be a constant. Let the aberration function, $V(\sigma, x'', y'')$, be the deviation of this wavefront from a spherical one. It is obvious that the deviation at $P''(x'', y'')$ is a function of x'', y''. The deviation of a given system also depends upon the displacement of the object from the axis, or more elegantly, upon σ, the displacement of the corresponding Gaussian image.

Then

$$x''^2 + y''^2 + z''^2 = [R + V(\sigma, x'', y'')]^2 \tag{A.30}$$

Assuming that $(V/R)^2 \ll 1$ we get

$$x''^2 + y''^2 + z''^2 - R^2 - 2RV(\sigma, x'', y'') = 0 \tag{A.31}$$

Then the ratio of the direction cosines of a ray passing through the point P'' is given by

$$x'' - R\frac{\partial V}{\partial x''} : y'' - R\frac{\partial V}{\partial y''} : z'' \tag{A.32}$$

Hence the equation of the ray is given by

$$\frac{x-x''}{x''-R\frac{\partial V}{\partial x''}} = \frac{y-y''}{y''-R\frac{\partial V}{\partial y''}} = \frac{z-z''}{z''} \tag{A.33}$$

The intercept of the ray with the image plane defined by $z = 0$ is

$$x = R\frac{\partial V}{\partial x'} \qquad \text{and} \qquad y = R\frac{\partial V}{\partial y''}$$

Changing into polar coordinates

$$x = \frac{R}{a}\left[\sin\phi\,\frac{\partial V}{\partial r} + \frac{\cos\phi}{r}\,\frac{\partial V}{\partial \phi}\right] \tag{A.34}$$

and

$$y = \frac{R}{a}\left[\cos\phi\,\frac{\partial V}{\partial r} - \frac{\sin\phi}{r}\,\frac{\partial V}{\partial \phi}\right] \tag{A.35}$$

The locus of the intercepts of the rays from a zone r = constant on the wavefront will be a closed curve on the plane z = 0. This curve is called the aberration curve.

The aberration function V can be expanded[11] in a power series of the rational invariants σ^2, r^2 and $\sigma r \cos\phi$, each term representing a single aberration. A typical term in the expansion is given by

$$b'_{\ell nm}\,\sigma^{2\ell+m}\,r^n\cos^m\phi \tag{A.36}$$

or by

$$b_{\ell nm}\,\sigma^{2\ell+m}\,r^n\cos m\phi \tag{A.37}$$

where ℓ, n and m are integers ≥ 0, while $n > m$ and $n - m$ is even. $b_{\ell nm}$ is the aberration coefficient. Following Nijboer, we use the second expansion with the following classification of aberrations (lower order) as shown in Table 2.

Substituting (A.37) into (A.34) and (A.35) we get an aberration curve due to a circular zone r = const on the wavefront given by

$$x = b_{\ell nm}\,\sigma^{2\ell+m}\,\frac{R}{a}\left\{-\frac{n+m}{2}\,r^{n-1}\sin(m-1)\,\phi + \frac{n-m}{2}\,r^{n-1}\sin(m+1)\,\phi\right\} \tag{A.38}$$

$$y = b_{\ell nm}\, \sigma^{2\ell+m}\, \frac{R}{a} \left\{ \frac{n+m}{2}\, r^{n-1} \cos(m-1)\,\phi + \frac{n-m}{2}\, r^{n-1} \cos(m+1)\,\phi \right\} \qquad (A.39)$$

when V = 0, corresponding to the perfect case all rays converge to P.

TABLE 2*

n=1	-	distortion (r cos ϕ)	-
n=2	curvature of the field (r^2)	-	1st astigmatism (r^2 cos 2ϕ)
n=3	-	1st coms (r^3 cos ϕ)	-
n=4	1st spherical aberration (r^4)	-	2nd astigmatism (r^4 cos 2ϕ)
n=5	-	2nd coma (r^5 cos ϕ)	-
n=6	2nd spherical aberration (r^6)	-	3rd astigmatism (r^6 cos 2ϕ)
		etc.	

An examination of (A.38) and (A.39) will reveal that the main features of the aberration curve e.g., the general shape, symmetry etc. are determined by the value of m, while n determines the details of the curve and the particular value of ℓ seems to be immaterial. For example, when m = 0, (A.38) and (A.39) yeild

$$x = b_{\ell no}\, \sigma^{2\ell}\, \frac{R}{a} \left\{ n r^{n-1} \sin \phi \right\} \qquad (A.40)$$

and

$$y = b_{\ell no}\, \sigma^{2\ell}\, \frac{R}{a} \left\{ n r^{n-1} \cos \phi \right\} \qquad (A.41)$$

* More generally the order of aberrations are designated according to the value of n, i.e., the power of r. Thus what Nijboer calls 1st coma is known as 3rd order coma since the value of n is 3 and so on.

The aberration curve in this case is a circle with P' as the center. This is called spherical aberration. One complete revolution along r = const circle corresponds to one revolution along the aberration curve.

If m = 1, Equations (A.38) and (A.39) reduce to

$$x = b_{\ell n1}\, 0^{2\ell+1}\, \frac{R}{a} \left\{ \frac{n-1}{2}\, r^{n-1} \sin 2\phi \right\} \tag{A.42}$$

$$y = b_{\ell n1}\, 0^{2\ell+1}\, \frac{R}{a} \left\{ \frac{n+1}{2}\, r^{n-1} + \frac{n-1}{2} \cos 2\phi \right\} \tag{A.43}$$

Equations (A.42) and (A.43) represent a circle of radius proportional to r^{n-1} in the image plane but the center of the circle is displaced by an amount also proportional to r^{n-1} on the y axis. Hence the family of circles corresponding to various zones at the aperture has an envelope which is a pair of straight lines as shown in Figure 34.

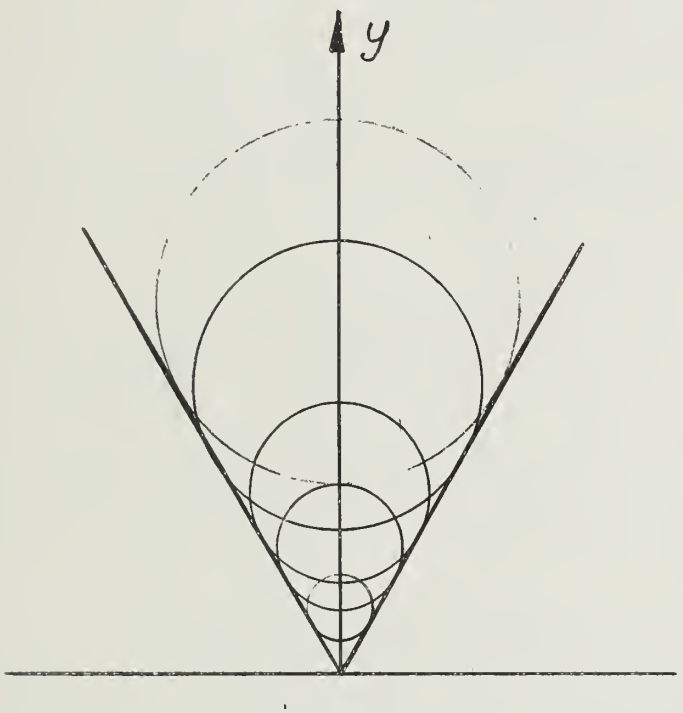

FIGURE 34

Thus the geometrical optics image of a point object at P has a comet-shaped appearance with its Gaussian image P' as its apex. It is important to note that the aberration curve in this case is not symmetrical except with respect to the y-axis. This is called coma aberration. Two complete revolutions of the aberration curve corresponds to one revolution of r = constant circle.

By putting m = 2 in Equations (A.38) and (A.39) we obtain aberration curves which are symmetrical with respect to both x and y axes. These curves are characterized by the fact that they reduce to either a horizontal or a vertical focal line as the receiving plane is moved on either side of the Gaussian image. This is called astigmatism.

Higher values of m will produce other aberrations which were first studied by Nijboer . Without going into the details of these aberrations it can be seen that the aberration curves will be symmetrical with respect to both x and y axes for even values of m and symmetrical only with respect to the y axis for odd values of m .

The field at any point Q in the image space for uniformly illuminated aperture is given by

$$u(Q) \propto \int_0^1 \int_0^{2\pi} \frac{e^{-ik(s+V)}}{s} \, r.dr \, d\phi \qquad (A.44)$$

where s represents the distance of a typical point P'' on the wavefront to Q.

With V = 0, the isophoto lines on the image plane are a set of concentric circles with P' as the center. When the expansion of V i.e.

$\Sigma b_{\ell nm} O^{2\ell+n} r^n \cos m\phi$ is used for V in (A.44), Nijboer has shown that the resultant diffraction patterns are symmetrical with respect to both x and y axes only for the terms corresponding to both spherical aberration and astigmatism and higher aberrations involving even values of m, Whereas the patterns do not possess the same symmetry for the terms corresponding to coma and higher aberration terms involving odd values of m. All the terms having odd values of m including coma produce patterns symmetrical with respect to the y axis only.

For the two dimensional case, since there is no variation in the ϕ direction, the aberration function is

$$V = \sum_n C_n y^n \qquad (A.45)$$

where C_n includes the factor $O^{2\ell}$. It can be seen from the foregoing considerations that all terms with even values of n represent spherical aberration while all terms with odd values of n represent coma aberration. Astigmation is absent.

Following the treatment of the three dimensional case by Nijboer it can be shown that the diffraction pattern will be symmetrical with respect to the z axis for a system with only spherical aberration. On the other hand with coma the pattern is asymmetrical about z axis. Thus in the case of a two dimensional zoned mirror the two secondary maxima of the intensity distribution along y axis on either side of the principal will be equal for a system with no coma. Any inequality of the two can be attributed to the coma effect only, while for a three dimensional case their inequality is due to both coma and other higher aberrations

corresponding to all odd values of m. Therefore the ratio of the magnitude of the two secondary maxima will provide a measure of the coma effect for a two dimensional case. In case this ratio is nearly unity, the change in the magnitude of the secondary maxima is a measure of the spherical aberration.

ADDENDUM

At the time when this report was in the printer's hands, a report on the "Experimental Study of a Diffraction Reflector" by J. H. Provencher, Air Force Cambridge Research Center (April 1959) was received. These authors are pleased to add that Provencher's experimental results are generally in quite good agreement with those obtained in this report, although not on an exact quantitative basis, for Provencher's investigation is made on a three-dimensional model and its focal length and aperture are also different from the example computed in this report. For a scan angle equal to 17.5^{o} the drop in gain as reported by Provencher is about 2 db, while for the cylindric mirror investigated here it is considerably better, about 0.5 db. This might be due to less inherent aberrations of a cylindric system as explained in this report. However, Provencher's beam width and minor lobe level seem to deteriorate slightly less than those computed in this report up to 17.5 scan angle. This apparent contradiction to the last statement might possibly be explained by the fact that Provencher's F-number is larger than the one considered here, and also his reflector is illuminated by a flared horn, probably not uniformly, as witnessed by the measured half-power beamwidth which is greater than that of a uniformly illuminated dish of the same aperture. It is also of interest to point out in Provencher's measurements for normal incidence that (1) the gain of zoned mirror is less than that of a corresponding smooth paraboloid and (2) the minor lobe level of the former is greater than that of the latter. This result agrees with these authors. The second effect is already explained in this report (P. 83), while, for the first one, as the computation (Figure 18) indicates, is due to the diffraction effect by the edges of all the

zones. It is therefore doubtful that the diffraction effect in this sense plays an essential role in the coma-correction for a zoned mirror in spite of the fact that this effect tends to make the two secondary maxima slightly closer to equality (See Figures 18 - 23).

ERRATA

Page 9, line 15, delete P at end of line

Page 10, Equation (3.8) should be $E_{Diff} = - E_{z_{inc}}$

Page 12, Equation (3.13) should be $\frac{k^2}{i\omega} \int_{\text{strip } i} I_i(s) g(s,s') ds + \ldots$

Equation (3.15) should be $= - E_{z_{inc}}$

Equation (3.16) should have small n above the $\sum_{\substack{j=1 \\ j \neq i}}$ and $\sum_{\substack{k=1 \\ k \neq j}}$

Page 13, Equation (3.18) should be $\int_{\text{strip } i} I_{ij}^{(1)}(s) \ldots$

Page 14, Equation (3.19) should be $= E(s')$

Page 18, first paragraph, curl $\bar{E} = - \bar{B}$

Page 21, Equation (4.19), the second half of the equation in the numerator should read, $Ho_{\eta}^{(2)}(\xi_o) Se_n(\eta) So_n(\eta_o)$

Equation (4.20), should read

$$\ldots + \left\{ \int_o^{\infty} I_z(y,\alpha) H_o^{(2)}(kr) dy \right.$$

Page 27, line 7, should be $s = k^2 h^2, \ldots$

Page 29, line 6, should read, I_{h_B} is the current .....

Page 37, the first equation on the page is Equation (5.12)

Page 44, line 2, should be Let $A = \sqrt{2kr} \cos \alpha/2$

Page 45, line 12, should be $H_o^{(2)}[k|x-x'|]dx'$

Page 46, line 2, should be $H_o^{(2)}[k(x'-x)]dx'$

line 6, the end of the equation should be $dt\, dx'$

Page 47, line 4, the equation should be

$$\int_1^\infty \frac{e^{-ik(h\pm x)t}}{(1+t)^r\sqrt{t^2-1}}\,dt = e^{-ik(h\pm x)} \int_o^\infty \frac{e^{-ik(h\pm x)z}}{(2+z)^{r+\frac{1}{2}}\sqrt{z}}\,dz$$

line 8, the denominator should read $(2+z)^{r+\frac{1}{2}}\sqrt{z}$

line 15, the denominator should read $(2+z)^{r+\frac{1}{2}}\sqrt{z}$

Page 49, line 7, insert equation number (5.39)

Page 58, Figure 10, line 2, Observation (Angle of Incidence $\alpha = 0$)

Page 70, Figure 20 should read, Image Pattern on the Focal Plane

Page 74, line 10, Figure 26 should be Figure 31

Page 78, zoned minor should read zoned mirror

Page 79, the numbers on the left side should be 0, -1, -2, and zoned minor should be zoned mirror

Page 80, zoned minor should read zoned mirror

Page 82, zoned minor should read zoned mirror and the caption for Figure 30 should be Minor Lobe Level of the Radiation Pattern ....

Page 87, Number 14 and 15, Kellar should be spelled Keller

Page 88, Number 30 should read "Die Beugung und ...."

Page 89, line 6 should be (a) The Fourier expansion of Se(s,x) i,e

line 7 should be $Se_n(s,x) = ...$

Page 91, lines 3, 8, and 17 asynptotic should be spelled asymptotic

Page 91, line 9 should be with $n = 0$ i,e $\nu = 1$ ....

Page 92, Equations (A.10) and (A.11) should read respectively

$$\Big]\Big/ y_1 \qquad x=\pi/2 \qquad\qquad \Big]\Big/ y_{2'} \qquad x=\pi/2$$

Page 92, line 17 should read ..., only if $y_1(s, \frac{\pi}{2} - \rho)$, ...

Page 93, Equation (A.16)
$$Je_r(s,x) \sim \frac{[F_0(x) \cos \varphi + F_1(x) \sin \varphi]}{s^{1/4} \sqrt{\cosh x}}$$

Equation (A.17)
$$Ne_r(s,x) \sim \frac{[F_0(x) \sin \varphi - F_1(x) \cos \varphi]}{s^{1/4} \sqrt{\cosh x}}$$

Page 97, line 6, should read $dS = \sqrt{(\frac{dx_1}{dx})^2 + (\frac{dy_1}{dx})^2} \cdot d\psi = ...$

line 7, should be Field at F_1 due ....

line 8, should read

$$E_z(F_1) = f\, e^{i\,\pi/4} \int_{-\Theta_1}^{\Theta_1} \frac{\cos(\psi/2 + \delta)}{\cos^2 \psi/2}\, e^{-ik[\rho' - f(\tan \psi/2} \ldots$$

Page 98, Equation (A.28) $\frac{x''}{a} = r \sin \phi$ and $\frac{y''}{a} = r \cos \phi$

ANTENNA LABORATORY
TECHNICAL REPORTS AND MEMORANDA ISSUED

Contract AF33(616)-310

"Synthesis of Aperture Antennas," Technical Report No. 1, C.T.A. Johnk October, 1954

"A Synthesis Method for Broad-band Antenna Impedance Matching Networks," Technical Report No. 2, Nicholas Yaru, 1 February 1955.

"The Asymmetrically Excited Spherical Antenna," Technical Report No. 3, Robert C. Hansen, 30 April 1955.

"Analysis of an Airborne Homing System," Technical Report No. 4, Paul E. Mayes. 1 June 1955, (CONFIDENTIAL)

"Coupling of Antenna Elements to a Circular Surface Waveguide," Technical Report No. 5, H. E. King and R. H. DuHamel, 30 June 1955

"Input Impedance of a Spherical Ferrite Antenna wigh a Latitudinal Current," Technical Report No. 6, W. L. Weeks, 20 August 1955.

"Axially Excited Surface Wave Antennas," Technical Report No. 7, D. E. Royal, 10 October 1955

"Homing Antennas for the F-86F Aircraft (450-2500mc)," Technical Report No. 8 P. E. Mayes, R. F. Hyneman, and R. C. Becker, 20 February 1957. (CONFIDENTIAL)

"Ground Screen Pattern Range," Technical Memorandum No. 1, Roger R. Trapp, 10 July 1955

Contract AF33(616)-3220

"Effective Permeability of Spheroidal Shells," Technical Report No. 9, E. J. Scott and R. H. DuHamel, 16 April 1956.

"An Analytical Study of Spaced Loop ADF Antenna Systems," Technical Report No. 10, D. G. Berry and J. B. Kreer, 10 May 1956.

"A Technique for Controlling the Radiation from Dielectric Rod Waveguides," Technical Report No. 11, J. W. Duncan and R. H. DuHamel, 15 July 1956.

"Directional Characteristics of a U-Shaped Slot Antenna," Technical Report No. 12, Richard C. Becker, 30 September 1956

"Impedance of Ferrite Loop Antennas," Technical Report No. 13, V. H. Rumsey and W. L. Weeks, 15 October 1956.

"Closely Spaced Transverse Slots in Rectangular Waveguide" Technical Report No. 14, Richard F. Hyneman, 20 December 1956.

"Distributed Coupling to Surface Wave Antennas," Technical Report No. 15. Ralph Richard Hodges, Jr., 5 January 1957.

"The Characteristic Impedance of the Fin Antenna of Infinite Length," Technical Report No. 16, Robert L. Carrel, 15 January 1957.

"On the Estimation of Ferrite Loop Antenna Impedance," Technical Report No. 17, Walter L. Weeks, 10 April 1957

"A Note Concerning a Mechanical Scanning System for a Flush Mounted Line Source Antenna," Technical Report No. 18, Walter L. Weeks, 20 April 1957.

"Broadband Logarithmically Periodic Antenna Structures," Technical Report No. 19, R. H. DuHamel and D. E. Isbell, 1 May 1957.

"Frequency Independent Antennas," Technical Report No. 20, V. H. Rumsey, 25 October 1957

"The Equiangular Spiral Antenna," Technical Report No. 21, J. D. Dyson, 15 September 1957

"Experimental Investigation of the Conical Spiral Antenna," Technical Report No. 22, R. L. Carrel, 25 May 1957.

"Coupling Between a Parallel Plate Waveguide and a Surface Waveguide," Technical Report No. 23, E. J. Scott, 10 August 1957

"Launching Efficiency of Wires and Slots for a Dielectric Rod Waveguide," Technical Report No. 24, J. W. Duncan and R. H. DuHamel, August 1957.

"The Characteristic Impedance of an Infinite Biconical Antenna of Arbitrary Cross Section," Technical Report No. 25, Robert L. Carrel, August 1957.

"Cavity-Backed Slot Antennas," Technical Report No. 26, R. J. Tector, 30 October 1957.

"Coupled Waveguide Excitation of Traveling Wave Slot Antennas," Technical Report No. 27, W. L. Weeks, 1 December 1957.

"Phase Velocities in Rectangular Waveguide Partially Filled with Dielectric," Technical Report No. 28, W. L. Weeks, 20 December 1957.

"Measuring the Capacitance per Unit Length of Biconical Structures of Arbitrary Cross Section," Technical Report No. 29, J. D. Dyson, 10 January 1958.

"Non-Planar Logarithmically Periodic Antenna Structure," Technical Report No. 30, D.W Isbell, 20 February 1958.

"Electromagnetic Fields in Rectangular Slots," Technical Report No. 31, N.J. Kuhn and P.E. Mast, 10 March 1958.

"The Efficiency of Excitation of a Surface Wave on a Dielectric Cylinder," Technical Report No. 32, J.W. Duncan, 25 May 1958.

"A Unidirectional Equiangular Spiral Antenna," Technical Report No. 33, J D. Dyson, 10 July 1958.

"Dielectric Coated Spheroidal Radiators," Technical Report No. 34, W.L. Weeks, 12 September 1958.

"A Theoretical Study of the Equiangular Spiral Antenna," Technical Report No. 35, P.E Mast, 12 September 1958.

Contract AF33(616)-6079

"Use of Coupled Waveguides in a Traveling Wave Scanning Antenna," Technical Report No. 36, R.H. MacPhie, 30 April 1959.

DISTRIBUTION LIST

One copy each unless otherwise indicated

Armed Services Technical Information
Agency
Arlington Hall Station
Arlington 12, Virginia
3 copies, 1 repro.

Commander
Wright Air Development Center
Wright-Patterson Air Force Base, Ohio
ATTN: WCLRS-6, Mr. F. E. Burnham
3 copies

Commander
Wright Air Development Center
ATTN: WCLNQ-4, Mr. M. Draganjac
Wright-Patterson Air Force Base, Ohio

Commander
Wright Air Development Center
ATTN: WCOSI, Library
Wright-Patterson Air Force Base, Ohio

Director
Evans Signal Laboratory
ATTN. Technical Document Center
Belmar, New Jersey

Commander
U. S. Naval Air Test Center
ATTN: ET-315, Antenna Section
Patuxent River, Maryland

Chief
Bureau of Ordnance
Department of the Navy
ATTN: Mr. C.H Jackson, Code Re 9a
Washington 25, D. C.

Commander
Hq. A. F. Cambridge Research Center
Air Research and Development Command
Laurence G. Hanscom Field
ATTN: CRRD, R. E. Hiatt
Bedford, Massachusetts

Commander
Air Force Missile Test Center
Patrick Air Force Base, Florida
ATTN: Technical Library

Director
Ballistics Research Laboratory
ATTN: Ballistics Measurement Lab.
Aberdeen Proving Ground, Maryland

Office of the Chief Signal Officer
ATTN: SIGNET-5
Eng. & Technical Division
Washington 25, D. C.

Commander
Rome Air Development Center
ATTN: RCERA-1 D. Mather
Griffiss Air Force Base
Rome, New YOrk

Airborne Instruments Lab., Inc.
ATTN: Dr. E. G. Fubini
Antenna Section
160 Old Country Road
Mineola, New York
M/F Contract AF33(616)-2143

Andrew Alford Consulting Engineers
ATTN: Dr. A. Alford
299 Atlantic Avenue
Boston 10, Massachusetts
M/F Contract AF33(038)-23700

Bell Aircraft Corporation
ATTN: Mr. J. D. Shantz
Buffalo 5, New York
M/F Contract W-33(038)-14169

Chief
Bureau of Ships
Department of the Navy
ATTN: Code 838D, L. E. Shoemaker
Washington 25, D.C.

DISTRIBUTION LIST (CONTINUED)

McDonnell Aircraft Corporation
ATTN Engineering Library
M F Contract AF33(600)-8743
Lambert Municipal Airport
St Louis 21, Missouri

Dr. L. Cutrona
University of Michigan
Aeronautical Research Center
M F Contract AF33(038)-21573
Willow Run Airport
Ypsilanti, Michigan

Professor H J. Zimmermann
Research Lab of Electronics
Massachusetts Institute of Technology
M F Contract AF33(616)-2107
Cambridge, Massachusetts

Dr. J.A. Marsh
North American Aviation, Inc.
Aerophysics Laboratory
M F Contract AF33(038)18319
12214 Lakewood Boulevard
Downey, California

Mr. Dave Mason
Engineering Data Section
North American Aviation, Inc.
M F Contract AF33(038)18319
Los Angeles International Airport
Los Angeles 45, California

Northrop Aircraft, Incorporated
ATTN Northrop Library
Dept 2135
M F Contract AF33(600)-22313
Hawthorne, California

Radioplane Company
M F Contract AF33(600)-23893
Van Nuys, California

Lockheed Aircraft Corporation
ATTN C.L. Johnson
P O Box 55
M F NOa(s)-52-763
Burbank, California

Robert Borts
Raytheon Manufacturing Company
Wayland Laboratory, Wayland, Mass

Republic Aviation Corporation
ATTN: Engineering Library
M F Contract AF33(038)-14810
Farmingdale
Long Island, New York

Sperry Gyroscope Company
ATTN: Mr. B. Berkowitz
M F Contract AF33(038)-14524
Great Neck
Long Island, New York

Mr. George Cramer
Temco Aircraft Corporation
Contract AF33(600)21714
Garland, Texas

George Giffin
Farnsworth Electronics Co.
Marked: For Cont. AF33(600)-25523
Ft. Wayne, Indiana

Mr James D Leonard
North American Aviation, Inc
Contract NOa(s) 54-323
4300 E. Fifth Avenue
Columbus, Ohio

Mr. P.D. Newhouser
Development Engineering
Westinghouse Electric Corporation
Air Arm Division
Contract AF33(600)-27852
Friendship Airport, Maryland

Air Force Development Field
Representative
ATTN: Capt. Carl B. Ausfahl
Code 1010
Naval Research Laboratory
Washington 25, D.C.

Chief of Naval Research
Department of the Navy
ATTN: Mr Harry Harrison
Code 427
Room 2604, Bldg. T-3
Washington 25, D C.

DISTRIBUTION LIST (CONTINUED)

Sylvania Electric Products, Inc.
Electronic Defense Laboratory
M.F Contract DA 36-039-sc-75012
P.O Box 205
Mountain View, California

Stanford Electronics Laboratory
Stanford University
ATTN: Applied Electronics Lab.
Document Library
Stanford, California

Radio Corporation of America
R.C.A. Laboratories Division
Princeton, New Jersey

Electrical Engineering Res. Lab.
University of Texas
Box 8026, University Station
Austin, Texas

Dr. Robert Hansen
8356 Chase Avenue
Los Angeles 45, California

Technical Library
Bell Telephone Laboratories
463 West Street
New York 14, New York

Dr. R.E. Beam
Microwave Laboratory
Northwestern University
Evanston, Illinois

Dr. H.G. Booker
Department of Electrical Engineering
Cornell University
Ithaca, New York

Applied Physics Laboratory
Johns Hopkins University
8621 Georgia Avenue
Silver Spring, Maryland

Exchange and Gift Division
The Library of Congress
Washington 25, D.C.

Ennis Kuhlman
% McDonnell Aircraft
P.O. Box 516
Lambert Municipal Airport
St. Louis 21, Missouri

Mr. Roger Battie
Supervisor, Technical Liaison
Sylvania Electric Products, Inc.
Electronic Systems Division
P.O. Box 188
Mountain View, California

Physical Science Lab.
ATTN: R. Dressel
New Mexico College of A and MA
State College, New Mexico

Mrs. E.L. Hufschmidt, Librarian
Technical Reports Collection
303 A Pierce Hall
Harvard University
Cambridge 38, Massachusetts

Dr. R.H. DuHamel
Collins Radio Company
Cedar Rapids, Iowa

Dr. R.F. Hyneman
5116 Marburn Avenue
Los Angeles 43, California

Director
Air University Library
ATTN: AUL-8489
Maxwell AFB, Alabama

Mary Lou Fields, Acquisitions
Stanford Research Institute
Documents Center
Menlow Park, California

Dr. Harry Letaw, Jr.
Research Division
Raytheon Manufacturing Co.
Waltham 54, Massachusetts

Canoga Corporation
5955 Sepulveda Boulevard
M/F Contract AF08(603)-4327
P.O. Box 550
Van Nuys, California

DISTRIBUTION LIST (CONTINUED)

Beech Aircraft Corporation
ATTN: Chief Engineer
6600 E. Central Avenue
Wichita 1, Kansas
M/F Contract AF33(600)-20910

Land-Air, Incorporated
Cheyenne Division
ATTN: Mr. R. J. Klessig
Chief Engineer
Cheyenne, Wyoming
M/F Contract AF33(600)-22964

Director, National Security Agency
RADE 1GM. ATTN: Lt. Manning
Washington 25, D.C.

Melpar, Inc.
3000 Arlington Blvd.
Falls Church, Virginia
ATTN: K. S. Kelleher

Naval Air Missile Test Center
Point Mugu, California
ATTN: Antenna Section

Fairchild Engine & Airplane Corp.
Fairchild Airplane Division
ATTN: L. Fahnestock
Hagerstown, Maryland
M/F Contract AF33(038)-18499

Federal Telecommunications Lab.
ATTN: Mr. A. Kandoian
500 Washington Avenue
Nutley 10, New Jersey
M/F Contract AF33(616)-3071

Ryan Aeronautical Company
Lindbergh Drive
San Diego 12, California
M/F Contract W-33(038)-ac-21370

Republic Aviation Corporation
ATTN: Mr. Thatcher
Hicksville, Long Island, New York
M/F Contract AF18(600)-1602

Lockheed Aircraft Corporation
Missile Systems Division
ATTN: E. A. Blasi
Department 54-12, Building 130
Sunnyvale, California
M/F Contract AF33(616)-6022

General Electric Co.
French Road
Utica, New York
ATTN: Mr. Grimm, LMEED
M/F Contract AF33(600)-30632

Motorola, Inc.
Defense Systems Lab.
ATTN: Mr. A. W. Boekelheide
3102 N. 56th Street
Phoenix, Arizona
M/F Contract NOa(s)-53-492-c

Stanford Research Institute
Southern California Laboratories
ATTN: Document Librarian
820 Mission Street
South Pasadena, California
Contract AF19(604)-1296

Prof. J. R. Whinnery
Dept. of Electrical Engineering
University of California
Berkeley, California

Professor Morris Kline
Mathematics Research Group
New York University
45 Astor Place
New York, N. Y.

Prof. A. A. Oliner
Microwave Research Institute
Polytechnic Institute of Brooklyn
55 Johnson Street - Third Floor
Brooklyn, New York

Dr. C. H. Papas
Dept. of Electrical Engineering
California Institute of Technology
Pasadena, California

DISTRIBUTION LIST (CONTINUED)

Sylvania Electric Products, Inc.
Electronic Defense Laboratory
P.O. Box 205
Mountain View, California
M/F Contract DA 36-039-sc-75012

Stanford Electronics Laboratory
Stanford University
Stanford, California
ATTN: Applied Electronics Lab.
Document Library

Radio Corporation of America
R.C.A. Laboratories Division
Princeton, New Jersey

Electrical Engineering Res. Lab.
University of Texas
Box 8026, University Station
Austin, Texas

Dr. Robert Hansen
8356 Chase Avenue
Los Angeles 45, California

Technical Library
Bell Telephone Laboratories
463 West St.
New York 14, N. Y.

Dr. R. E. Beam
Microwave Laboratory
Northwestern University
Evanston, Illinois

Department of Electrical Engineering
Cornell University
Ithaca, New York
ATTN: Dr. H. G. Booker

Applied Physics Laboratory
Johns Hopkins University
8621 Georgia Avenue
Silver Spring, Maryland

Exchange and Gift Division
The Library of Congress
Washington 25, D.C.

Ennis Kuhlman
c/o Mc Donnell Aircraft
P.O. Box 516
Lambert Municipal Airport
St. Louis 21, Mo.

Mr. Roger Battie
Supervisor, Technical Liaison
Silvania Electric Products, Inc.
Electronic Systems Division
P.O. Box 188
Mountain View, California

Physical Science Lab.
New Mexico College of A and MA
State College, New Mexico
ATTN: R. Dressel

Technical Reports Collection
303 A. Pierce Hall
Harvard University
Cambridge 38, Mass.
ATTN: Mrs. E. L. Hufschmidt, Librarian

Dr. R. H. DuHamel
Collins Radio Company
Cedar Rapids, Iowa

Dr. R. F. Hyneman
5116 Marburn Avenue
Los Angeles 43, California

Director
Air University Library
ATTN: AUL-8489
Maxwell AFB, Alabama

Stanford Research Institute
Documents Center
Menlo Park, California
ATTN: Mary Lou Fields, Acquisitions

Dr. Harry Letaw, Jr.
Research Division
Raytheon Manufacturing Co.
Waltham 54, Massachusetts

Canoga Corporation
5955 Sepulveda Boulevard
P.O. Box 550
Van Nuys, California
M/F Contract AF08(603)-4327

DISTRIBUTION LIST (CONTINUED)

Radiation, Inc.
Technical Library Section
ATTN: Antenna Department
Melbourne, Florida
M/F Contract AF33(600)-36705

Westinghouse Electric Corporation
ATTN: Electronics Division
Friendship International Airport
Box 746
Baltimore 3, Maryland
M/F Contract AF33(600)-27852

Ta-Mar, Incorporated
2339 Cotner Avenue
Los Angeles 64, California
M/F Contract AF33(604)-18651
ATTN: Rex Beam

Motorola, Inc.
8201 E. McDowell Rd.
Phoenix, Arizona
ATTN: R. C. Huntington

Ohio State Univ. Research Foundation
ATTN: Dr. T. E. Tice
1314 Kinnear Road
Columbus 8, Ohio

Smyth Research Associates
ATTN: J. B. Smyth
3555 Aero Court
San Diego 11, California

Army Rocket and Guided Missile Agency
U.S. Army Ordnance Missile Agency
ATTN: ORDXR-GMR
Redstone Arsenal, Alabama

Republic Aviation Corporation
Missile Systems Division
233 Jericho Turnpike
ATTN: Mr. Samuel Baig
Chief, Library Section
Mineola, Long Island, New York

University of Denver
Denver Research Institute
University Park
Denver 10, Colorado

Commander
Air Technical Intelligence Center
ATTN: AFCIN-4cb, Mr. Leroy Hay
Wright Patterson AFB, Ohio

Commander
801st Air Division (SAC)
ATTN: DCTT, Major Witry
Lockbourne Air Force Base, Ohio

Dr. D. E. Royal
Ramo-Wooldridge, Div. of
Thompson Ramo Wooldridge, Inc.
P.O. Box 90534 Airport Station
Los Angeles 45, California

Director
Air University Library
ATTN: AUL-9642
Maxwell Air Force Base, Alabama

Chief
Bureau of Aeronautics
Department of the Navy
ATTN: Aer-EL-931